INVESTIGATION OF FLOWS AROUND A TWO DIMENSIONAL HYDROFOIL SUBJECT TO A HIGH REDUCED FREQUENCY GUST LOADING

By

PHILIP MARIO DELPERO

B.S. Nuclear Engineering
Pennsylvania State University (1978)

Submitted to the Department of
OCEAN ENGINEERING
In Partial Fulfillment of the Requirements
For the Degrees of

MASTER OF SCIENCE IN NAVAL ARCHITECTURE AND MARINE ENGINEERING

and

MASTER OF SCIENCE IN MECHANICAL ENGINEERING

at the

MASSACHUSETTS INSTITUTE OF TECHNOLOGY
February, 1992

Signature of Author_____
Department of Ocean Engineering
September 26,1991

Certified by_____
Professor Justin E. Kerwin
Thesis Supervisor

Certified by_____
Professor Patrick Leehey
Thesis Reader

Accepted by_____
A. Douglas Carmichael, Chairman
Departmental Graduate Committee
Department of Ocean Engineering

INVESTIGATION OF FLOWS AROUND A TWO DIMENSIONAL HYDROFOIL SUBJECT TO A HIGH REDUCED FREQUENCY GUST LOADING

By

PHILIP MARIO DELPERO

Submitted to the Department of
OCEAN ENGINEERING
on September 26, 1991
in partial fulfillment of the Requirements
for the degrees of

MASTER OF SCIENCE IN NAVAL ARCHITECTURE AND MARINE ENGINEERING

and

MASTER OF SCIENCE IN MECHANICAL ENGINEERING

ABSTRACT

A system was designed to create a sinusoidal gust with a reduced frequency of 10 for use in the water tunnel in the Marine Hydrodynamics Laboratory. The system will be used to study and obtain data on the unsteady flow field over an instrumented two-dimensional hydrofoil.

Two NACA 0025 hydrofoils with a chord length of 3 inches are used to create the gust. The foils oscillate at an maximum angle-of-attack of ±6° with an oscillation frequency up to 60 hertz. Detailed analysis of the foils showed the maximum angle of twist and the maximum midspan deflection to be low enough that the resultant shed vortex is considered two-dimensional.

Initial installation and shakedown of the system showed satisfactory operation up to an oscillation frequency of 15 hertz. Corrective actions to reduce excessive foundation vibrations are being analyzed and are underway. Initial velocity profiles at a reduced frequency of one shows the hydrodynamic disturbances was measurable and sinusoidal.

Thesis Supervisor: Professor Justin E. Kerwin
Title: Professor of Ocean Engineering

Table of Contents

List of Symbols

SYMBOL	DESCRIPTION	UNITS
a	Nondimensional Separation Distance	
c	Oscillating Foil Chord Length	inches
C	Stationary Foil Chord Length	inches
C(k)	Theodorsen's Function	
d	Separation Distance Between Pivot and Centroid	inches
E	Young's Modulus	psi
f_o	Maximum Camber	inches
G	Shear Modulus	psi
h	Heave	inches
$\dot{h}$	Heave Velocity	ft/sec
$\ddot{h}$	Heave Acceleration	ft/sec^2
J	Polar Moment of Inertia About Pivot Point	lbm ft^2
J_o	Polar Moment of Inertia About Centroid	lbm ft^2
k	Reduced Frequency	
k_b	Bending Stress Concentration Factor	

k_T	Torsional Stress Concentration Factor	
l_a	Length of Shaft From Bearing to Foil Section	inches
L	Lift	lbf
M_y	Moment About Foil Pivot	ft-lbf
M_z	Bending Moment	ft-lbf
P	Instantaneous Power	hp
P_a	Average Power	hp
r	Radius of Cylindrical ends on Foils	inches
R_e	Reynolds number	
s	Foil Span	inches
t	Time	seconds
t_o	Maximum Foil Thickness	inches
T	Torque	ft-lbf
U_∞	Free Stream Water Velocity	ft/sec
V	Shear Force	lbf
w	Load Distribution	lbf/ft
W	Work	ft-lbf
Z	Section Modulus	in^3
α	Angle of Attack	degrees
α_{max}	Maximum Angle of Attack	degrees

$\dot{\alpha}$	Angular Velocity	radians/sec
$\ddot{\alpha}$	Angular acceleration	radians/sec^2
ϕ	Phase Shift	radians
θ	Angle of Twist	radians
ρ_{foil}	Oscillating Foil Density	lbm/ft^3
ρ_{water}	Tunnel Water Density	lbm/ft^3
σ	Normal Stress	psi
ν	Kinematic Viscosity	lbm/ft-sec
ω	Radial Frequency	radians/sec
τ_{torque}	Shear Stress Caused by Applied Torque	psi
τ_{lift}	Shear Stress Caused by Lift	psi
μ	Transmission Angle	degrees

List of Figures

List of Tables

Acknowledgements

This research was performed under the direction of Professor Justin Kerwin and Dr. David Keenan. Their direction in the overall performance of this project and their latitude in the accomplishment of this project were greatly appreciated.

Support for this research was provided by the Office of Naval Research and Defense Advanced Research Projects Agency under Contract N000A4-89-J-3194.

This project could have not been accomplished without the aid and assistance of many individuals. I would like to acknowledge the following individuals for their support of the project:

1) Mr. Charles Mazel of the Marine Hydrodynamics Laboratory for his diligence and persistence in the development of the software and hardware to acquire the data for the experiment. Without his expertise and dedication, the lab would be much less than it is today.

2) Mr. Paul Sicard of Wie Sic Experimental Machine in Lowell for his continued patience and flexibility in the manufacture of the many parts to build the flapping foil system. His flexibility in accepting my many changes and in resolving my shortcomings in defining the part geometries, as well as his company's flawless workmanship, were one of the shining lights in the performance of this project.

3) Mr. Brian Bosey of B & B Machine and Engineering Inc. in Stoughton for his patience in developing the foil design and his company's flawless workmanship in the foil manufacture.

Last, but not least, I would like to thank my wife, Kathleen, for her patience in dealing with the demands of my MIT experience and for her invaluable assistance in the preparation of this manuscript. Without her support my time at MIT would have been much more challenging.

Philip M. Delpero

Chapter 1

Introduction

1.1 Background

This thesis is part of a three year research program to obtain experimental data on the flow over a hydrofoil in an unsteady flow field. The overall goal of the research program is to obtain high quality data for the flow around a two-dimensional, stationary, hydrofoil subject to a high reduced frequency gust loading and a high Reynolds number. Reduced frequency and Reynolds number are defined as:

$$k = \frac{\omega C}{2U_\infty} \tag{1.1}$$

$$R_e = \frac{U_\infty C}{\nu_{water}} \tag{1.2}$$

C = 18 inches
U_∞ = 30 ft/sec maximum

Data will be obtained for Reynolds numbers and reduced frequencies far exceeding the values of previous experiments.[1] Reynolds number will be of the order 4 x 10^6 and reduced frequency approximately 10. The data will be used to:[2]

---

[1] J.E. Kerwin and D.P. Keenan, *A Proposal for Continuation of An Experimental Investigation of the Unsteady Boundary Layer Structure of a Lifting Body Subject to Cross Flow Gusts*, 20 March 1991.

[2] J.E. Kerwin and D.P. Keenan, *Progress Report for Unsteady Foil Experiment from 1 June 1990 to 31 November 1990.*

1) provide insight to modify the classical Kutta condition used in unsteady potential flow analysis,

2) provide data for validation of unsteady Navier-Stokes codes.

The work performed in the first phase of this research program consisted of the following:[3]

1) Computer programs were written to characterize the flow field induced by a pair of oscillating foils and to predict the resultant flow field over an instrumented two-dimensional stationary hydrofoil.

2) The stationary hydrofoil was designed and manufactured. The stationary hydrofoil was formed from a NACA 16 thickness form with a maximum thickness of t_o/C of 11.56% and a NACA a = 0.8 mean camber line with f_o/C = 3.36%. This unbounded profile was modified to account for tunnel wall effects by sizing the manufactured foil to ensure the lift coefficient of the bounded and unbounded profiles matched. The final manufactured foil shape has a maximum thickness (i.e., t_o/C) of 8.84% and a maximum camber (i.e., f_o/C) of 2.576%.

3) The scheme to measure surface pressures on the foil was analyzed and small cylindrical pressure transducers were selected. The transducers were mounted onto tubing which fits into machined holes in the foil cross section with pressure taps to the foil surface.

---

[3] J.Q. Rice, *MIT: Thesis Investigation of A Two Dimensional Hydrofoil in Steady and Unsteady Flows:* June, 1991.

4) Initial concepts of the system used to generate the sinusoidal gusts and power estimates for the drive system were developed. Figure 1.1 shows the experimental concept.

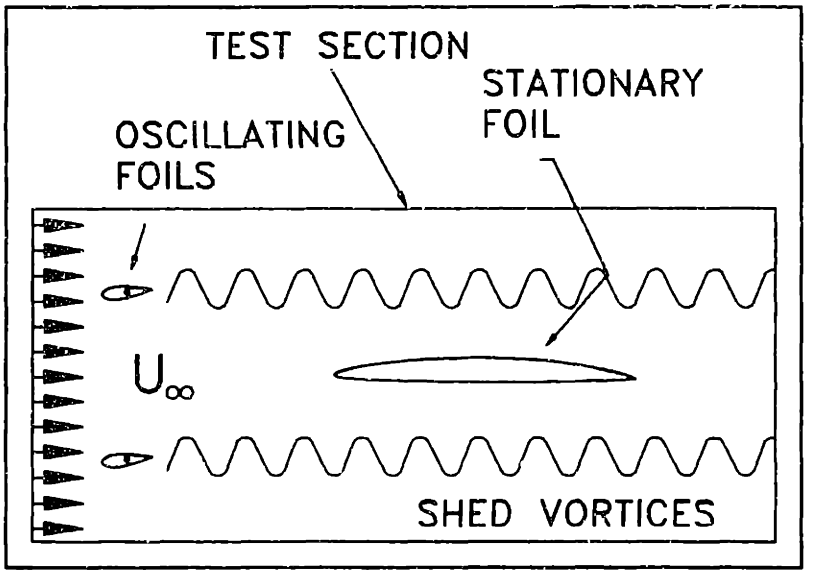

Figure 1.1 Experimental Concept

5) Steady state pressure and velocity measurements were taken on the two-dimensional, stationary hydrofoil. Reynolds number was 4×10^6 based on an 18 inch foil length.

1.2 Objectives

The objectives of the current research are :

1) to perform the detailed design and procurement of the oscillating foils (i.e.,flappers) used to create the sinusoidal gust,

2) to perform the detailed design and procurement of the mechanical system used to drive the oscillating foils,

3) to develop the data acquisition software for the unsteady experiment,

4) to install and shakedown the flapping foil system and obtain unsteady flow data to show the experimental concept works,

5) to complete the mapping of steady state flow data for the two-dimensional, stationary hydrofoil. Comparisons of the flow data obtained in the first and second parts of the research program will be made to validate consistency between different tests.

Chapter 2

Theory

2.1 Introduction

Before any design work can begin, the basic mathematical equations that describe the physical phenomena governing the flapping foil system must be developed. The goal of the drive system is to rotate two foils to create a sinusoidal gust over a stationary foil. The forces and moments (i.e., torque) on the oscillating foils are the result of inertial and hydrodynamic effects. These are separate and independent physical phenomena and their effects can be evaluated separately and linearly added to obtain the total effect on the foils.

In this chapter, the basic mathematical equations needed to calculate the forces and moments on the oscillating foils will be developed. Specifically, the following relationships will be developed:

1) equations of motion to describe the angle of attack, angular velocity, and angular acceleration of the oscillating foils,

2) equations to calculate the torque necessary to overcome the inertia of the foil mass,

3) equations to calculate the lift and torque on the oscillating foils due to hydrodynamic effects,

4) equations to calculate the power necessary to drive the oscillating foils.

2.2 Equations of Motion

The goal of the drive system used to rotate the oscillating foils is to create a sinusoidal gust. The angle of attack of the oscillating foils is assumed to vary sinusoidally with time and can be represented by the following equations:

$$\alpha(t) = \alpha_{max} \sin(\omega t + \phi) \tag{2.1}$$

or in complex form,[4]

$$\alpha(t) = -\alpha_{max}\, i\, \exp^{i(\omega t + \phi)} \tag{2.2}$$

The angular velocity of the oscillating foils is the derivative of the angular position and can be represented by the following equations:

$$\dot{\alpha}(t) = \frac{\partial \alpha(t)}{\partial t} \tag{2.3}$$

$$\dot{\alpha}(t) = \alpha_{max}\omega \cos(\omega t + \phi) \tag{2.4}$$

or in complex form,

$$\dot{\alpha}(t) = \alpha_{max}\, \omega\, \exp^{i(\omega t + \phi)} \tag{2.5}$$

The angular acceleration of the foils is the second derivative of the angular position and can be mathematically represented by the following equations:

---

[4] The real part of the complex number is assumed.

$$\ddot{\alpha}(t) = \frac{\partial^2 \alpha(t)}{\partial t^2} \tag{2.6}$$

$$\ddot{\alpha}(t) = -\alpha_{max}\, \omega^2 \sin(\omega t + \phi) \tag{2.7}$$

or in complex form,

$$\ddot{\alpha}(t) = \alpha_{max} \omega^2\, i\, \exp^{i(\omega t + \phi)} \tag{2.8}$$

Figures 2.1, 2.2, and 2.3 show the variation of angle of attack, angular velocity, and angular acceleration over one cycle of oscillation.

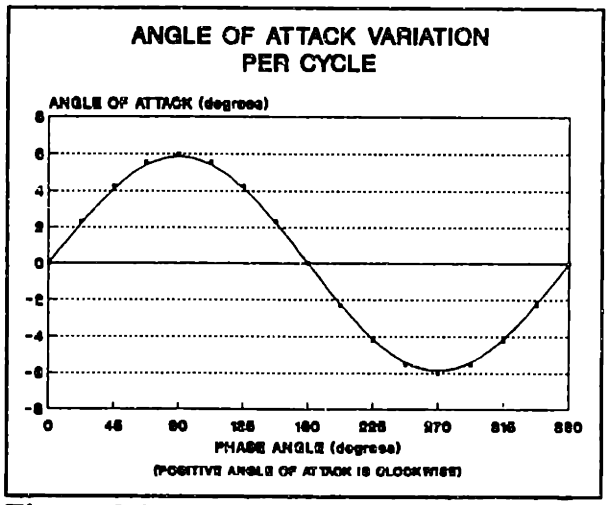

Figure 2.1 Variation of Angle of Attack Per Cycle

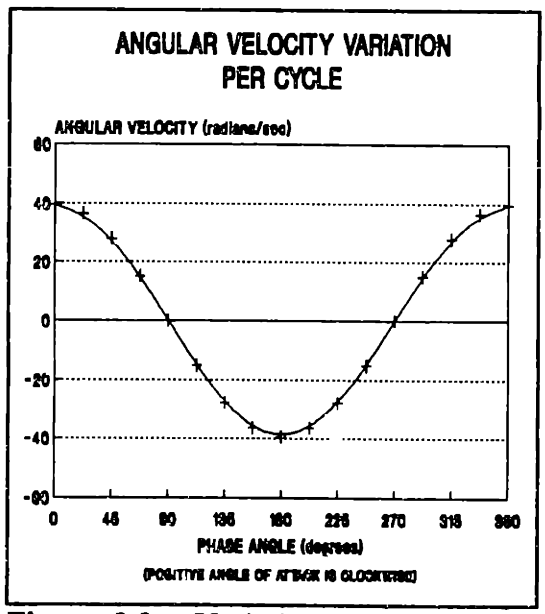

Figure 2.2 Variation of Angular Velocity Per Cycle

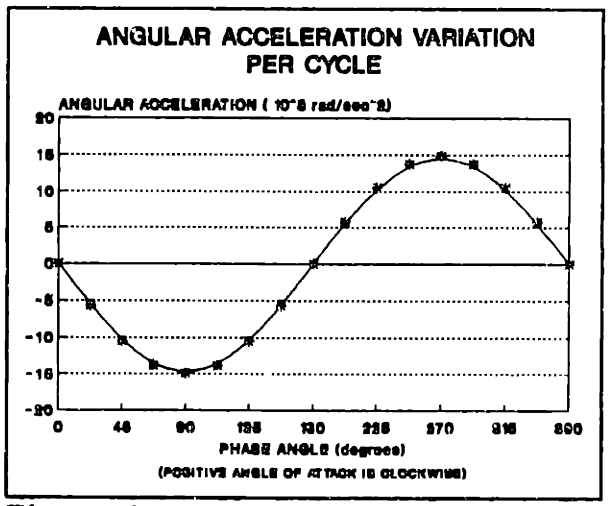

Figure 2.3 Variation of Angular Acceleration Per Cycle

2.3 Inertial Torque

A torque must be applied to the oscillating foil to overcome the inertia of the foil mass and develop the required angular acceleration. The torque can be calculated by the following equation:

$$T = J\,\ddot{\alpha}(t) \tag{2.9}$$

If the foil is modeled as an ellipse, the moment of inertia about the centroid is:[5]

$$J_o = \rho_{foil}\,\frac{s\pi ct}{64}\,(c^2 + t^2) \tag{2.10}$$

Taking into account the pivot point may not be at the centroid of the section, the parallel axis theorem can be applied to obtain the polar moment of inertia about the pivot point:

$$J = \rho_{foil}\,\frac{s\pi ct}{4}\left(\frac{c^2 + t^2}{16} + d^2\right) \tag{2.11}$$

Equations 2.7, 2.8, and 2.11 can be combined to obtain the final equation for the torque that must be applied to overcome the foil inertia:

$$T = -\rho_{foil}\,\frac{s\pi ct}{4}\left[\frac{c^2 + t^2}{16} + d^2\right]\alpha_{max}\,\omega^2\sin(\omega t + \phi) \tag{2.12}$$

or in complex form,

$$T = \rho_{foil}\,\frac{s\pi ct}{4}\left[\frac{c^2 + t^2}{16} + d^2\right]\alpha_{max}\omega^2\, i\, \exp^{i(\omega t + \phi)} \tag{2.13}$$

---

[5] Ferdinand P. Beer and E. Russell Johnston, Jr., *Vector Mechanics For Engineers:Statics*, second edition (New York: McGraw-Hill Book Company, 1972), p. 344-345.

2.4 Hydrodynamic Lift and Torque

The problem of determining the hydrodynamic lift and torque on a foil subject to heaving and oscillating motion has been previously solved.[6,7] The lift and moment are:

$$L = \rho_{water} s \pi \frac{c^2}{4}[\ddot{h} + U_\infty \dot{\alpha} - d\ddot{\alpha}] + 2\rho_{water} \pi U_\infty \frac{c}{2} C(k)[\dot{h} + U_\infty \alpha + \frac{c}{2}(\frac{1}{2} - \frac{d}{\frac{c}{2}})\dot{\alpha}] \tag{2.14}$$

$$M_y = \rho_{water} \pi s \frac{c^2}{4}[d\ddot{h} - U_\infty \frac{c}{2}(\frac{1}{2} - \frac{d}{\frac{c}{2}})\dot{\alpha} - \frac{c^2}{4}(\frac{1}{8} + \frac{d^2}{\frac{c^2}{4}})\ddot{\alpha}] + \rho_{water} 2\pi s U_\infty \frac{c^2}{4}(\frac{d}{\frac{c}{2}} + \frac{1}{2})C(k)[\dot{h} + U_\infty \alpha + \frac{c}{2}(\frac{1}{2} - \frac{d}{\frac{c}{2}})\dot{\alpha}] \tag{2.15}$$

Simplifying equations 2.14 and 2.15 by setting the heave terms to zero and defining the nondimensional separation distance as[8]

$$a = \frac{d}{\frac{c}{2}} \tag{2.16}$$

yields the following result:

---

[6] Raymond L. Bisplinghoff, Holt Ashley, and Robert L. Halfman, *Aeroelasticity*, (Cambridge, Mass.: Addison-Wesley Publishing Company, 1955), p. 251-273.

[7] Earl H. Powell, Howard C. Curtiss Jr., Robert H. Scanlan, and Fernando Sisto, *A Modern Course in Aeroelasticity*,(Dordrecht, The Netherlands: Kluwer Academic Publishers, 1989), p. 218-222.

[8] "a" is positive moving toward the trailing edge.

$$L = \rho_{water} s \pi \frac{c^2}{4} [U_\infty \dot{\alpha} - d\ddot{\alpha}] + 2\rho_{water} \pi U_\infty \frac{c}{2} C(k) [U_\infty \alpha + \frac{c}{2}(\frac{1}{2} - a)\dot{\alpha}] \quad (2.17)$$

$$M_y = \rho_{water} \pi s \frac{c^2}{4} [U_\infty \frac{c}{2}(\frac{1}{2} - a)\dot{\alpha} - \frac{c^2}{4}(\frac{1}{8} + a^2)\ddot{\alpha}] + \rho_{water} 2\pi s U_\infty \frac{c^2}{4}(a + \frac{1}{2}) C(k) [U_\infty \alpha + \frac{c}{2}(\frac{1}{2} - a)\dot{\alpha}] \quad (2.18)$$

The combination of equations 2.17 and 2.18 with the equations for the angular position, velocity, and acceleration is left to the reader. Figure 2.4 shows the variation of the inertial, hydrodynamic and total torque per cycle. Figure 2.5 shows the variation in lift per cycle of oscillation.

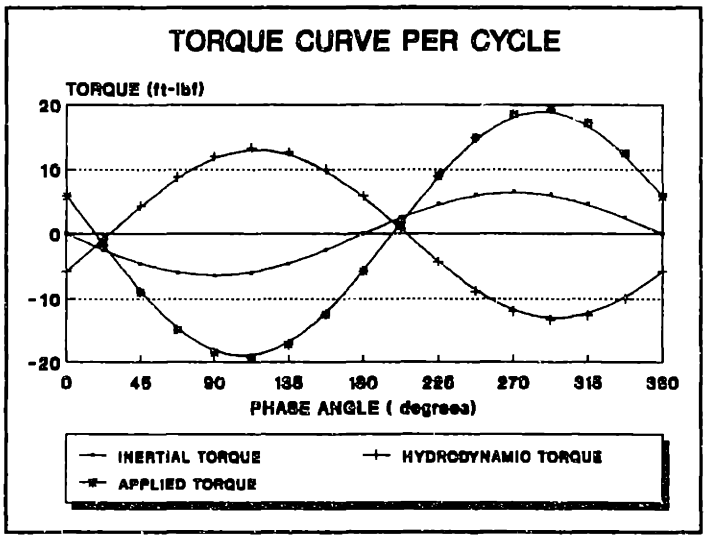

Figure 2.4 Torque Variation Per Cycle

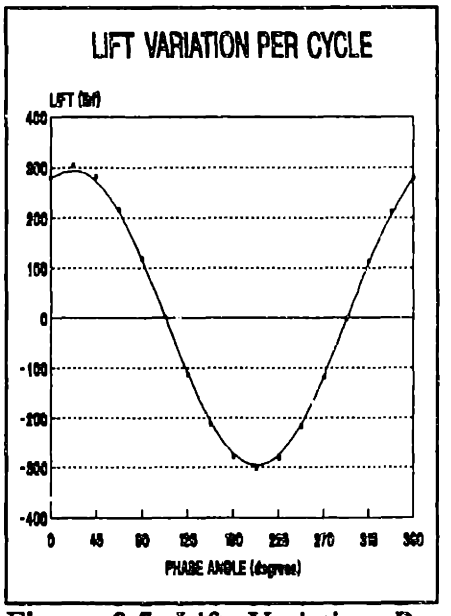

Figure 2.5 Lift Variation Per Cycle

2.5 Power

Calculation of power required to move the oscillating foils is necessary to size the drive motor. The goal of the power calculations is to develop an algorithm that can be used on a computer to calculate the average power. Average power, not peak power, is the determining factor for motor sizing. A flywheel will be used to absorb or supply energy variations from the average.

Power can be most readily calculated by starting with the work done in moving the foils a given distance, changing the movement to incremental distances, taking derivatives and integrals, and converting integrals to sums. Work is simply force times distance, or for the rotational case, torque times angle.

$$W = T\alpha \tag{2.19}$$

Using the incremental form and taking time derivatives yields,

$$\partial W = T\partial\alpha \tag{2.20}$$

$$\frac{\partial W}{\partial t} = T\frac{\partial\alpha}{\partial t} \tag{2.21}$$

Instantaneous power is the time rate of change of work. Therefore,

$$P = \frac{\partial W}{\partial t} \tag{2.22}$$

and

$$P = T\dot{\alpha} \tag{2.23}$$

The remainder of this section will develop the formulas to calculate average power. The average power is defined as the average of the instantaneous power over a complete cycle. In integral form, this statement translates to

$$P_a = \frac{1}{t}\int_0^t T\,\dot{\alpha}\,\partial t \tag{2.24}$$

where t in the time for one cycle. Converting equation 2.24 to a form useful for a computer yields:

$$P_a = \frac{1}{t}\sum^{cycle} T\,\Delta\alpha \tag{2.25}$$

Chapter 3

Design Requirements

3.1 Introduction

A logical first step in the design development is to generate a set of requirements the design must meet. In the broadest sense, the unsteady test apparatus must produce a gust that creates a measurable response over the stationary foil at a reduced frequency of approximately 10 and a Reynolds number of 4×10^6. The next step in the design process is to translate this broad guidance into detailed design and performance requirements.

3.2 Design Requirements

The unsteady test apparatus must be designed to meet the following requirements:

1) create a gust that is measurable over the stationary foil,

2) create a gust with a reduced frequency of approximately 10,

3) produce a two dimensional flow,

4) operate safely at rated conditions,

5) be easily installed and removed with no permanent modifications to the water tunnel that would hinder the performance of another experiment,

6) manufactured at a reasonable cost (i.e., $10,000).

3.3 Design Approach

Having established the detailed system design requirements, the next step in the design process is to establish a logical plan to progress through the design. The most frequently used plan in the marine engineering community is the design spiral first introduced in 1959.[9] The spiral starts with the requirements and develops from the requirements through preliminary design to the detailed design. With each iteration through the spiral, the design becomes further and further refined. The design spiral for this project is shown in Figure 3.1.

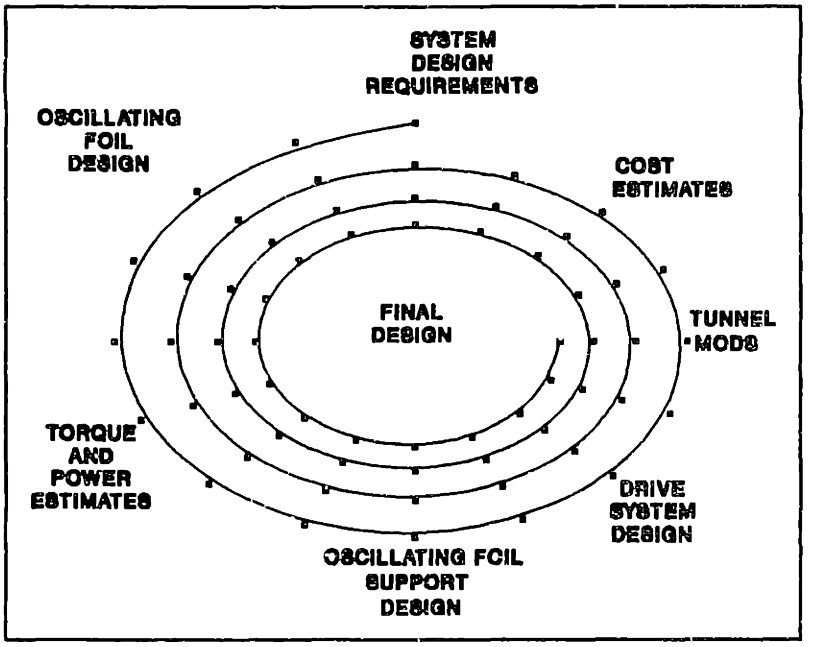

Figure 3.1 Design Spiral

Three revolutions through the design spiral were required to finalize the design. The major changes that occurred as the design evolved were:

1) change of oscillating foil material selection from stainless steel to aluminum due to cost,

2) change of oscillating foil support system to allow for high stresses in the foil,

---

[9] J.H. Evans., *Basic Design Concepts*, ASNE Journal, Nov. 1959.

3) change of drive system linkage design since original linkage was not compatible with drive system requirements,

4) simplification of part design to facilitate manufacturing and reduce cost.

3.4 Preliminary Design

The preliminary design of the drive system was performed by Mr. Dean Lewis[10] and is shown in figure 3.2. This concept established a good starting point for the detailed design to follow.

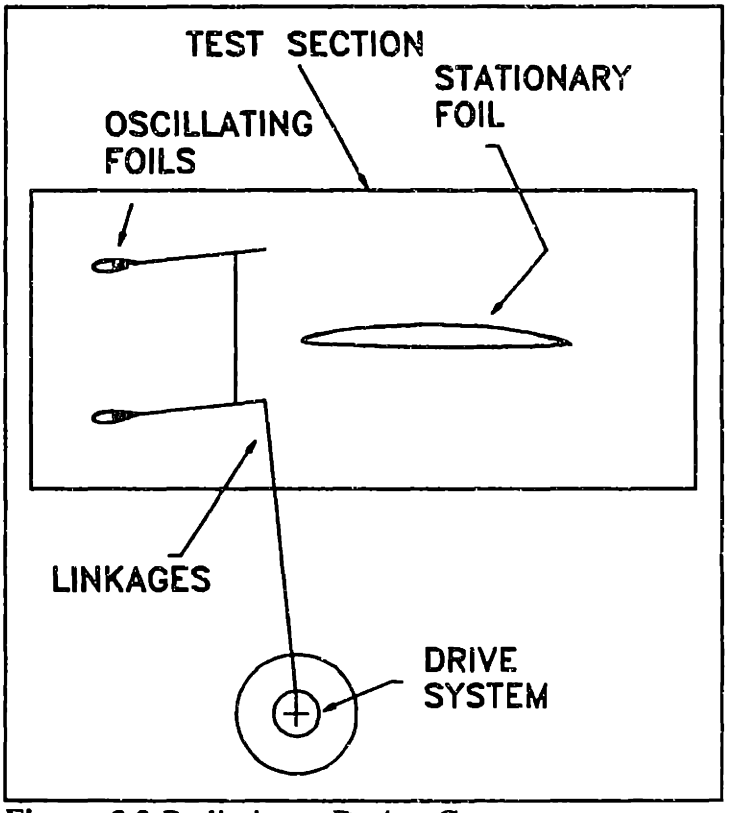

Figure 3.2 Preliminary Design Concept

3.5 Detailed Design

The overall system design consisted of four basic parts:

1) modifications to the water tunnel to support and power the drive system,

2) design of the oscillating foils and support structure,

3) design of the support structure for the oscillating foils,

4) design of the drive system.

[10] Mr. Lewis was previously a laboratory engineer in the Marine Hydrodynamics Laboratory.

Modifications to the water tunnel involved adding two electrical outlets to power and control the variable speed DC motor used in the drive system, and drilling holes in the plexiglass windows to support installation of the oscillating foils. These modifications proved to be fairly straightforward.

The only complication was the additional window modifications required for the upcoming vorticity optical probe experiment. These modifications involved machining a recess in the laser side, plexiglass window to recess the holding nuts for the stationary foil below the window surface. This provided a smooth surface for the lenses used in the vorticity optical probe experiment.

The remaining elements of the design are discussed in the next two chapters.

Chapter 4

Oscillating Foil Design

4.1 Background

In the first part of the research program, an analysis was conducted to determine the general characteristics of the oscillating foils (i.e., flappers). The analysis determined two oscillating foils with a chord length of 3 inches, positioned equidistant between the tunnel centerline and walls, would result in a pressure distribution on the instrumented, main foil that should be readily measurable.[11] These characteristics provided the starting point for the oscillating foil design.

4.2 Design Requirements

The first step in designing the oscillating foils (i.e., flappers) was to develop a set of design requirements. The flappers had to meet the following requirements:

1) Chord length of at least three inches to create the required vorticity.

2) Minimum twist at maximum applied torque to keep the experiment two dimensional. Any twist would cause a streamwise shift in the shed vortex. The design goal was to keep the streamwise shift in the shed vortex to 1/8 inch over the 20 inch tunnel width.

3) Minimum midspan deflection to keep the experiment two dimensional.

---

[11] Rice, p. 36.

4) No expected stall up to an angle of attack of 10° .

5) Mechanical properties great enough to withstand the expected stresses using a factor of safety of 2. Fatigue properties sufficient to allow for a 500 hour life (i.e., 1×10^8 cycles).

6) Power to drive the flappers less than 1.5 horsepower to support use of an existing variable speed DC motor.

7) Reasonable cost.

The above criteria do not take into account the interface between the flappers and the associated systems used to support, seal, and drive the flappers. When these interfaces are considered, the following additional design criteria are required:

1) wide enough to be compatible with the associated systems that interface with the flapper,

2) geometry outside the foil section compatible with the associated systems that interface with the flappers.

4.3 Design Optimization

Having defined the detailed design requirements, the next step was to develop some optimization criterion. Hydrodynamically, the chord length and angle of attack needed to be as large as possible to increase the magnitude of the shed vortex. Mechanically, the chord length and maximum angle of attack needed to be small to keep the stresses and deflections within the design requirements. Additionally, the power to drive the

flappers had to be below 1.5 hp to allow use of an existing motor.

The optimization was to make the chord length and angle of attack as large as possible without exceeding the design requirements. In this regard, it was important to decide what parameters were important to focus on. The selected parameters were maximum lift and torque for structural integrity and average power for motor sizing. Selecting maximum lift and torque will help ensure structural integrity. Selecting average, not peak power, is appropriate since a flywheel will be used to supply or store the power variations from the average.

4.4 Calculation of Foil Stresses and Deflections

The stresses on the foils are caused by two separate and independent mechanisms. The torque on the foil causes a shear stress and twist. The lift on the foil causes a shear stress at the bearing supports. This shear stress causes a bending moment, normal stress, and vertical deflection throughout the foil length.

4.4.1 Calculation of Foil Stresses

The shear stress in the foil caused by the torque is:[12]

$$\tau_{torque} = \frac{16\,T}{\pi\, c\, t_0^2} \tag{4.1}$$

[12] Raymond J. Roark and Warren C. Young, *Formulas for Stress and Strain*, fifth ed. (New York: McGraw-Hill Inc, 1975), p. 290

The shear stress in the cylindrical ends of the foil caused by the torque is:[13]

$$\tau_{torque} = \frac{2T}{\pi r^3} \tag{4.2}$$

The shear stress and normal stress caused by the lift will be determined by classical equilibrium methods and the use of shear force and bending moment diagrams. Figure 4.1 shows the geometry of the foil. Lift is the only vertical force acting on the system and is assumed to be evenly distributed over the foil span. The weight of the foils is negligible compared to the lift. Two bearings are used to support the foils.

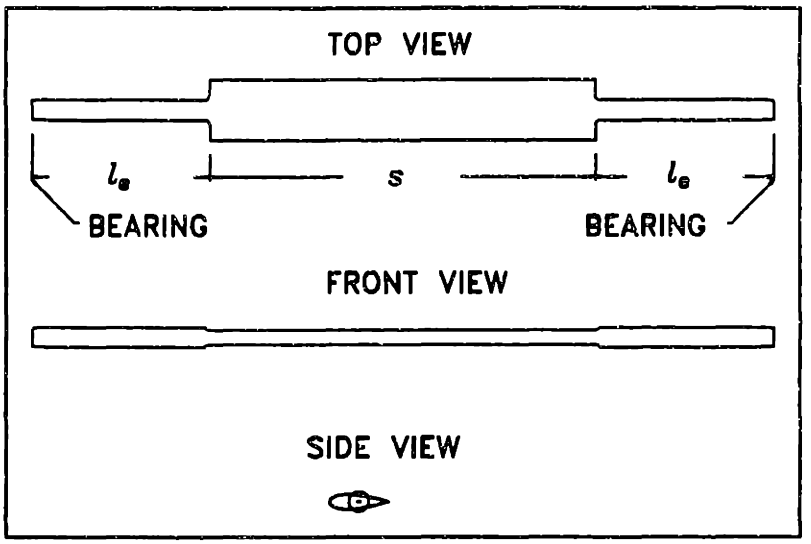

Figure 4.1 Foil Geometry

The shear force is defined as:[14]

$$\frac{\partial V}{\partial x} = -w \tag{4.3}$$

Integrating the load curve for this problem yields:

---

[13] Roark, p. 290.

[14] Irving H. Shames, *Introduction to Solid Mechanics*, second ed. (Englewood Cliffs, NJ: Prentice Hall, 1989) p. 258.

$$
\begin{aligned}
V &= -\frac{L}{2} && 0 \le x \le l_e \\
V &= -\frac{L}{2} + \frac{L}{s}(x - l_e) && l_e \le x \le s + l_e \\
V &= \frac{L}{2} && l_e + s \le x \le 2l_e + s
\end{aligned}
\tag{4.4}
$$

To obtain the bending moment, the type of end support needs to be defined. The mounted bearings are treated as simple supports since the shaft is not constrained to have a zero slope through the bearing. The bending moment is defined as:[15]

$$
\frac{\partial M_z}{\partial x} = -V \tag{4.5}
$$

Integration of the shear force yields the bending moment provided appropriate boundary conditions are specified. Boundary conditions for a simple support are zero bending moment at the support. Using these boundary conditions, the bending moment equations for this problem are:

$$
\begin{aligned}
M_z &= \frac{L}{2}x && 0 \le x \le l_e \\
M_z &= \frac{L}{2}x - \frac{L}{s}\frac{(x - l_e)^2}{2} && l_e \le x \le s + l_e \\
M_z &= -\frac{L}{2}(x - x_e - s) && l_e + s \le x \le 2l_e + s
\end{aligned}
\tag{4.6}
$$

Figure 4.2 shows the load, shear force, and bending moment diagrams for the foil along with the respective maximums. Having determined the shear force and bending moments, the next step is to translate these quantities into stress. The stresses are:

[15] Shames, p. 258.

$$\tau_{lift} = \frac{V}{\pi r^2} \qquad \text{in ends (4.7)}$$

$$\tau_{lift} = \frac{4V}{\pi c t_0} \qquad \text{in foil section (4.8)}$$

$$\sigma_{max} = \frac{M_z}{Z} \qquad (4.9)$$

$$\sigma_{max} = \frac{4M_z}{\pi r^3} \qquad \text{in ends (4.10)}$$

$$\sigma_{max} = \frac{32M_z}{\pi c t_0^2} \qquad \text{in foil section (4.11)}$$

4.4.2 Estimation of Stress Concentrations

As shown in figure 4.1, the foil cross section is not continuous from end-to-end. The foil has cylindrical ends and a typical foil shape in the center. In the transition from one cross section to

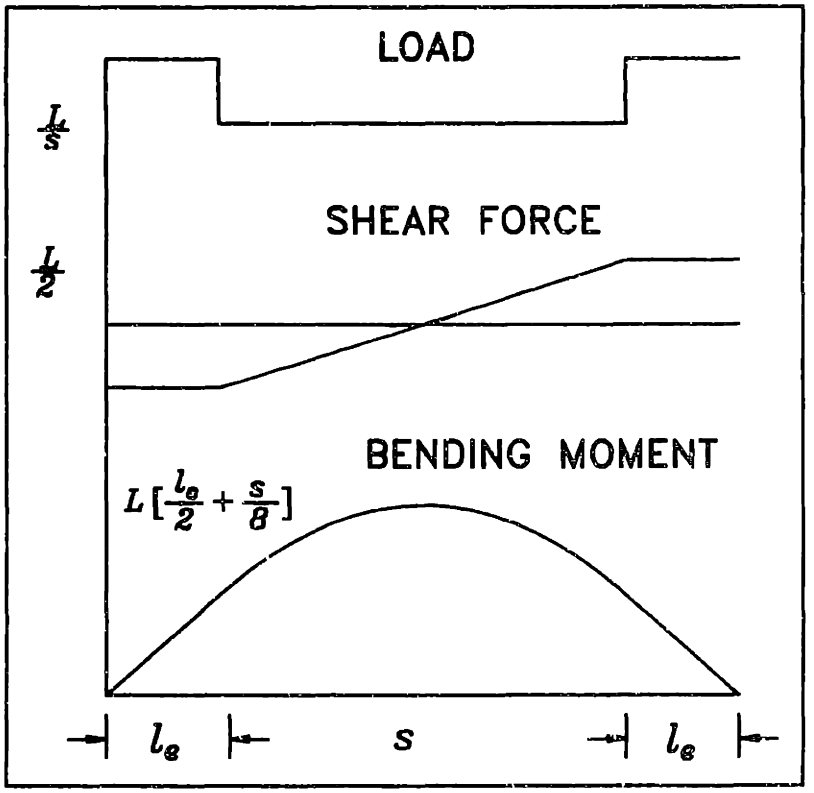

Figure 4.2 Load, Shear Force and Bending Moment Diagrams

the other, some stress concentrations will occur. The stress concentration factors were estimated modeling the geometry as a square shoulder with a fillet joining a circular shaft. For this geometry, the stress concentration factors are:[16]

$$\begin{aligned} k_b &= 1.4 \\ k_T &= 1.2 \end{aligned} \tag{4.12}$$

4.4.3 Estimation of Stress Magnitudes

The critical areas to evaluate the stresses are at the transition from the circular to foil cross sections and at the midspan of the foil. These are the locations where the maximum stresses would be expected.

At the transition from one cross section to the other, the maximum stresses would be in the circular cross section since the cross sectional area is smaller compared to the center elliptical section. The stresses would be:

$$\tau_{lift} = \frac{L}{2\pi r^2} \tag{4.13}$$

$$\tau_{torque} = k_T \frac{2T}{\pi r^3} \tag{4.14}$$

$$\sigma = k_b \frac{4}{\pi r^3} \frac{L}{2} l_e \tag{4.15}$$

[16] Roark, p. 600.

Table 4.1: Final Design Values			
r	0.5 inches	L	304 lbs
s	19.8 inches	T	20 ft-lbs
l_e	5.5 inches	material	aluminum
c	3.0 inches	E	10×10^6 psi
t_0	0.75 inches	G	3.8×10^6 psi

Substituting the quantities in table 4.1 yields the following stresses:

$$\tau_{lift} = 194 \text{ psi}$$

$$\tau_{torque} = 1430 \text{ psi}$$

$$\sigma = 11{,}921 \text{ psi}$$

At midspan, the stresses would be:

$$\tau_{lift} = 0$$

$$\tau_{torque} = \frac{16\,T}{\pi\, c\, t_0^2} \qquad (4.16)$$

$$\sigma = \frac{32}{\pi\, c\, t_0^2}\left(\frac{L}{2}\left(l_e + \frac{s}{4}\right)\right)$$

Substituting the values in Table 4.1 yields:

$$\tau_{lift} = 0 \text{ psi}$$

$$\tau_{torque} = 706 \text{ psi}$$

$$\sigma = 9{,}587 \text{ psi}$$

One interesting observation from the data presented above is the magnitude of the normal stress. The normal stress is eight times larger than the torsional shear stress. The high normal stress is the result of the bearing support being 5.5 inches from the transition from the foil cross section to the circular cross section. This large distance represented a compromise to provide a simple bearing support system and easy foil

installation.

4.4.4 Establishment of Failure Criterion

The failure criterion was established very conservatively as no yielding on any part of the foil. To evaluate this, the Tresca maximum shear stress theory was used.[17] This criterion states that yielding will not occur if the maximum shear stress is kept below half the yield strength. Mathematically,

$$\frac{1}{2}(\tau_{max} - \tau_{min}) \leq \frac{\sigma_y}{2} \tag{4.17}$$

Applying a safety factor of 2 yields:

$$\frac{1}{2}(\tau_{max} - \tau_{min}) \leq \frac{\sigma_y}{4} \tag{4.18}$$

For the data presented in section 4.4.3, the results are:

$$\frac{1}{2}(\tau_{max} - \tau_{min}) = 6129\,psi$$

$$\frac{\sigma_y}{4} = 8750\,psi$$

$$\therefore \textit{no yielding}$$

4.4.5 Calculation of Deflections

The foil encounters two types of deflections: twisting due to the applied torque, and bending due to the lift. The amount of twist the foil experiences in the test section is:[18]

---

[17] Shames, p. 225-226.

[18] Roark, p. 290.

$$\theta = \frac{Ts}{KG} \tag{4.19}$$

Where,

$$K = \frac{\pi c^3 t_0^3}{16(c^2 + t_0^2)} \tag{4.20}$$

Substitution yields,

$$\theta = \frac{T}{G}\left(\frac{16(c^2 + t_0^2)s}{\pi c^3 t_0^3}\right) \tag{4.21}$$

Substituting the values from table 4.1 yields:

$$\theta = 0.0502 \text{ radians or } 0.30°$$

This translates into a 0.08 inch streamwise shift in the shed vortex over the length of the foil and is less than the design requirement of 0.125 inches.

The amount of deflection due to bending can be found by applying the equation[19]

$$\frac{\partial^2 y}{\partial x^2} = \frac{M_z}{E I_{zz}} \tag{4.22}$$

and integrating twice. However, the problem can be simplified by realizing that the deflection in the test section is of primary interest. The goal is to keep the flow two

[19] Shames, p. 371.

dimensional. The deflection in the test section is:[20]

$$\delta_{max} = \frac{5 \frac{L}{s} s^4}{384 E I_{zz}} \tag{4.23}$$

Substituting values from table 4.1 yields

$$\delta_{max} = 0.049 \text{ inches}$$

4.4.6 Summary of Stress and Deflection Calculations

The results in the previous sections can be summarized as follows:

1) The ability to have no yielding at any point on the foil is primarily governed by the lift on the foil. To increase lift a thicker foil would be required to reduce the stress. Alternatively, a less conservative failure criterion or a material with a higher yield strength could be used.

2) The ability to keep the shed vortex two dimensional is governed by the torque and angle of twist on the foil and the lift and vertical deflection of the foil. The angle of twist and vertical deflection can be reduced by increasing thickness, elastic modulus, or shear modulus since:

$$\theta \propto \frac{1}{G} \frac{1}{t_0^3} \qquad \text{and} \qquad \delta \propto \frac{1}{E r^3}$$

[20] S. Timoshenko and D. H. Young, *Elements of Strength of Materials*, fifth ed. (New York: D. Van Nostrand Company, 1968), p. 213.

4.5 Design Procedure

Having established the relationships among lift, torque, stress, and deflections, the remainder of the oscillating foil design can be broken down into five separate areas. These are:

1) optimization of pivot point location,

2) determination of chord length and maximum angle of attack,

3) determination of maximum thickness,

4) selection of foil material,

5) generation of foil shape.

4.6 Pivot Point Optimization

Equations 2.12 and 2.18 provide the fundamental relationships for evaluating the effect of shifting the pivot point on torque and power. The optimization of pivot point location was performed assuming an aluminum foil. Optimization was based on minimization of torque and power.

Figure 4.3 shows how the total torque and power vary with pivot point location. The minimum torque occurs when the pivot point is 4% forward of the centroid. The minimum power occurs when the pivot point is 50% aft of the midpoint or centroid. A pivot point at the centroid was selected as a good compromise. Shifting the pivot point further aft to reduce power would have been impractical. The increased torque would have increased the stresses and angle of twist.

One interesting observation from figure 4.3 is the average power goes to zero as the pivot point is moved toward the trailing edge. The underlying cause for this result is the movement of the pivot point causes a phase shift in the hydrodynamic torque. When the pivot point is 50% aft of midchord, the hydrodynamic torque is 90° out of phase with the angular velocity. Consequently, average power is zero. The inertial torque causes no average power since the inertial torque is always 90° out of phase with angular velocity.

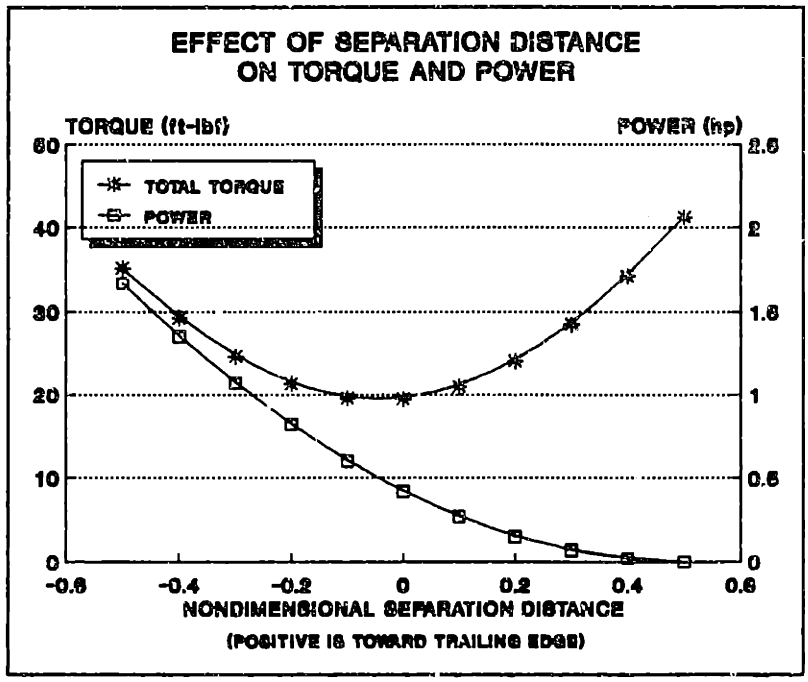

Figure 4.3 Pivot Point Optimization for An Aluminum Foil

4.7 Chord Length and Angle of Attack Optimization

Equations 2.12, 2.17. and 2.18 provide the fundamental relationships for evaluating the effect of chord length and angle of attack on torque, power, and lift.

Figures 4.4 and 4.5 show how the torque, power, and lift vary with chord length. Torque varies as L^3 and lift and power vary as L^2. Consequently, a small increase in length requires large increases in thickness to withstand the additional stresses and stiffen the foil to minimize twisting. Alternatively, a material with a higher yield strength, elastic modulus, and shear modulus could be used to accomplish the same goal. Because of the large effect of foil length on torque, power, and lift, foil length was kept to the design requirement of 3 inches.

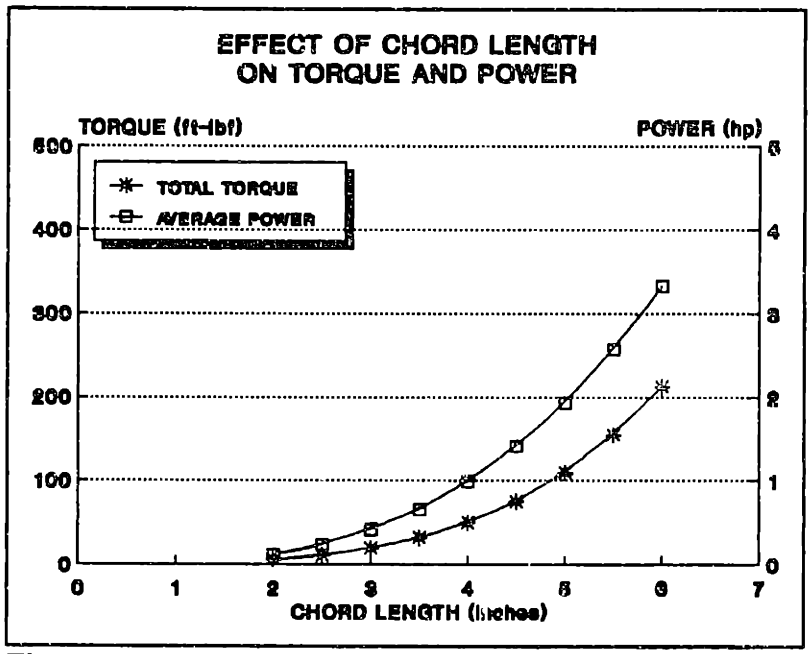

Figure 4.4 Variation of Torque and Power With Chord Length

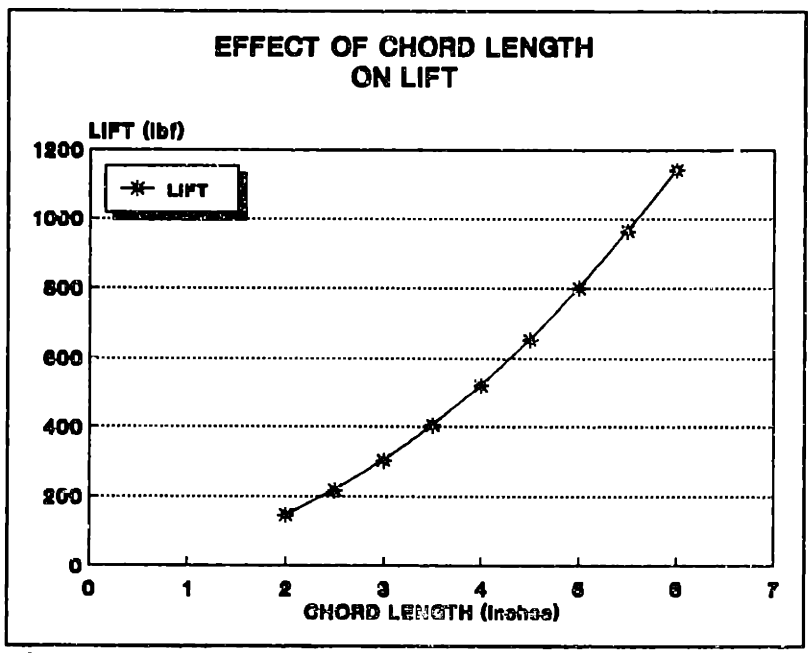

Figure 4.5 Effect of Chord Length on Lift

Figures 4.6 and 4.7 show how the torque, power, and lift vary with angle of attack. Review of equations 2.13, 2.17, 2.18, and 2.23 and these figures show the following:

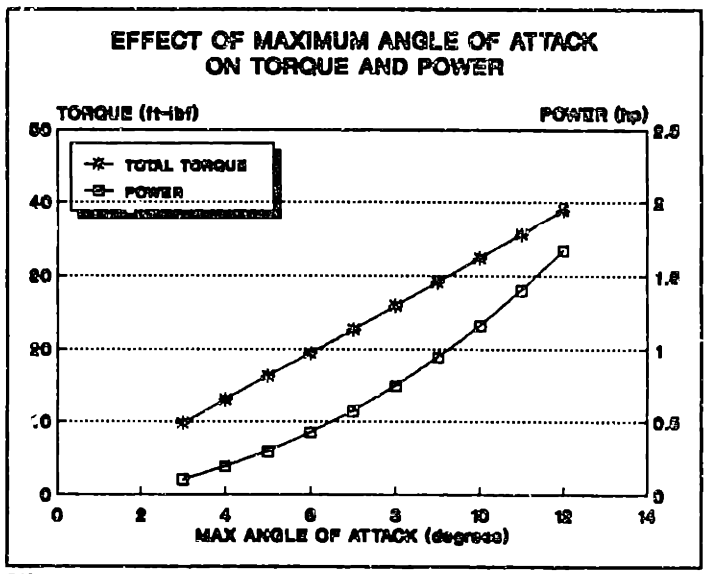

Figure 4.6 Effect of Angle of Attack on Torque and Power

$T \propto \alpha_{max}$

$P \propto \alpha_{max}^2$

$L \propto \alpha_{max}$

This data shows that increasing the angle of attack may prove to be an effective method of increasing the vorticity. A 20% increase in the angle of attack will increase the stresses and angle of twist by only 20%. The current design has sufficient margin to absorb these increases. The only practical limit on angle of attack is the foil should not stall.

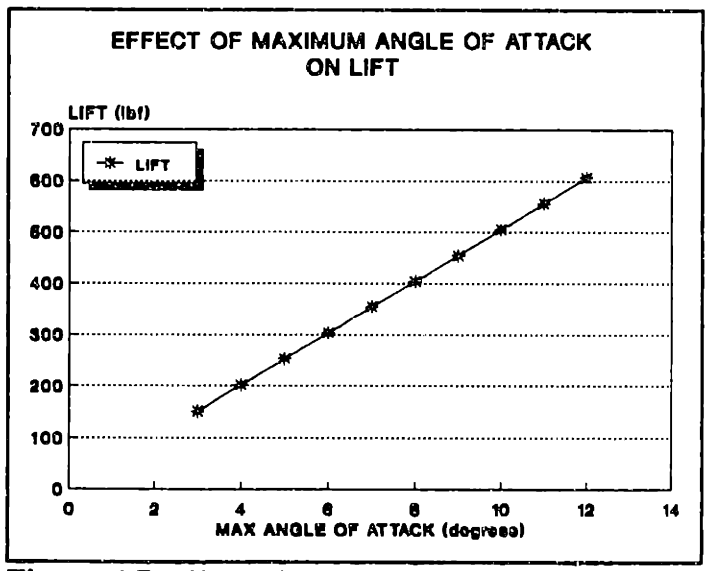

Figure 4.7 Effect of Angle of Attack on Lift

The design allows the angle of attack to be adjusted to 3°, 6°, or 8° with 6° being the operating point. An 8° angle of attack can be easily accommodated. The only change

required would be to repeat the dynamic balancing of the drive shaft assembly. An angle of attack above 8° can be easily achieved by manufacturing a new eccentric plate and drilling the required offset hole for mounting the drive link.

4.8 Selection of Foil Thickness

Foil thickness was picked to reduce the stresses and angle of twist. Section 4.4 showed the total stress was driven by the bending stress. Bending stress is proportional to $1/t_0^3$ or $1/r^3$. In order to keep the stresses in the foil and end sections within the design limits, a two tiered thickness was used. Figure 4.1 shows the foil profile. The cylindrical ends were 1 inch diameter and the foil section was 3/4 inch thick. This lowered the stresses in each section below the design limits.

4.9 Selection of Foil Material

The initial foil material started out as 300 series stainless steel. Stainless steel offered two advantages over aluminum.

The first advantage is the material is stiffer. Young's modulus and shear modulus for stainless steel is approximately three times greater than for aluminum. Since,

$$\theta \propto \frac{T}{G}$$

and

$$\delta \propto \frac{1}{E}$$

the deflections for a stainless steel foil would be 1/3 the deflections of an aluminum foil.

One factor that would slightly offset the angle of twist difference is the stainless steel would weigh three times the weight of the aluminum foil. The increased weight would require higher inertial torques, but not higher hydrodynamic torques. The net torque increase would be about 50%. Consequently, the angle of twist for stainless steel foil would be 1/2 not 1/3 the twist of an aluminum foil.

The second advantage of stainless steel is corrosion protection. However, aluminum foils have been successfully used in the water tunnel provided they are hard coat anodized.

The major disadvantage of stainless steel is cost. The raw material costs for a stainless steel foil are over 5 times the costs for an aluminum foil. When the increased difficulty of machining stainless steel vice aluminum is considered, the final cost of a stainless steel foil is 2-3 times the cost of an aluminum foil. Consequently, aluminum was selected as the foil material. The calculated deflections and angle of twist were low enough that the resulting flow field could still be considered two dimensional with an aluminum foil.

The type of aluminum chosen was alloy 6061, temper T6. This alloy and temper were selected because of the improved fatigue properties compared to the higher strength aluminum alloys.[21]

4.10 Development of Foil Shape

The primary task in the development of the foil shape was to find a shape that did not stall at the maximum angle of attack. Additionally, a symmetric foil was needed to provide a symmetric gust. A NACA 0025 airfoil section was selected. No stall is expected up to an angle of attack of 18°.[22] The 25% thickness is more than adequate for the expected loads.

Having selected a generic profile for the wing section, the section had to be defined in sufficient detail for machining on a numerically controlled milling machine. For this task, an existing fortran program BPROP was used to generate 180 points around the foil surface.[23] The program generated fourth order B-spline sections given leading edge radius, trailing edge thickness, maximum thickness and chord length. B-spline vertices were continually modified until the profile generated by BPROP matched the

---

[21] Batelle Materials Ceramics and Information Center, *Structural Alloys Handbook*, 1990 ed. p.105.

[22] *Comprehensive Reference Guide to Airfoil Sections for Light Aircraft*, (Washington D.C.: Aviation Publications, 1982).

[23] Justin E. Kerwin, *Fortran Program BPROP*, December 3,1988.

NACA 0025 profile. The final vertices and profile coordinates are listed in appendix I. The NACA 0025 and final BPROP profiles are compared in figure 4.8 and are almost identical. This final shape was provided to the foil manufacturer for programming the numerically controlled milling machine.

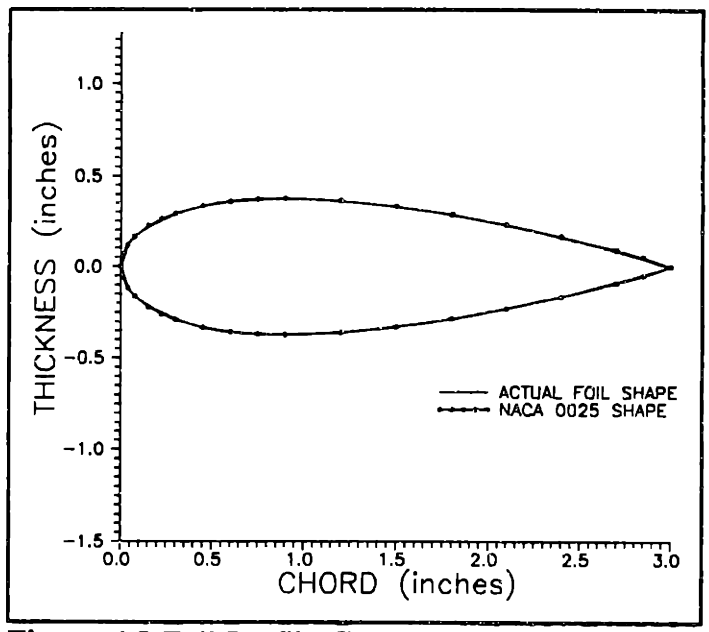

Figure 4.8 Foil Profile Compared To NACA 0025

(This page intentionally left blank.)

Chapter 5

Flapping Foil System Design

5.1 Introduction

Chapter 4 presented the detailed logic for how the design of the flapping foils evolved. The foils are the key element in the flapping foil system. However, the foils are but one part of an integrated system designed to provide a specific function. Each part of the system must perform its given function for the total system to operate satisfactorily.

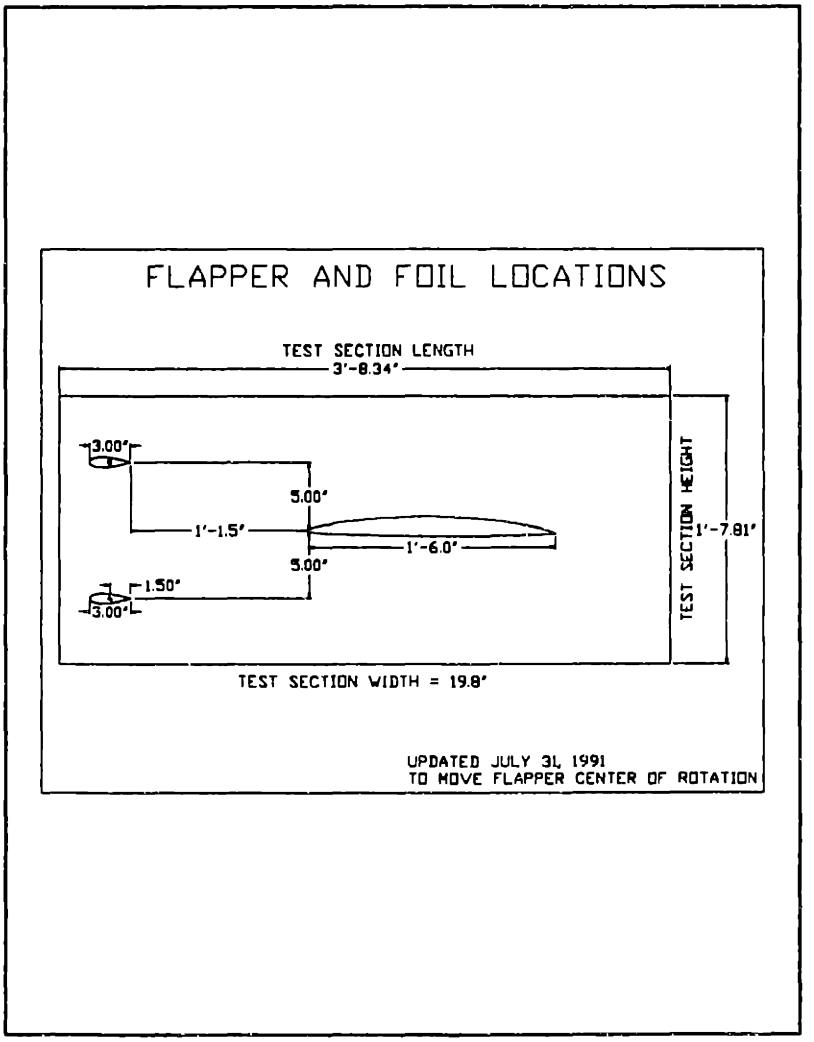

Figure 5.1 Tunnel Layout with Separation Distances

Figure 5.1 shows the location of the flapping foils in relation to the stationary foils. The foils are located as far away from the stationary foil as

allowed by the tunnel geometry. Figure 5.2 shows the overall configuration of the flapping foil system. The detailed design drawings can be found in appendix II. This chapter will discuss the rationale used in the design of the remaining portions of the flapping foil system. The areas that will be discussed are:

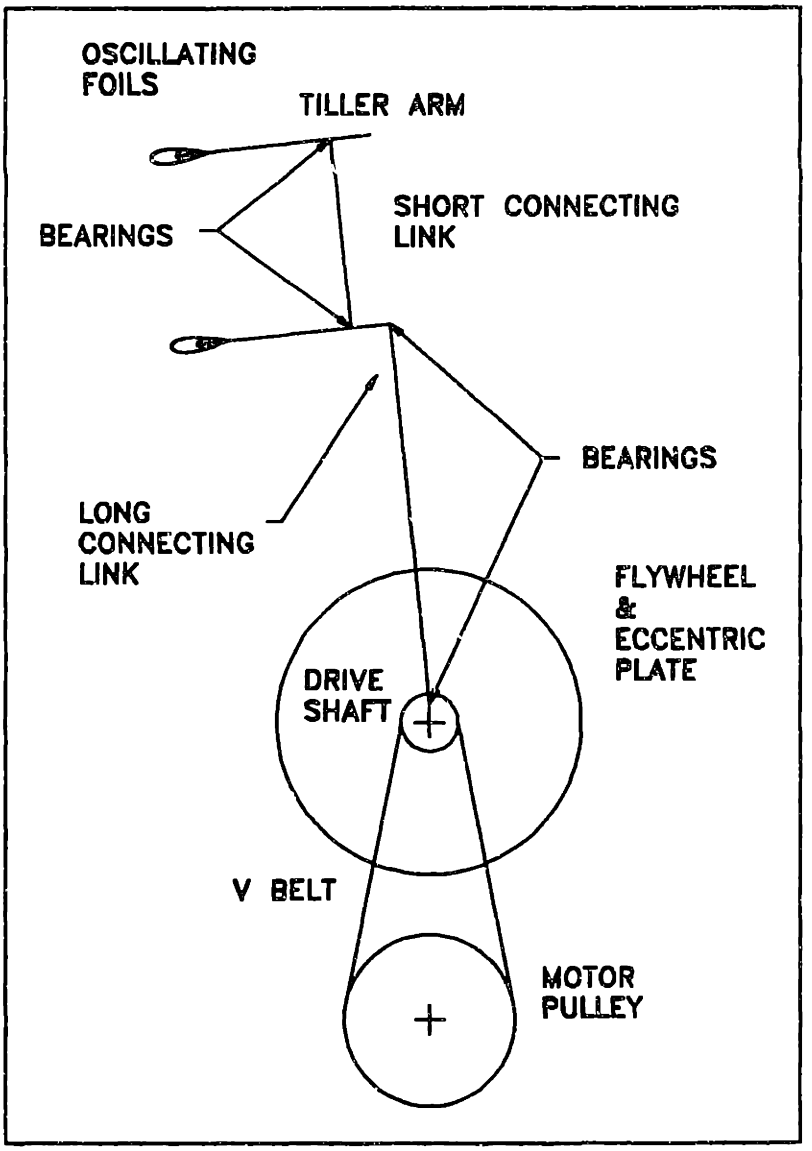

Figure 5.2 Overview of Flapping Foil System

1) shaft sealing,

2) mechanical support and bearing selection,

3) drive system design,

4) linkage design.

5.2 Shaft Sealing

The design of the shaft sealing system is identical to the system used for other shafts that penetrate the water tunnel. The system involves placing two, standard oil seals back-to-back with a water space between the seals. The water space is pressurized to a higher static pressure than can exist in the water tunnel.

This arrangement allows the seals to seal against pressures above and below atmospheric pressure. The outer seals seal against positive gage pressure and the inner-seals seal against a vacuum in the tunnel. The sealing arrangement is shown in figure 5.3.

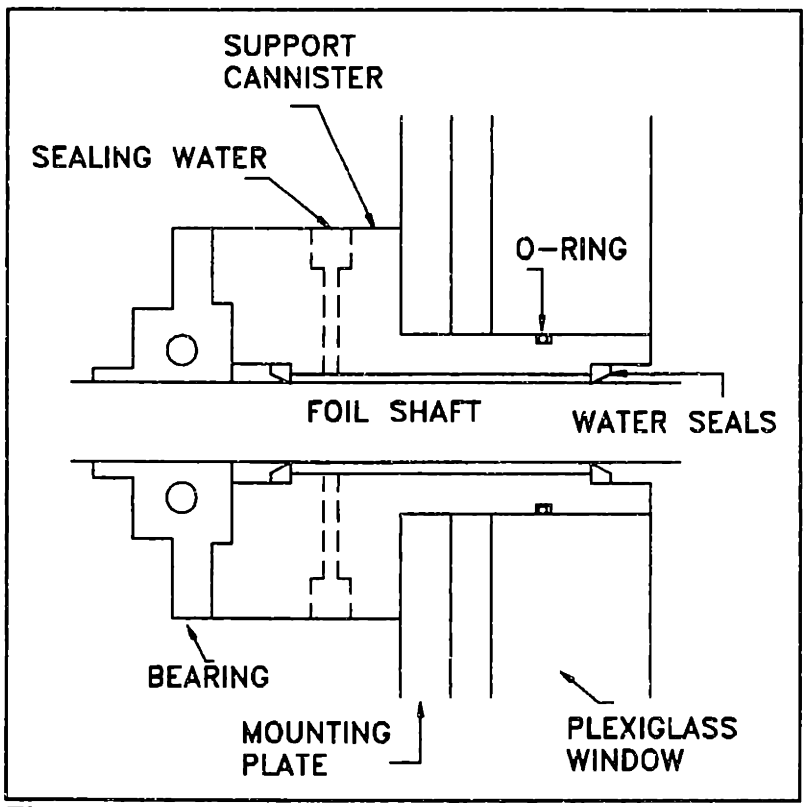

Figure 5.3 Support Canister and Shaft Sealing Arrangement

5.3 Mechanical Support and Bearing Design

5.3.1 Mechanical Support

The two key elements of the support system are the mounting plates and support canisters. These components are shown in figures 5.3 and 5.4.

The entire flapping foil system, except the drive motor, is mounted on the water tunnel. Two 5/8 inch thick mounting plates are used to support the various components. The plate outline and key loads are shown in figure 5.4. Each plate is rigidly attached to the water tunnel using nine 3/8 inch studs and nuts screwed into the existing window support bar, stud holes.

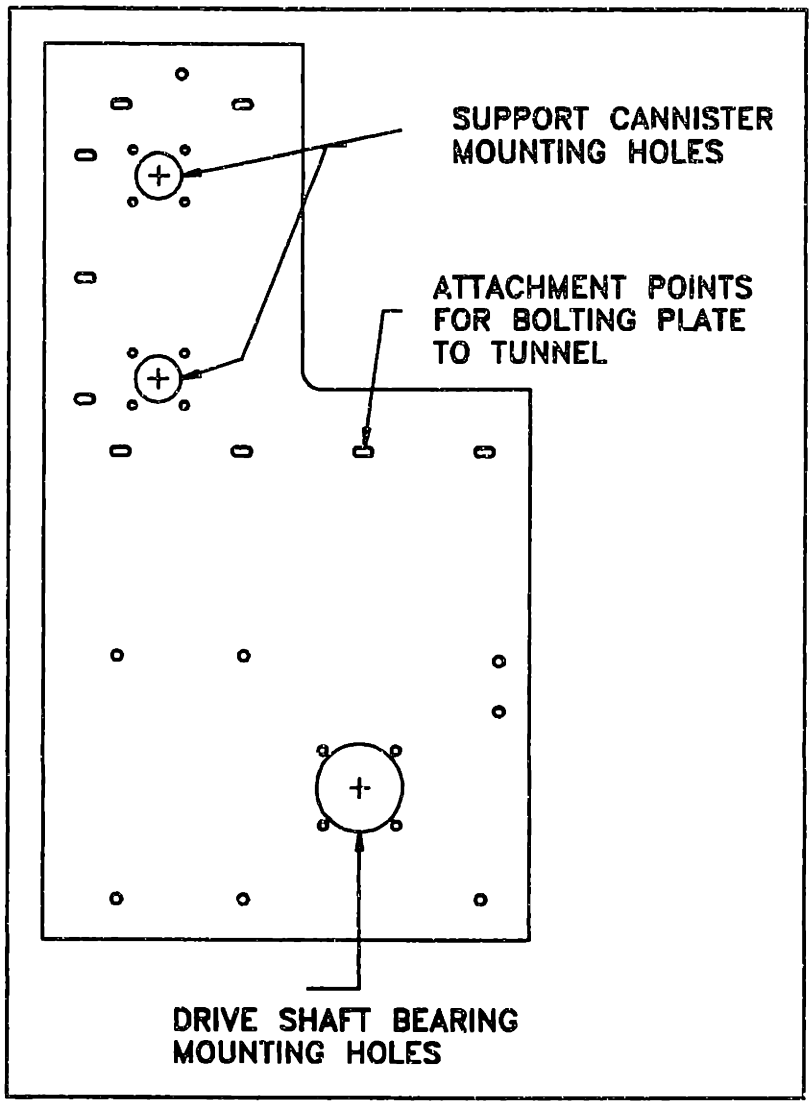

Figure 5.4 Mounting Plate with Main Loads

The support canisters are shown in figure 5.3. They are bolted to the mounting plate and are used to:

1) support the bearings that support the loads on the foils,

2) house the shaft seals and provide the sealing water cavity between the seals,

3) seal the holes in the plexiglass window with a standard o-ring.

5.3.2 Bearing Design

The flapping foil system is designed to be easily installed and removed from the water tunnel. The system will be installed only during performance of the many upcoming flapping foil experiments. These requirements ruled out using standard bearings with a press fit.

The key issue in bearing selection was to find a bearing that allowed the flapping foil system to be easily installed and removed. Additionally, the bearing had to provide a means to adjust and restrain the axial position of the foils.

After reviewing several bearing catalogs, mounted radial ball bearings were selected. These bearings offered several advantages:

1) the bearings came in their own housing eliminating the need to design and manufacture a bearing housing,

2) the bearings included two setscrews on the inner race to allow axial alignment and positioning of the shafts,

3) the bearings and housing allowed three degrees of rotational freedom to help absorb any misalignments,

4) the bearings rated speed and load were compatible with the need.

The final bearings selected were:

1) 1 inch diameter mounted radial ball bearings with a load rating of 757

pounds for the foils,

2) 1½ inch diameter mounted radial ball bearings with a rating of 1400 pounds for the drive shaft.

These bearings provided a factor of safety of 4 on maximum load and are designed for an average life of 2500 hours at the rated load.[24]

5.4 Drive System Design

The drive system was used to step up the speed from the 1200 rpm motor to 3600 rpm. A single V-belt with 9 inch and 3 inch diameter sheaves was used to transmit the torque from the drive motor to drive shaft. The motor was supported on its own foundation with means provided for adjusting belt tension. The foundation rested on a rubber pad to help isolate any motor vibrations from the water tunnel.

5.5 Linkage Design

The linkage served two main purposes:

1) to transmit the torque from the drive shaft to the flapping foils,

2) to cause the foils to oscillate in a sinusoidal pattern consistent with the assumed equations of motion developed in chapter 2.

---

[24] Browning Catalog #100 dated Dec. 1, 1986, p.1-40 - 1-42.

5.5.1 Linkage Design

The linkage system was designed by modeling the mechanism as a simple slider crank.[25] Consequently, the point where the tiller arm connected to the connecting link was assumed to move in a straight vertical path vice on the arc of a 20 inch diameter circle. This simplification introduced about a 4% error in the eccentric offset distance.

The ratio of eccentric offset to connecting link length was picked as 5% to achieve the assumed sinusoidal motion with minimal higher order terms. The resulting angle of attack, angular velocity, and angular acceleration of the oscillating foil were sinusoidal with a small higher order term because of the finite connecting link length. The higher order term caused a 5% shift in the actual foil motion from the assumed motion. The final

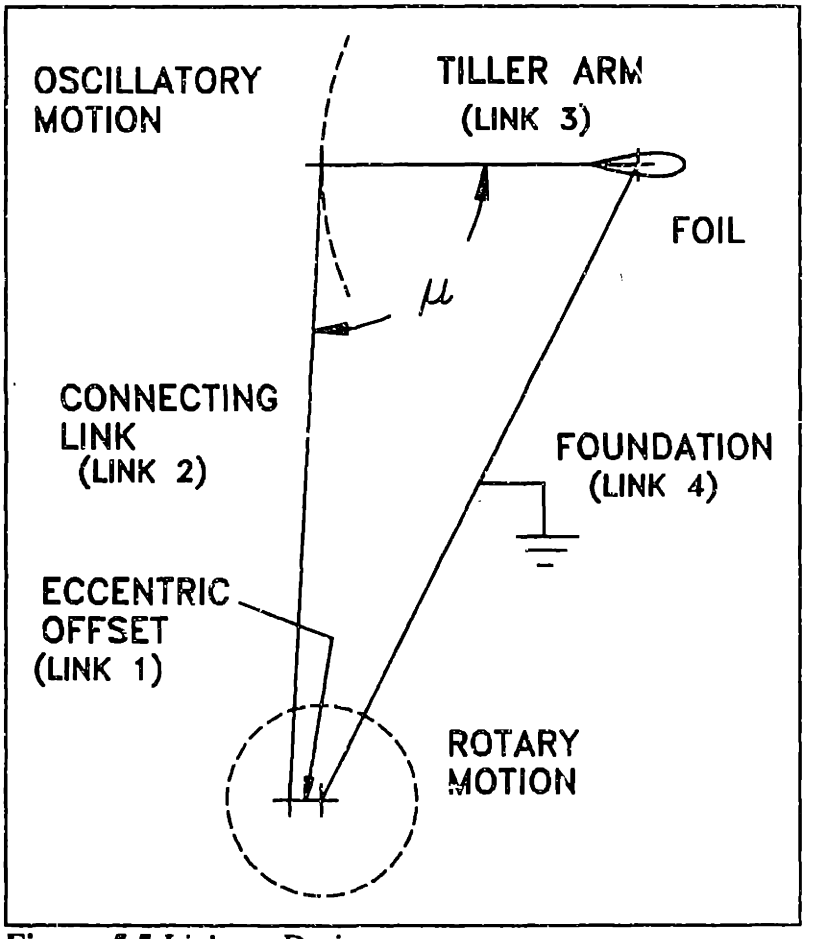

Figure 5.5 Linkage Design

[25] H.H. Mabie and F.W. Ocvirk, *Mechanisms and Dynamics of Machinery*, 3rd ed. (New York: John Wiley and Sons, Inc. 1975) p.19-20.

linkage design is shown in figure 5.5. The transmission angle, μ, was kept as close as possible to 90° to provide smooth operation.[26] The final transmission angle varied between 83.5° and 96.5° over one cycle.

The linkage design allows for the eccentric offset to be changed to three different values by simply rotating the eccentric plate 90°. This allows the maximum angle of attack to be adjusted to 3°, 6°, or 8°. However, since the initial dynamic balancing was performed assuming a 6° angle of attack, the dynamic balancing would need to be repeated if the system were run at high speeds.

5.5.2 Linkage Analysis

A detailed kinematic analysis was conducted on the final linkage arrangement. The linkage arrangement is a classic four bar link or a crank

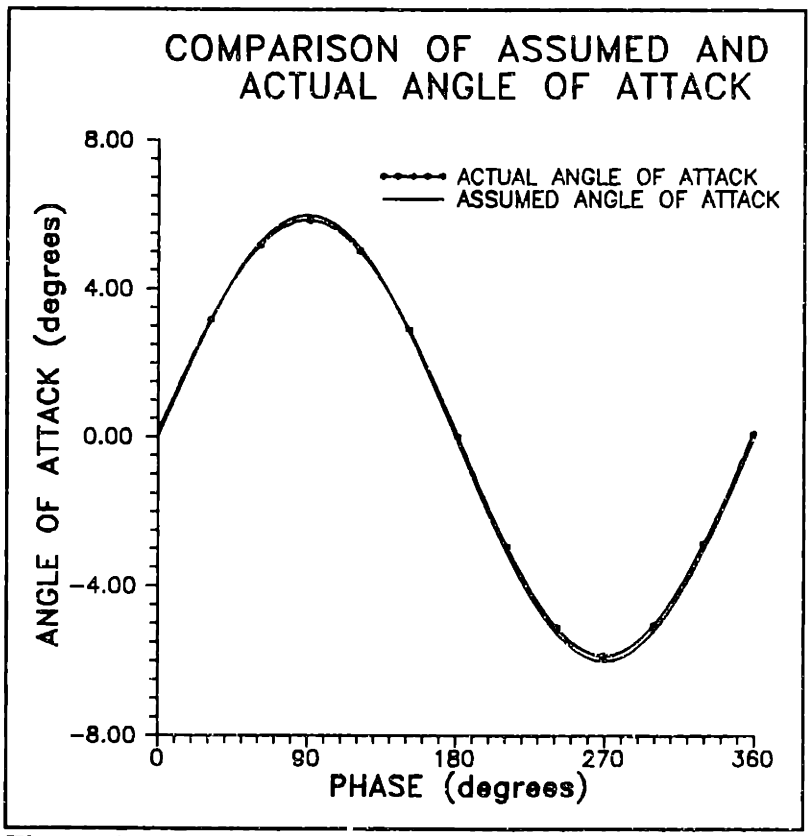

Figure 5.6 Comparison of Assumed and Actual Angle of Attack Over One Cycle of Oscillation

[26] Jacques Grosjean, *Kinematics and Dynamics of Mechanisms*, (London: McGraw-Hill Book Company, 1991) p.92.

and rocker mechanism.[27] The arrangement shown in figure 5.5 consisted of the following parts:

1) link 1 is the eccentric offset,

2) link 2 is the connecting link,

3) link 3 is the tiller arm,

4) link four is the foundation or common ground between the centers of rotary and oscillatory motion.

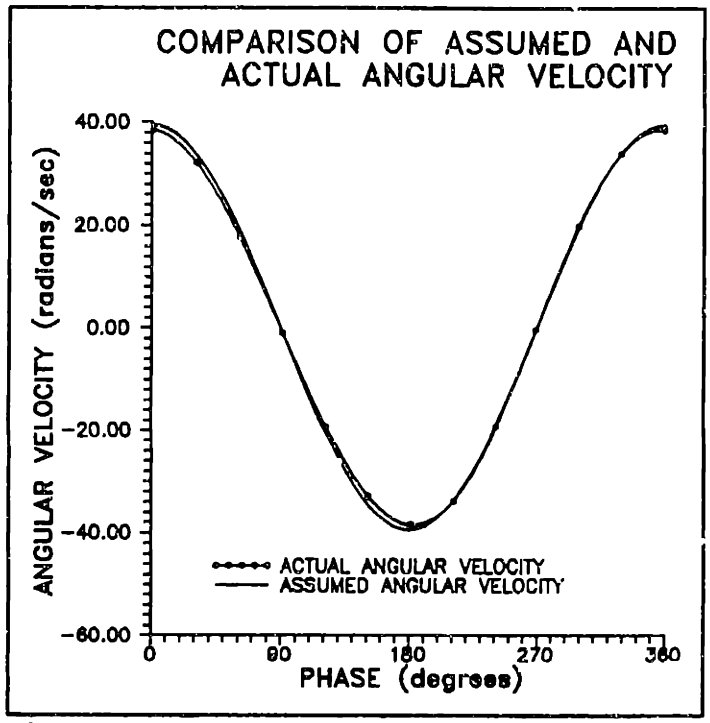

Figure 5.7 Comparison of Assumed and Actual Angular Velocity Over One Cycle of Oscillation

The analysis computed the angle of attack, angular velocity, and angular acceleration of the output link which is the tiller arm. The tiller arm is rigidly attached to the oscillating foil by means of a taper fit and key. Consequently, the tiller arm and foil have the same motion. The results of the analysis are shown in figures 5.6, 5.7, and 5.8. The analysis shows the linkage provided the assumed motions within 2.5%. A 0.025 inch, or 2.5%, increase in the eccentric offset would result in the assumed and actual motions almost identically matched.

[27] Grosjean, p.10-11,93-95.

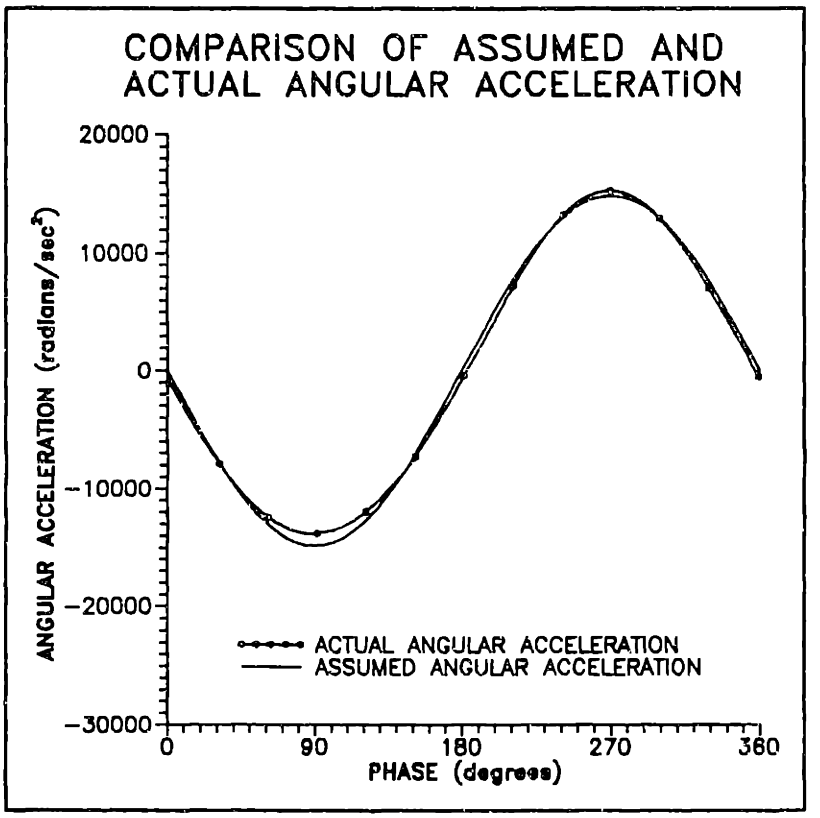

Figure 5.8 Comparison of Actual and Assumed Angular Acceleration Over One Cycle of Oscillation

Chapter 6

Steady State Velocity Profiles

6.1 Introduction

In the first phase of the research program, the steady state velocity profiles were mapped over the foil surface. Velocity profiles were taken at 10% increments on the upper and lower surfaces and 1 inch downstream of the trailing edge.

6.2 Steady State Data

In this part of the research program, more detailed steady state velocity profiles were obtained over the aft 40% of the foil and in the wake. The foil profile is shown in figure 6.1. Velocity profiles were taken every 5% starting with an X/C of 60%, and ½, 1, 1½, 2, 2½, 3, and 4 inches downstream of the trailing edge. The detailed velocity profiles are contained in Appendix III.

On the average a velocity deficit of at least 15 ft/sec (50%) on the upper surface and 10 ft/sec (30%) on the lower surface was measurable. Plotted with the velocity profiles is the standard deviation of the velocity measurements used to obtain the average velocity.

6.3 Comparison of Data

A comparison of data at 1 inch aft of the trailing edge with the previous experiment was performed. The two sets of data are shown in Figures 6.2 and 6.3. The data is not compared on the same plot because the data is almost identical. This verifies the data is repeatable from experiment.

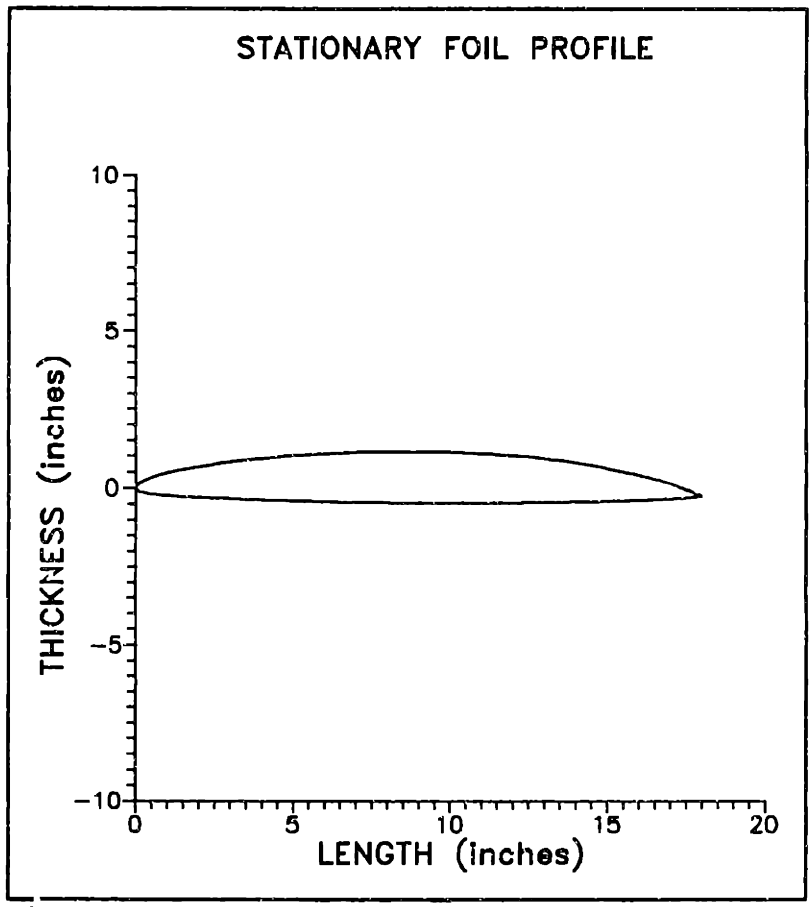

Figure 6.1 Stationary Foil Profile

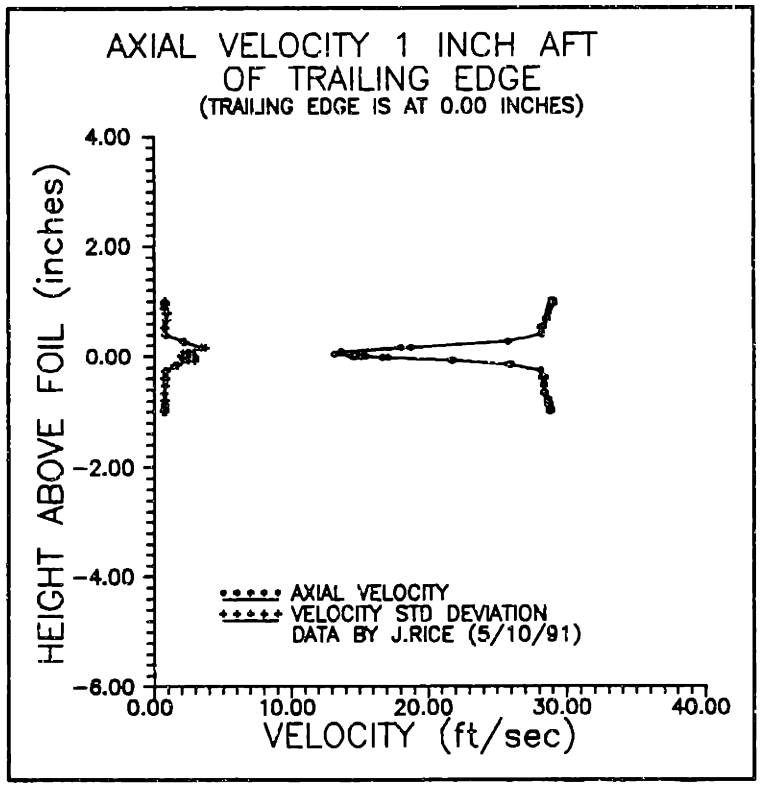

Figure 6.2 Velocity Profile 1 Inch Aft of Trailing Edge

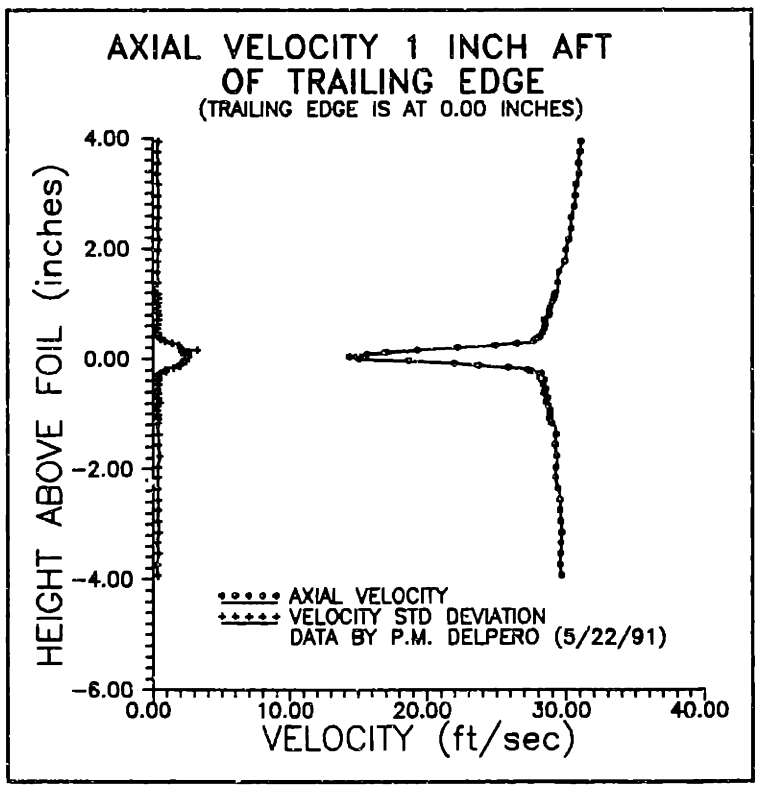

Figure 6.3 Velocity Profile 1 inch Aft of Trailing Edge

(This page intentionally left blank.)

Chapter 7

Unsteady Testing

7.1 Introduction

The purpose of the unsteady test program of this project was to:

1) install and shakedown the flapping foil system,

2) obtain unsteady flow data to see if the experimental concept worked.

7.2 System Shakedown

The initial shakedown of the system was designed to gradually bring the system up to its maximum capability while resolving and documenting problems as they occurred. The shakedown of the system consisted of:

1) dynamic balancing of the drive shaft,

2) installation check,

3) air testing,

4) water testing.

7.2.1 Dynamic Balancing

The drive shaft and all rotating parts were dynamically balanced as an assembly at Lindskog Dynamic Balancing in Action, Ma. The oscillating mass was replaced by an

equivalent mass for the balancing.[28] This mass was attached at the eccentric offset during the balancing procedure. The assembly was balanced to 0.12 in-lbs. A bump test determined the critical speed to be 6510 rpm.

7.2.2 Installation Check

The initial installation of the system went surprisingly well. The only difficulties were some minor fitup problems with the laser windows. Additionally, the method of bolting the support canisters to the mounting plates need to be altered to simplify the installation sequence.

7.2.3 Air Testing

Operational air testing followed the installation check. The system ran well up to 15 hertz where a severe vibration developed in the unsupported ends of the mounting plates. The 5/8 inch thick plates hang down 20 inches from the water tunnel where they are rigidly attached. The ends of the plates vibrated approximately ± ¼ inch. This vibration eventually caused one of the drive links to fall off its bearing at approximately 1500 rpm. The other problem encountered during air testing was the water seals around the oscillating foil shafts leaked excessively.

---

[28] Robert L Maxwell, *Kinematics and Dynamics of Machinery* (Englewood Cliffs, NJ: Prentice Hall, Inc 1960) p. 270-274.

7.2.4 Lessons Learned

During air testing, three problems were uncovered and were corrected or are being corrected. The problems encountered and corrective actions are:

1) Severe mounting plate vibration above 15 hertz. Stiffeners were manufactured to tie the unsupported ends of the plates into the supported ends. This solved the plate vibration problem and allowed the system to be operated up to 20 hertz were another severe vibration occurred. Additional troubleshooting is being performed to determine the cause of the vibrations at 20 hertz.

2) Water seals around the oscillating foil shafts did not seal against the design differential pressure of 3 psid. The spring-steel loaded seals were replaced with spring loaded seals. Retesting showed the seals did not leak at the design differential pressure of 3 psid. However, some leakage into the water tunnel did occur at high flow rates where the differential pressure across the seals is higher. Additional sealing water was added to solve the problem. Leak testing is being performed to determine if the leakage can be isolated to a specific seal.

3) The integrity of the press fit between the rod ends and cam followers on the connecting links needs to be improved. The rod ends were redesigned to allow for setscrew locking as well as press fitting the cam followers in place. Additionally, a locking compound for press fits was used as an added measure of confidence.

7.2.5 Initial Water Testing

Upon completion of air testing the system was disassembled and problems corrected. The system was reassembled and tested up to 20 hertz with the water tunnel operating over the entire range of flows. No problems in the operation of the system developed. The system will be run above 20 hertz once the cause of the severe vibrations are determined and corrected.

7.3 Unsteady Testing

Unsteady testing followed the initial shakedown of the system. Data acquisition ran flawlessly, the only problem being the angle encoder was reliable up to a maximum of 5 hertz. Data acquisition proceeded below this 5 hertz limit.

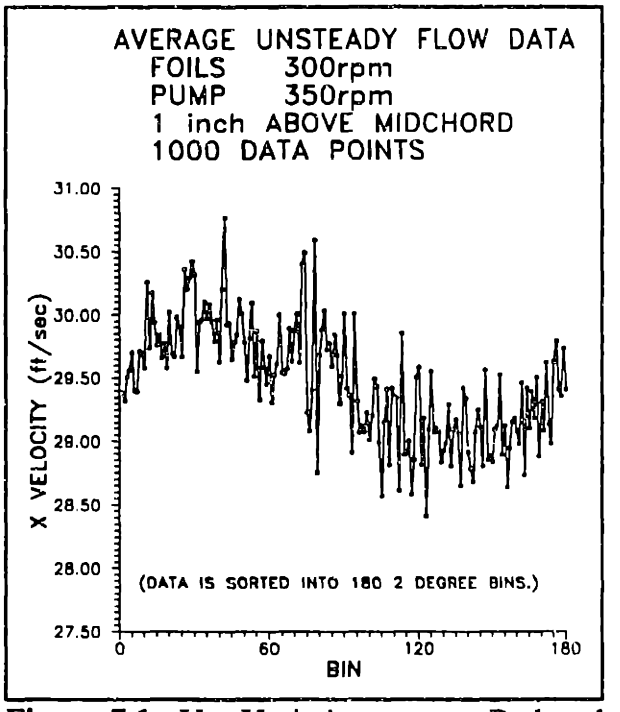

Figure 7.1 V_x Variation at a Reduced Frequency of 1.0

The initial data run consisted of 1000 data points at a position 1 inch above the stationary foil on the upper surface at midchord. The data was acquired at a reduced frequency of 1.0. Data consisted of x and y velocities and angular position of the drive shaft. The data was then grouped into 2° bins and the average and standard deviation were calculated for the x and y velocities in each bin. The average x and y

velocities are plotted in figures 7.1 and 7.2. The velocities follow a sinusoidal shape which would be expected given the motion of the flappers. The experiment was rerun at a reduced frequency of 1.2. 10,000 data points were taken 1½ inches above the midchord. The reduced data is shown in figures 7.3 and 7.4. The sinusoidal shape is more refined.

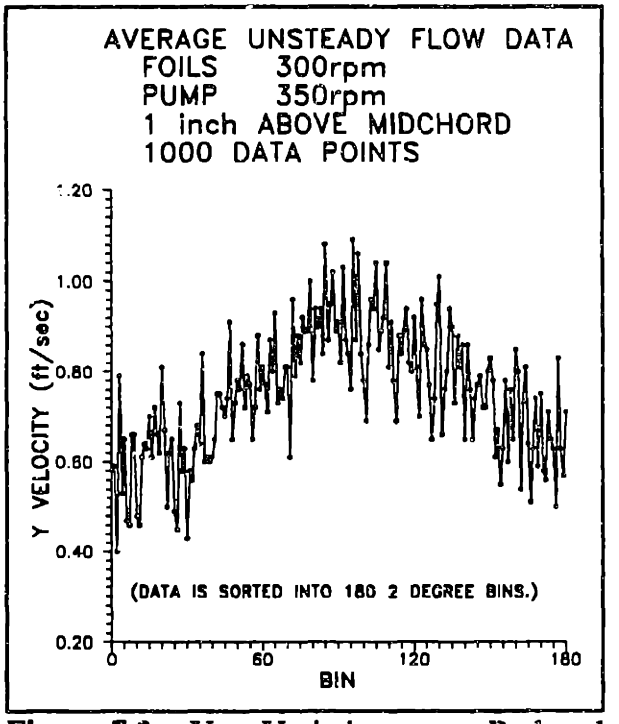

Figure 7.2 V_y Variation at Reduced Frequency of 1.0

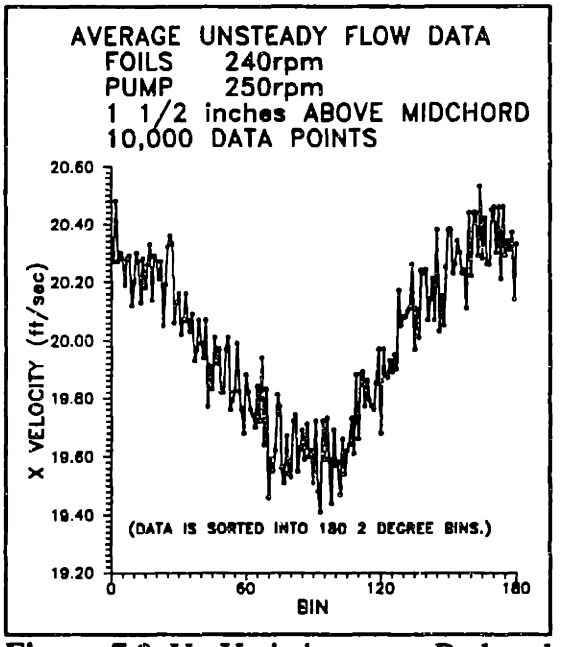

Figure 7.3 V_x Variation at a Reduced Frequency of 1.2

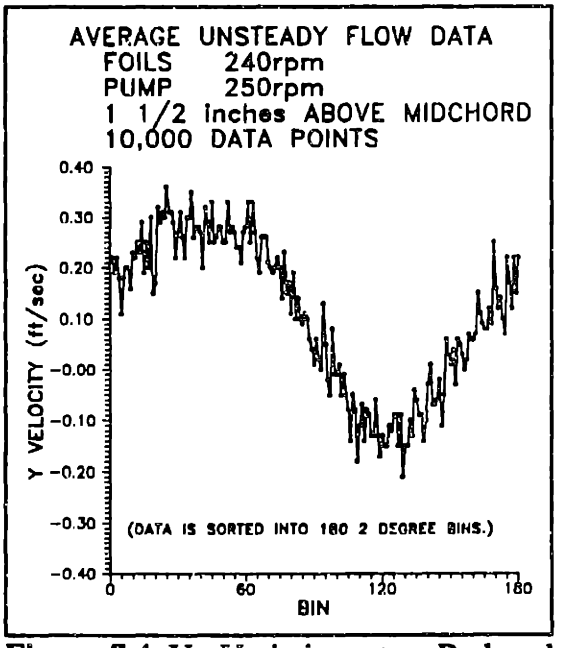

Figure 7.4 V_y Variation at a Reduced Frequency of 1.2

As a control, the connecting link was disconnected from the drive shaft and the unsteady data was taken with the drive shaft and motor running. The resulting reduced data is shown in figures 7.5 and 7.6. This data shows the sinusoidal profile obtained when the flappers are used is the result of the hydrodynamic effect of the flappers, not the vibrations caused by the drive system.

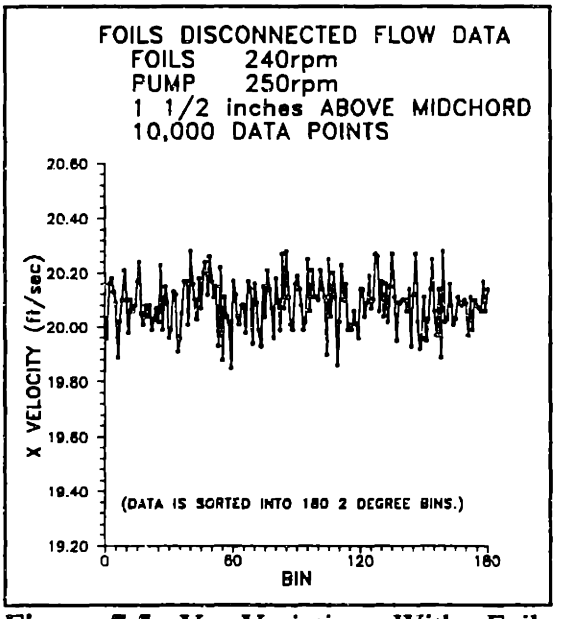

Figure 7.5 V_x Variation With Foils Disconnected and Motor Running

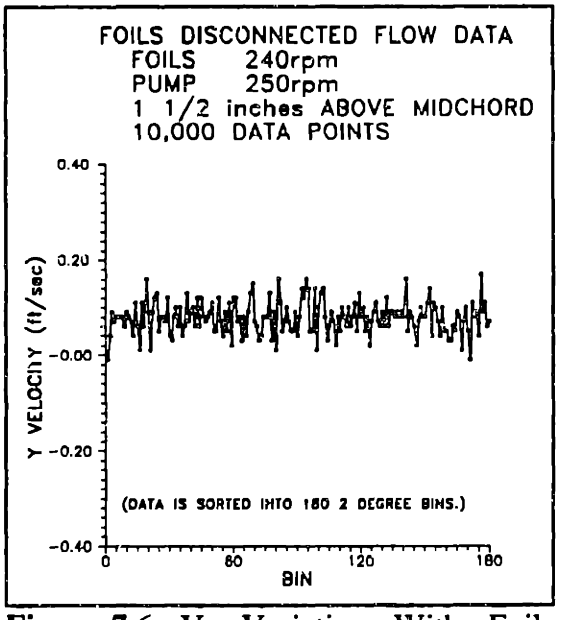

Figure 7.6 V_y Variation With Foils Disconnected and Motor Running

Chapter 8

Conclusions

8.1 Conclusions

The primary objective of this research was to design, build, install, and shakedown the flapping foil system. The data shown in Chapter 7 clearly shows the system worked. A measurable response was obtained at a reduced frequency of 1.0. Some additional work is required to solve the vibration problems and allow the system to be operated above a reduced frequency of 3.3 or a rotational frequency of 20 hertz.

(This page intentionally left blank.)

List Of References

Barton, Lyndon O. *Mechanism Analysis: Simplified Graphical and Analytical Techniques*. New York: Marcel Dekker Inc., 1984.

Batelle Materials and Ceramics Information Center. *Structural Alloys Handbook*. 1990 ed.

Baumeister, Theodore, Eugene A. Avallone, and Theodore Baumeister III. *Marks' Standard Handbook for Mechanical Engineers*. 8th ed. New York: McGraw Hill Book Company, 1978.

Beer, Ferdinand P. and E. Russell Johnston Jr. *Vector Mechanics for Engineers*. 2nd ed. Englewood, New York: McGraw-Hill Book Company.

Bisplinghoff, Raymond L., Holt Ashley, and Robert L. Halfman. *Aeroelasticity*. Cambridge, Mass: Addison-Wesley Publishing Company Inc., 1955.

Blake, Alexander. *Handbook of Mechanics, Materials, and Structures*. New York: John Wiley and Sons Inc., 1985..

Comprehensive Reference Guide to Airfoil Sections for Light Aircraft. Washington,D.C.: Aviation Publications, 1982.

Dowell, Earl H., Howard C. Curtis Jr., Robert H. Scanlan, and Fernando Sisto. *A Modern Course in Aeroelasticity*. 2nd ed. Dordrecht: Kluwer Academic Publishers, 1989.

Evans, J.H.. *Basic Design Concepts* ASNE Journal. Nov 1959.

Grosjean, Jacques. *Kinematics and Dynamics of Mechanisms*. New York: McGraw Hill Book Company, 1991.

Holowenko, A.R.. *Dynamics of Machinery*. New York: John Wiley and Sons Inc., 1955.

Kerwin, Justin E. and David P. Keenan. *A Proposal for Continuation of An Experimental Investigation of the Unsteady Boundary Layer Structure of a Lifting Body Subject to Cross Flow Gusts*. 20 March 1991.

Kerwin, J.E.. *Fortran Program BPROP*. December 3, 1988.

Kerwin, Justin E. and David P. Keenan. *Progress Report For Unsteady Foil Experiment.* 1 June 1990 to 31 Nov 1990.

Kerwin, Justin E. *13.04 Lecture Notes Hydrofoils and Propellers.* February 1990.

Mable, Hamilton H and Fred W. Ocvirk. *Mechanics and Dynamics of Machinery.* 3rd ed. New York: John Wiley and Sons Inc., 1975.

Maxwell, Robert L. *Kinematics and Dynamics of Machinery.* Englewood Cliffs, New Jersey: Prentice-Hall Inc., 1960.

Oberg, Erik, Franklin D. Jones and Holbrook L. Horton. *Machinery's Handbook.* 21st ed. New York:Industrial Press Inc., 1979.

Rice, James Q., *MIT Thesis Investigation of A Two Dimensional Hydrofoil in Steady and Unsteady Flows:* June, 1991.

Roark, Raymond J. and Warren C. Young. *Formulas for Stress and Strain.* 5th ed. New York: McGraw-Hill Book Company, 1975.

Shames, Irving H. *Introduction to Solid Mechanics.* 2nd ed. Englewood, NJ: Prentice Hall, 1989.

Shearer, J. Lowen, Arthur T. Murphy, and Herbert H. Richardson. *Introduction to System Dynamics.* Mass: Addison-Wesley Publishing Company, 1967.

Timoshenko, S. and D.H. Young. *Elements of Strength of Materials,* 5th ed. New York: D. Van Nostrand Company, 1968.

Appendix I

Flapping Foil Profile Coordinates

Foil Characteristics

CHORD=	3.000	YMAX=	0.375
YMIN=	-0.375	RLE=	0.206
TTE=	0.000	YLE=	-0.002
YTE=	0.000	ALPHA=	-0.036

Foil Vertices

3.00000	0.00000
2.10000	0.26725
0.75000	0.44542
0.24000	0.27385
-0.01044	0.12712
-0.01044	-0.12712
0.24000	-0.27388
0.75000	-0.44547
2.10000	-0.26728
3.00000	0.00000

Foil Profile Coordinates

3.00000,	0.00000
2.89545,	0.03054
2.79297,	0.05949
2.69258,	0.08687
2.59428,	0.11274
2.49808,	0.13712
2.40400,	0.16005
2.31204,	0.18157
2.22221,	0.20173
2.13453,	0.22055
2.04901,	0.23807
1.96564,	0.25434
1.88445,	0.26939
1.80544,	0.28325
1.72863,	0.29597
1.65401,	0.30758
1.58161,	0.31812
1.51143,	0.32763
1.44349,	0.33615
1.37779,	0.34371
1.31433,	0.35035
1.25314,	0.35611
1.19423,	0.36103
1.13759,	0.36514
1.08325,	0.36849
1.03120,	0.37110
1.00250,	0.37228
0.95408,	0.37382
0.90790,	0.37472
0.86389,	0.37500
0.82197,	0.37469
0.78206,	0.37382
0.74410,	0.37242
0.70800,	0.37052
0.67370,	0.36814
0.00027,	-0.01079
0.00093,	-0.01967
0.00197,	-0.02851
0.00339,	-0.03731
0.00520,	-0.04606
0.00739,	-0.05474
0.00996,	-0.06334
0.01291,	-0.07185
0.01625,	-0.08025
0.01997,	-0.08854
0.02407,	-0.09669
0.02856,	-0.10470
0.03130,	-0.10921
0.03639,	-0.11697
0.04186,	-0.12457
0.04771,	-0.13203
0.05395,	-0.13934
0.06058,	-0.14652
0.06759,	-0.15358
0.07499,	-0.16052
0.08277,	-0.16735
0.09095,	-0.17408
0.09951,	-0.18072
0.10846,	-0.18727
0.11779,	-0.19374
0.12752,	-0.20015
0.13764,	-0.20649
0.14815,	-0.21278
0.15904,	-0.21902
0.17033,	-0.22523
0.18202,	-0.23141
0.19409,	-0.23756
0.20656,	-0.24370
0.21943,	-0.24983
0.23268,	-0.25597

0.64111,	0.36531
0.61016,	0.36206
0.58078,	0.35841
0.55289,	0.35440
0.52641,	0.35005
0.50128,	0.34539
0.47741,	0.34045
0.45473,	0.33525
0.43317,	0.32982
0.41265,	0.32420
0.39309,	0.31840
0.37443,	0.31246
0.35658,	0.30640
0.33946,	0.30025
0.32302,	0.29404
0.30716,	0.28780
0.29182,	0.28155
0.28326,	0.27799
0.26859,	0.27179
0.25431,	0.26561
0.24044,	0.25946
0.22695,	0.25332
0.21386,	0.24718
0.20117,	0.24105
0.18887,	0.23491
0.17696,	0.22874
0.16545,	0.22256
0.15433,	0.21634
0.14359,	0.21007
0.13325,	0.20376
0.12330,	0.19740
0.11374,	0.19096
0.10457,	0.18446
0.09579,	0.17787
0.08740,	0.17120
0.07939,	0.16443
0.07177,	0.15755
0.06454,	0.15056
0.05769,	0.14345
0.05123,	0.13622
0.04516,	0.12884
0.24634,	-0.26212
0.26038,	-0.26828
0.27483,	-0.27447
0.28326,	-0.27802
0.29834,	-0.28426
0.31389,	-0.29051
0.32999,	-0.29674
0.34671,	-0.30293
0.36413,	-0.30904
0.38232,	-0.31505
0.40136,	-0.32094
0.42132,	-0.32667
0.44228,	-0.33221
0.46431,	-0.33754
0.48749,	-0.34264
0.51189,	-0.34746
0.53759,	-0.35200
0.56466,	-0.35620
0.59318,	-0.36006
0.62323,	-0.36354
0.65487,	-0.36662
0.68818,	-0.36926
0.72325,	-0.37144
0.76014,	-0.37313
0.79892,	-0.37431
0.83968,	-0.37494
0.88249,	-0.37500
0.92742,	-0.37446
0.97455,	-0.37329
1.00250,	-0.37233
1.05322,	-0.37011
1.10625,	-0.36719
1.16158,	-0.36352
1.21920,	-0.35907
1.27909,	-0.35380
1.34125,	-0.34766
1.40567,	-0.34063
1.47233,	-0.33266
1.54124,	-0.32372
1.61237,	-0.31378
1.68572,	-0.30278

0.03947,	0.12133
0.03416,	0.11366
0.03130,	0.10920
0.02659,	0.10128
0.02227,	0.09321
0.01833,	0.08500
0.01477,	0.07666
0.01160,	0.06821
0.00881,	0.05966
0.00640,	0.05103
0.00438,	0.04232
0.00274,	0.03354
0.00148,	0.02472
0.00060,	0.01586
0.00011,	0.00698
0.00000,	-0.00191
1.76128,	-0.29069
1.83903,	-0.27749
1.91898,	-0.26312
2.00110,	-0.24755
2.08540,	-0.23075
2.17185,	-0.21267
2.26045,	-0.19328
2.35119,	-0.17254
2.44406,	-0.15041
2.53905,	-0.12686
2.63615,	-0.10185
2.73535,	-0.07533
2.83663,	-0.04728
2.94000,	-0.01765
3.00000,	0.00000
3.00000,	0.00000

(This page intentionally left blank.)

Appendix II
Design Drawings

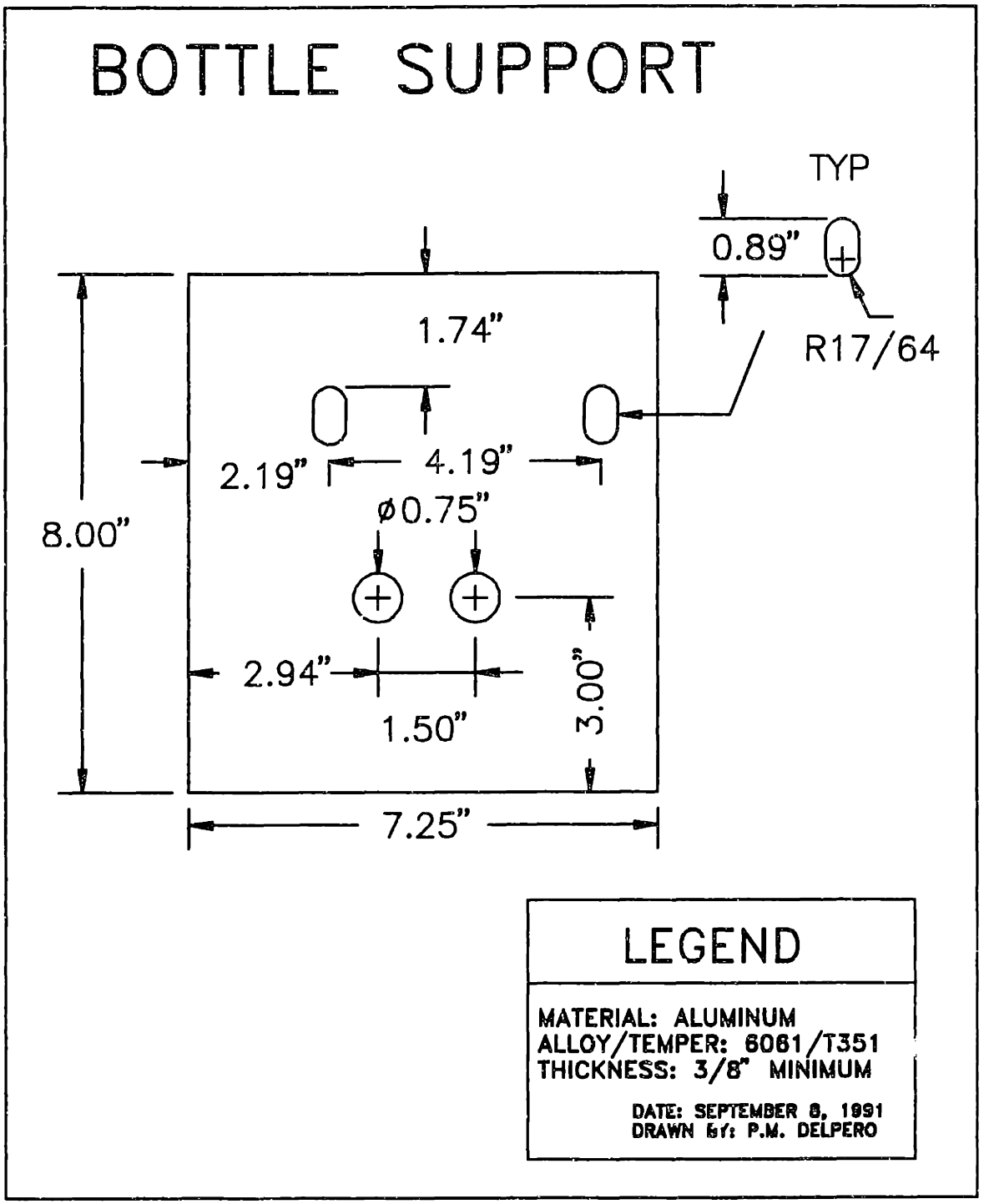

Figure II.1 Bottle Support

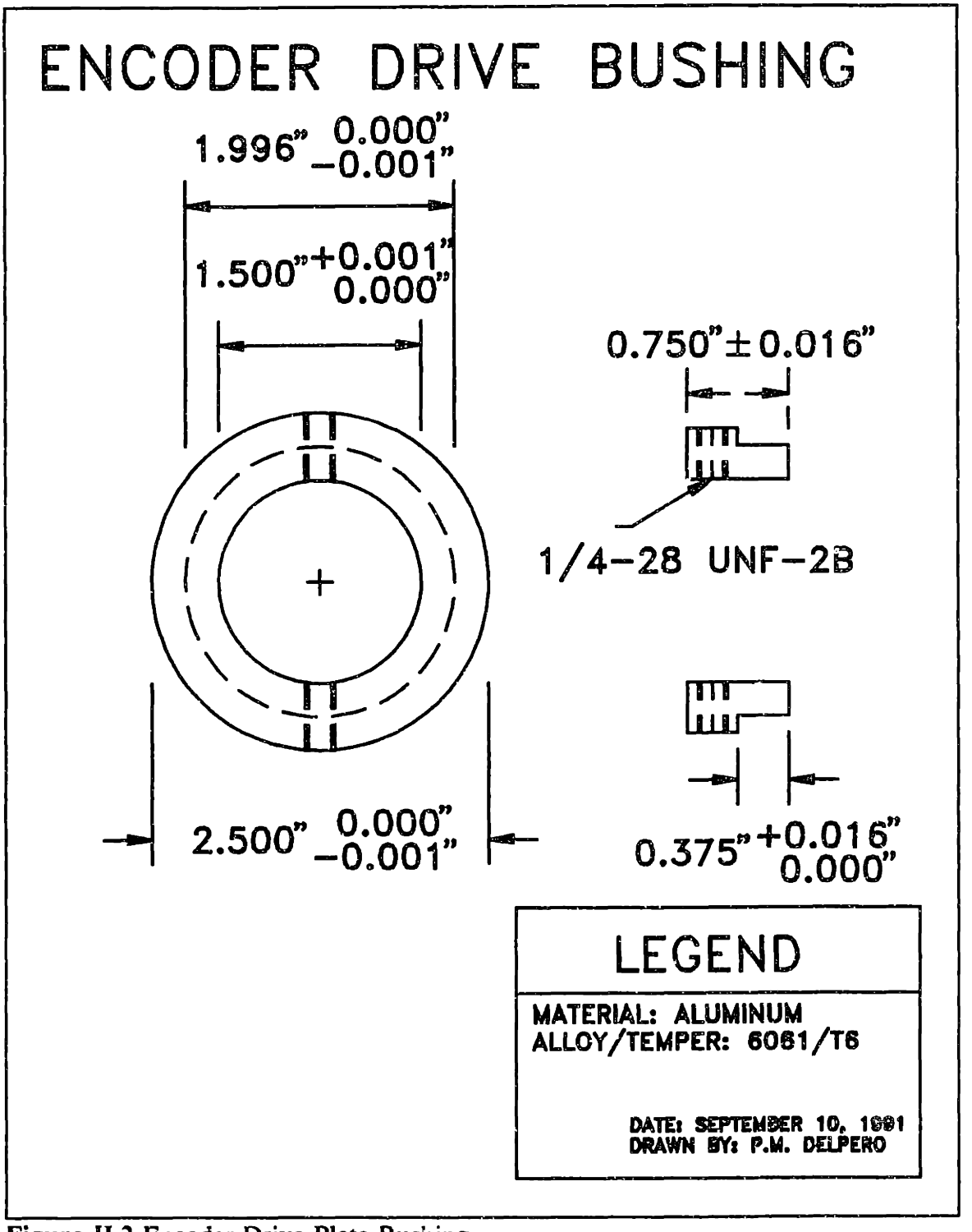

Figure II.2 Encoder Drive Plate Bushing

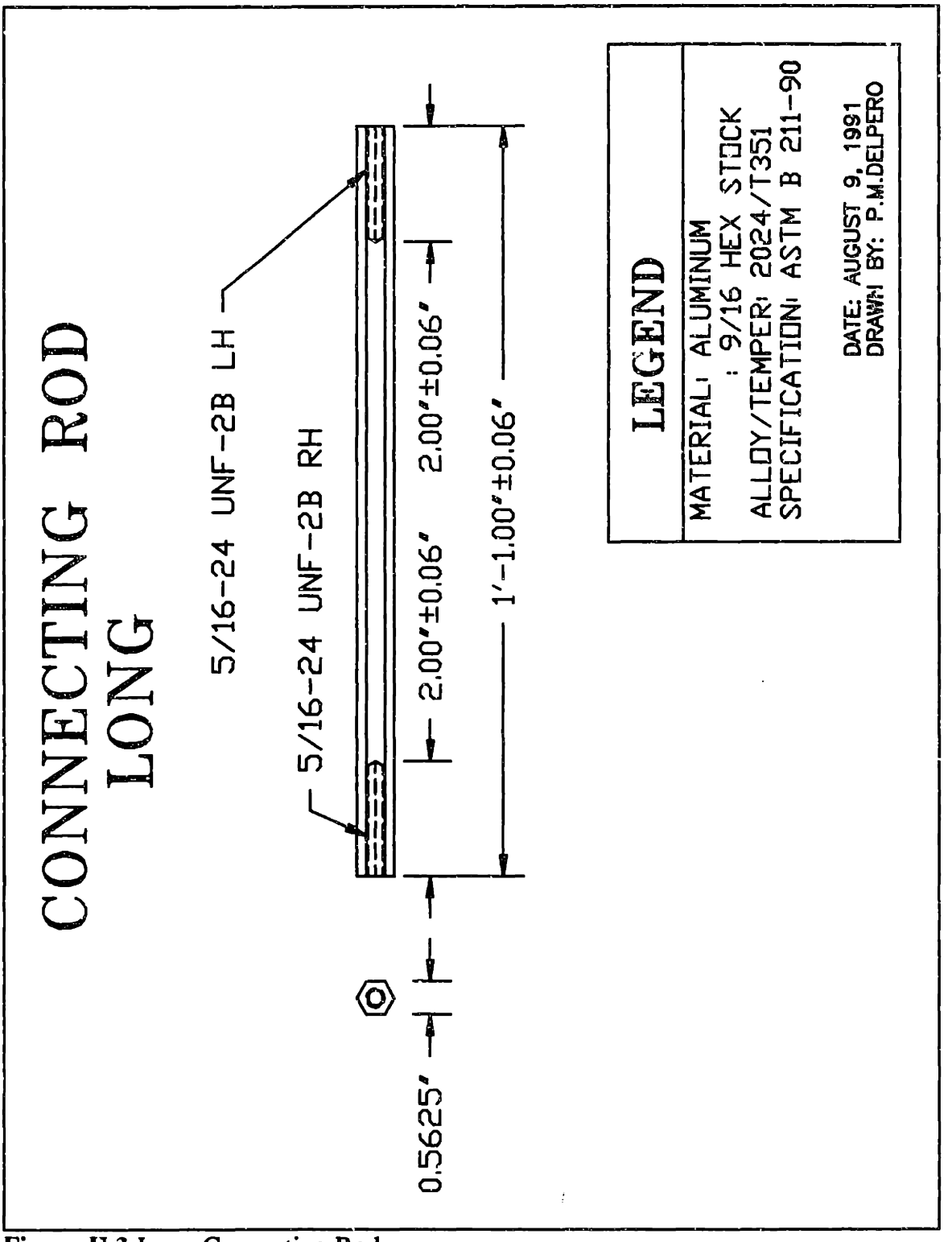

Figure II.3 Long Connecting Rod

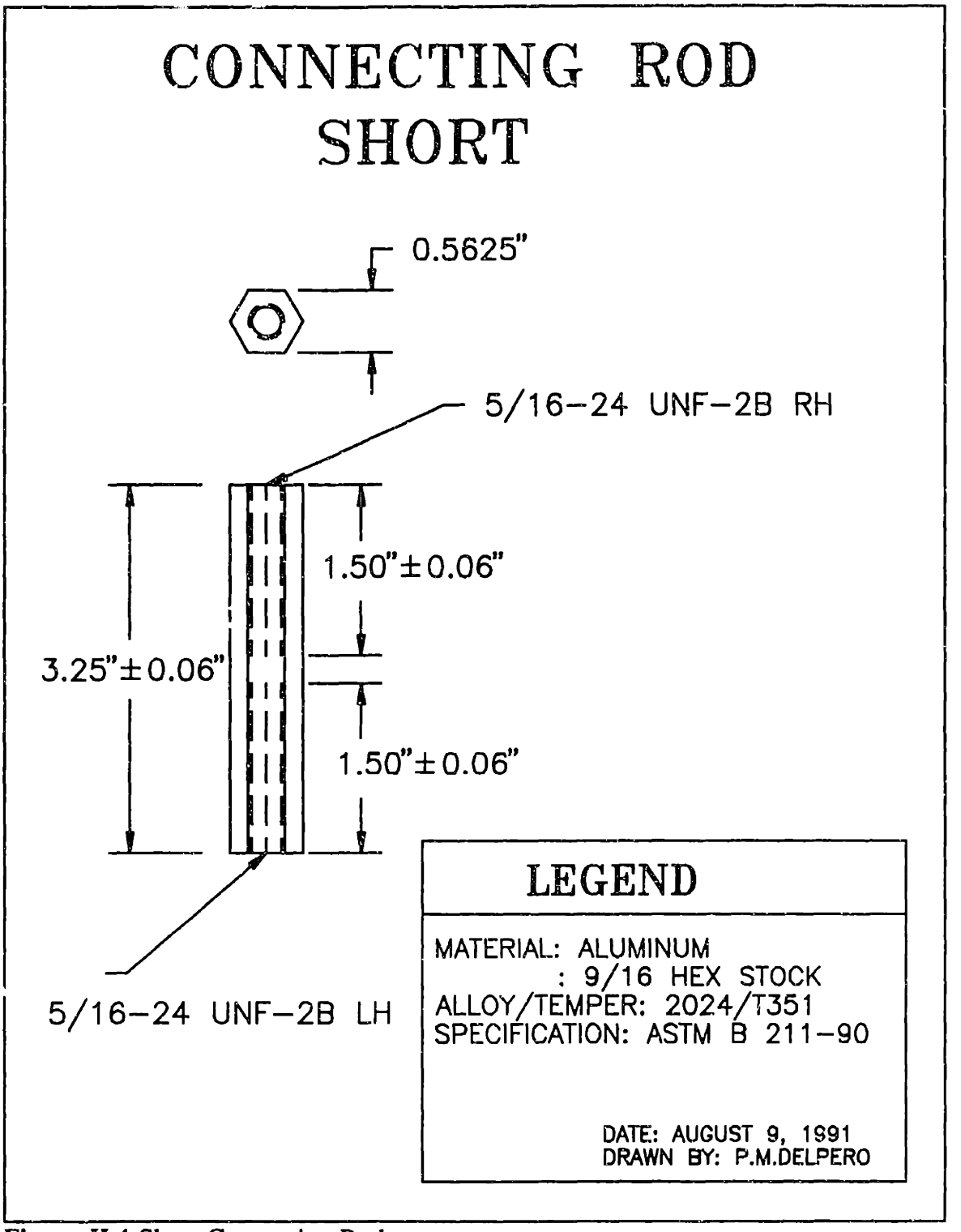

Figure II.4 Short Connecting Rod

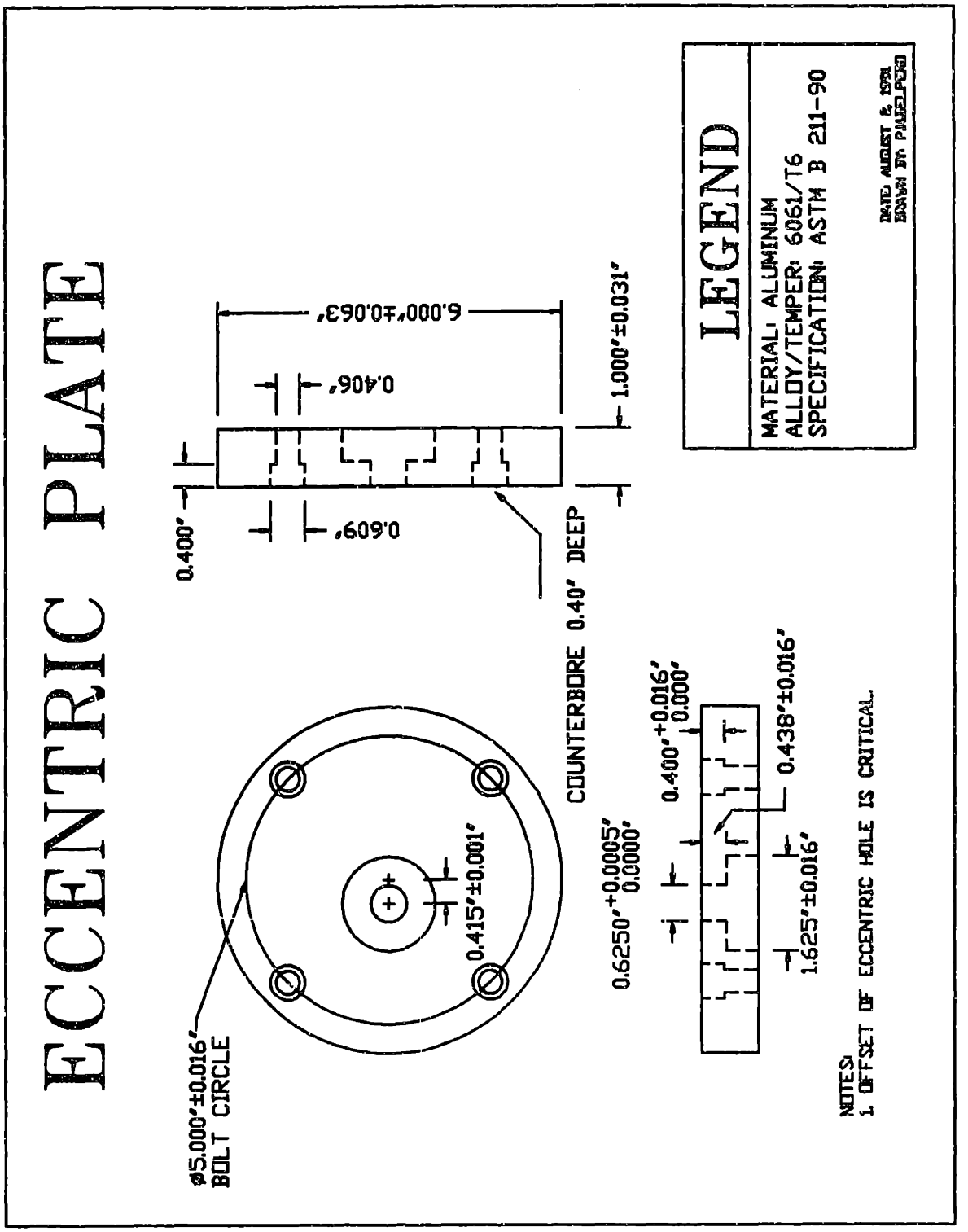

Figure II.5 Eccentric Plate

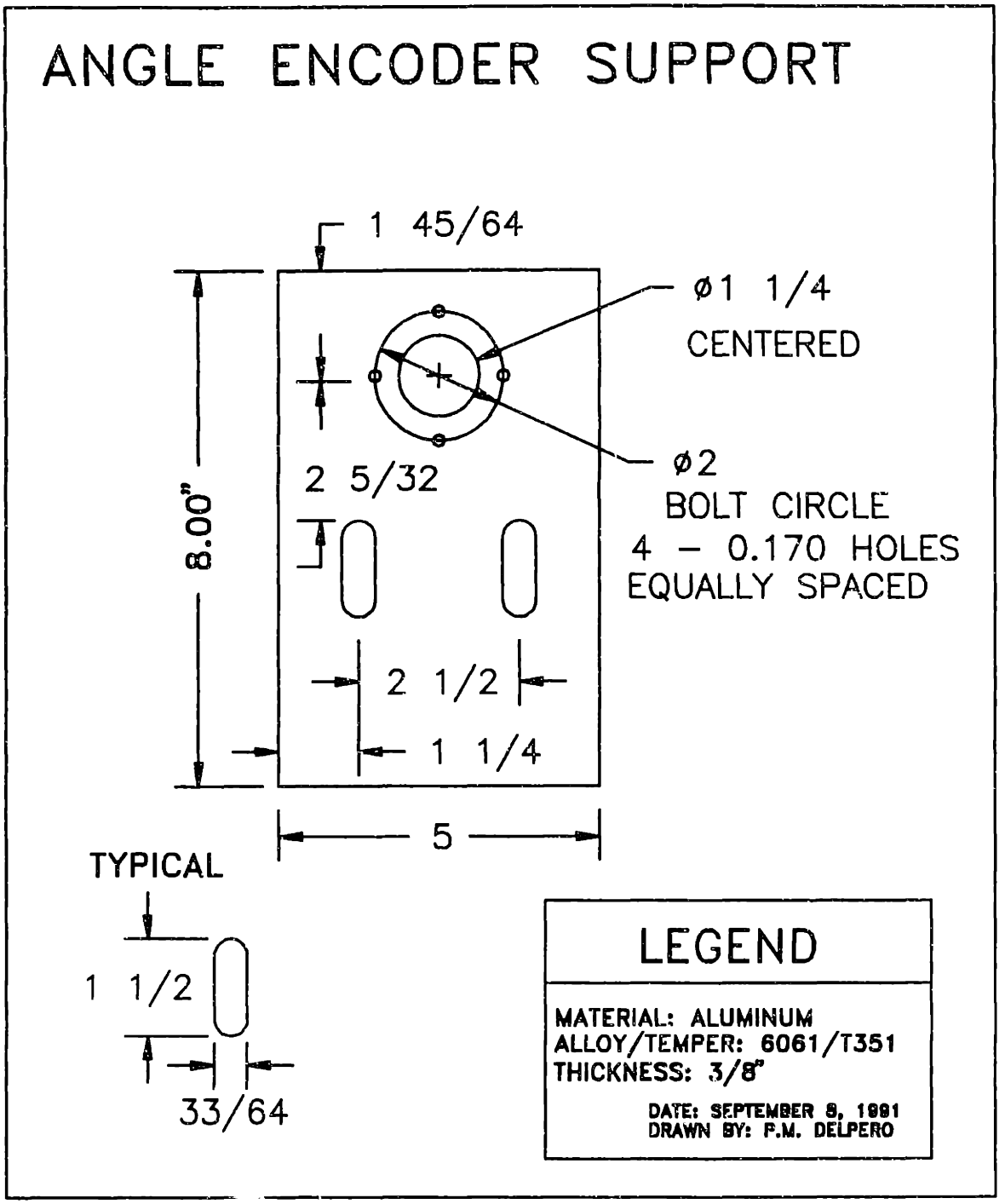

Figure II.6 Angle Encoder Mounting Plate

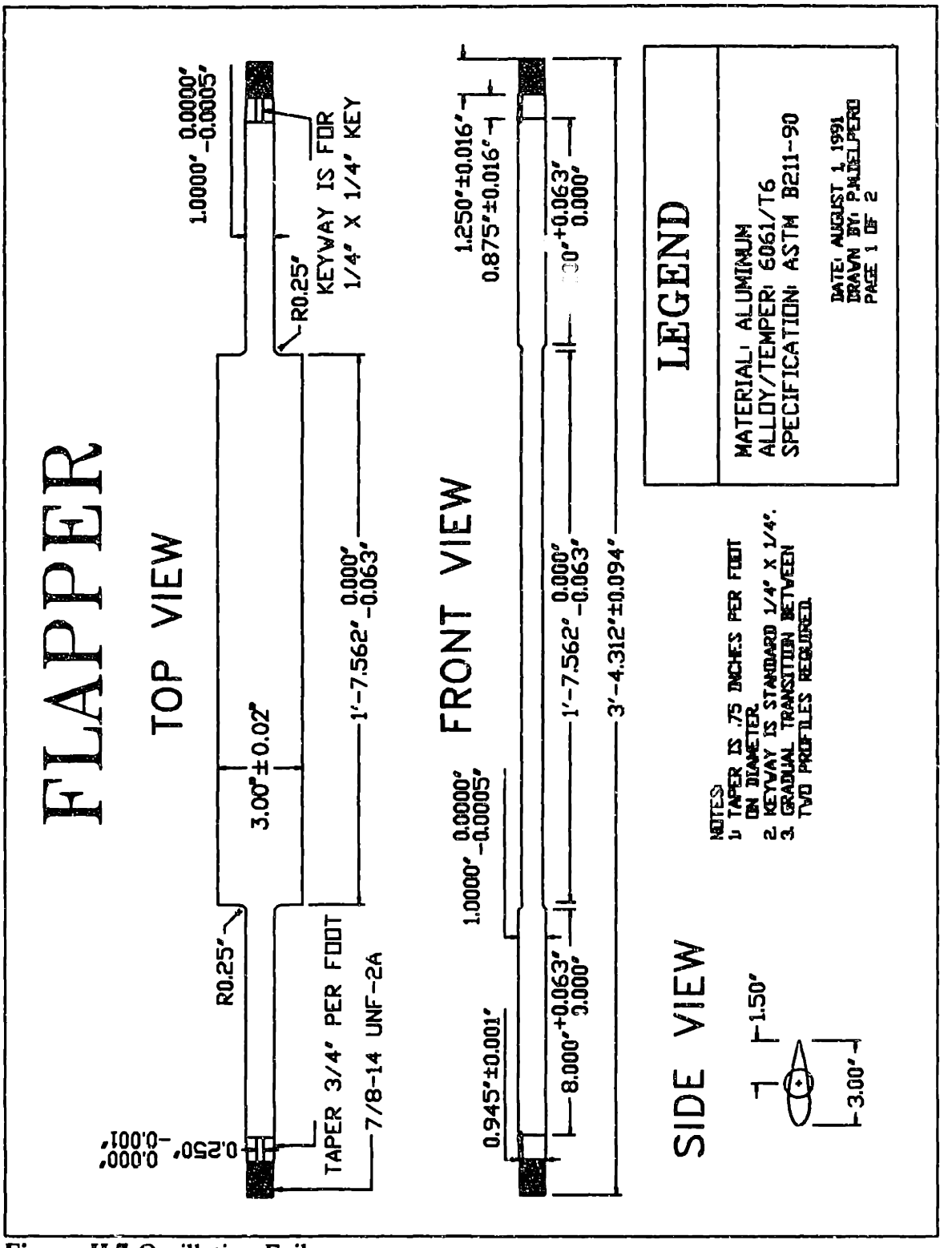

Figure II.7 Oscillating Foil

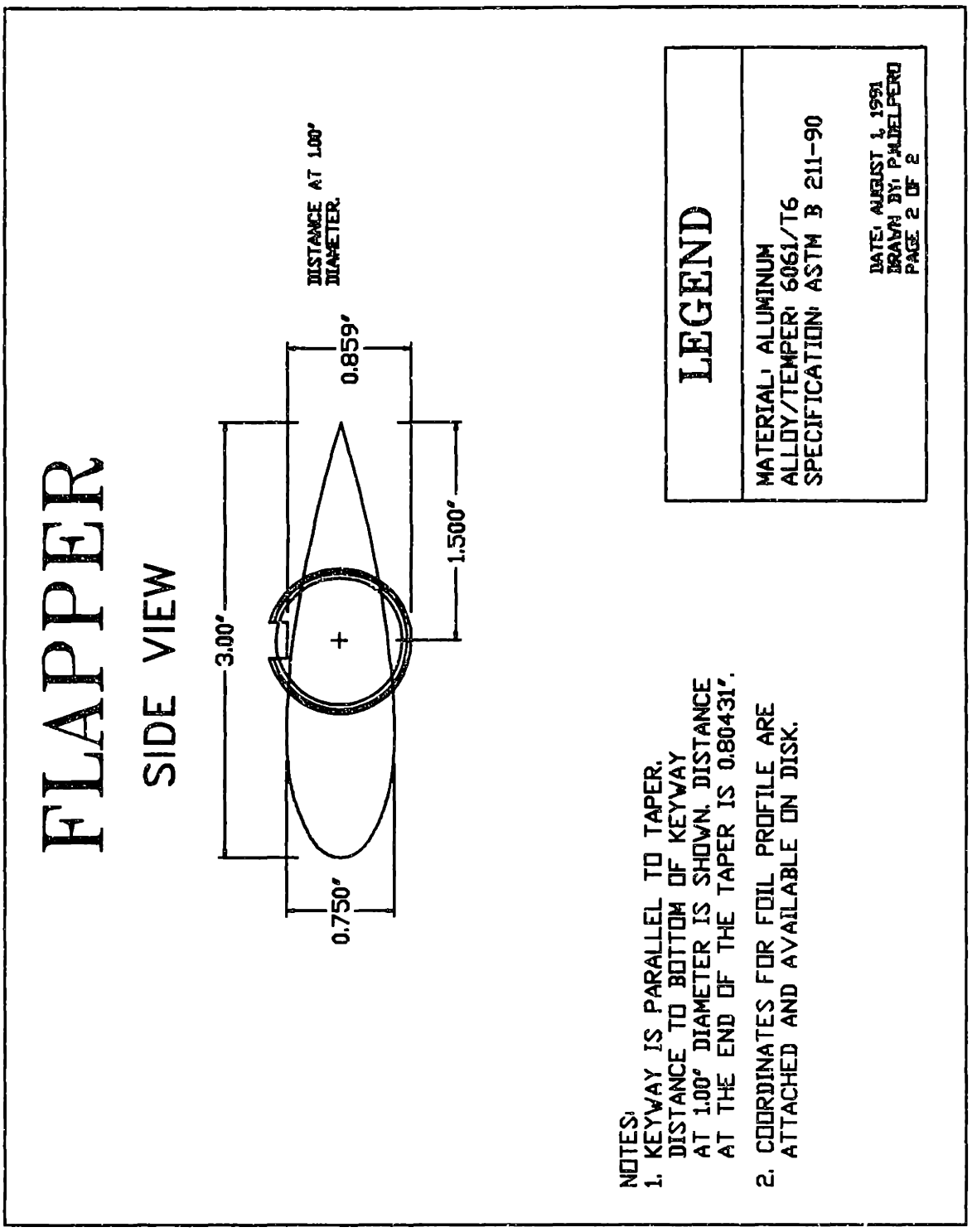

Figure II.8 Oscillating Foil (Side View)

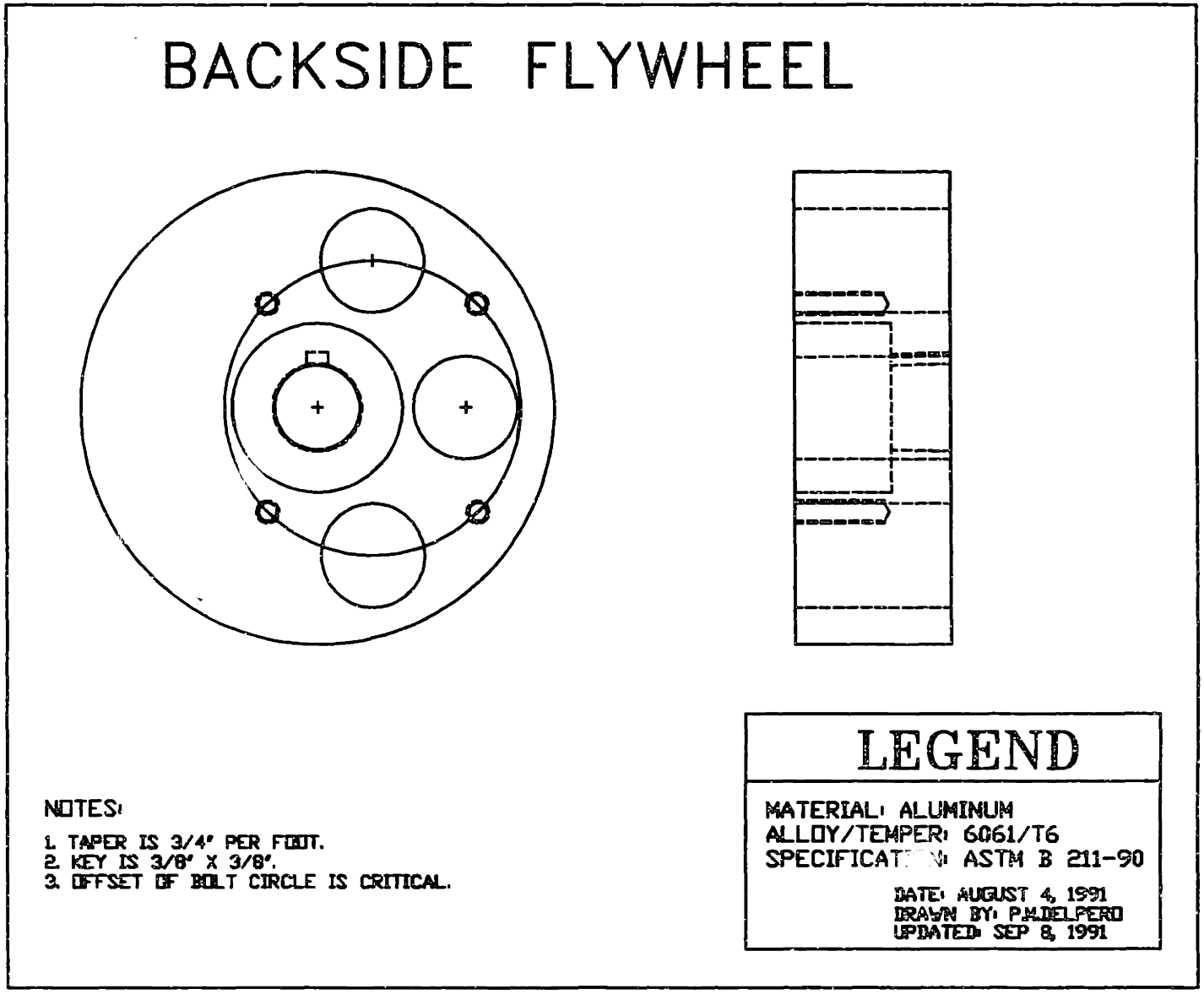

Figure II.9 Flywheel Outline

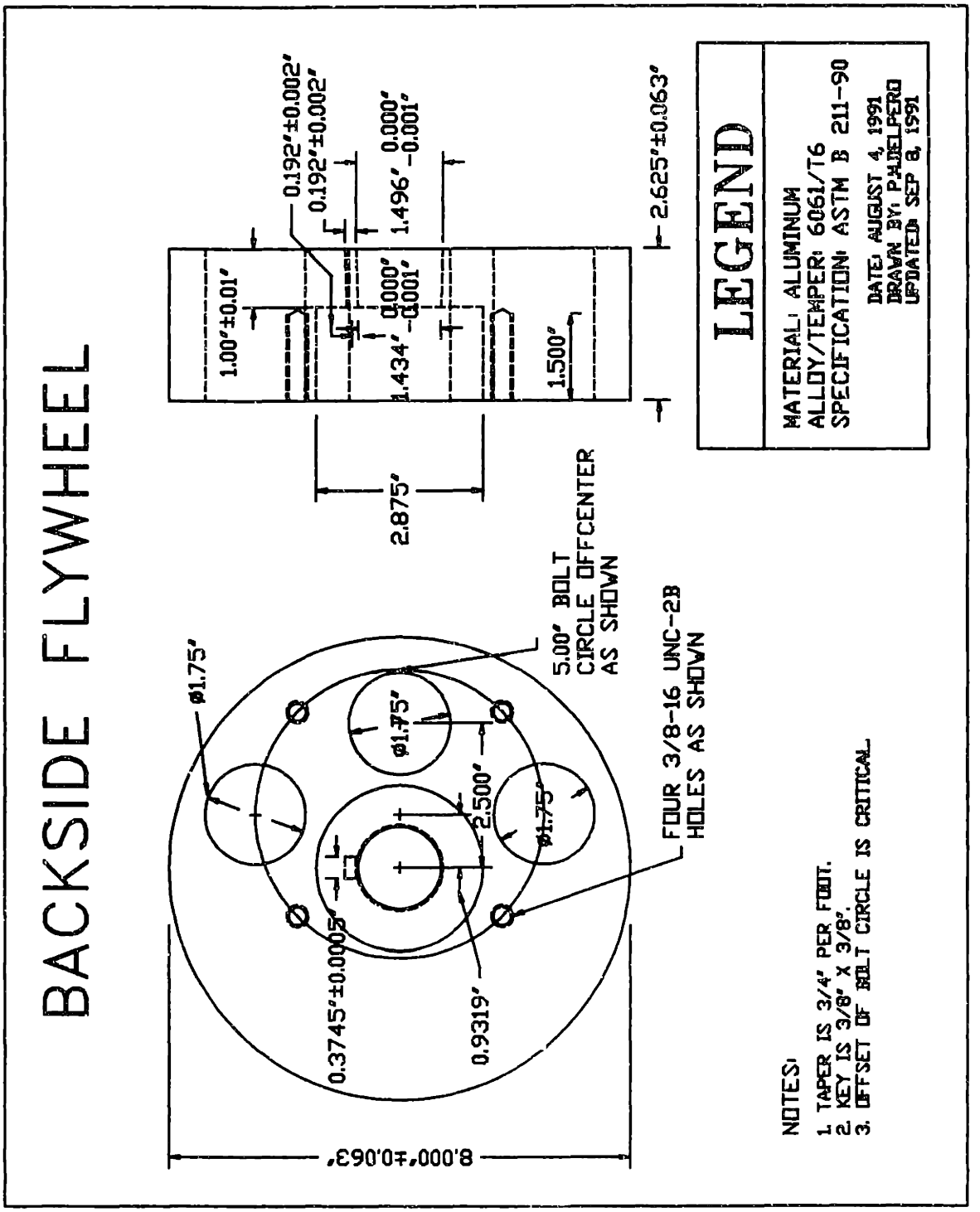

Figure II.10 Flywheel Detail Drawing

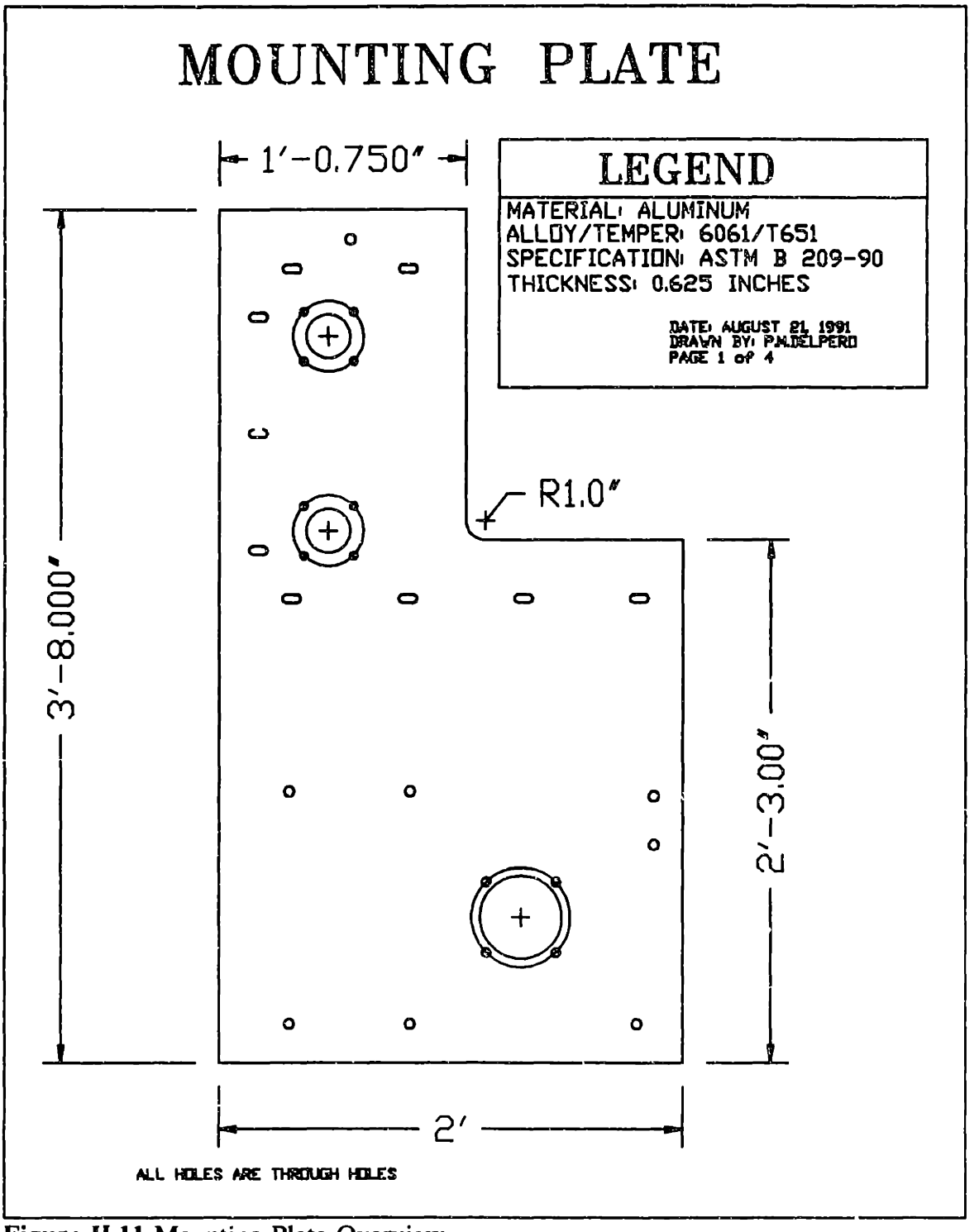

Figure II.11 Mounting Plate Overview

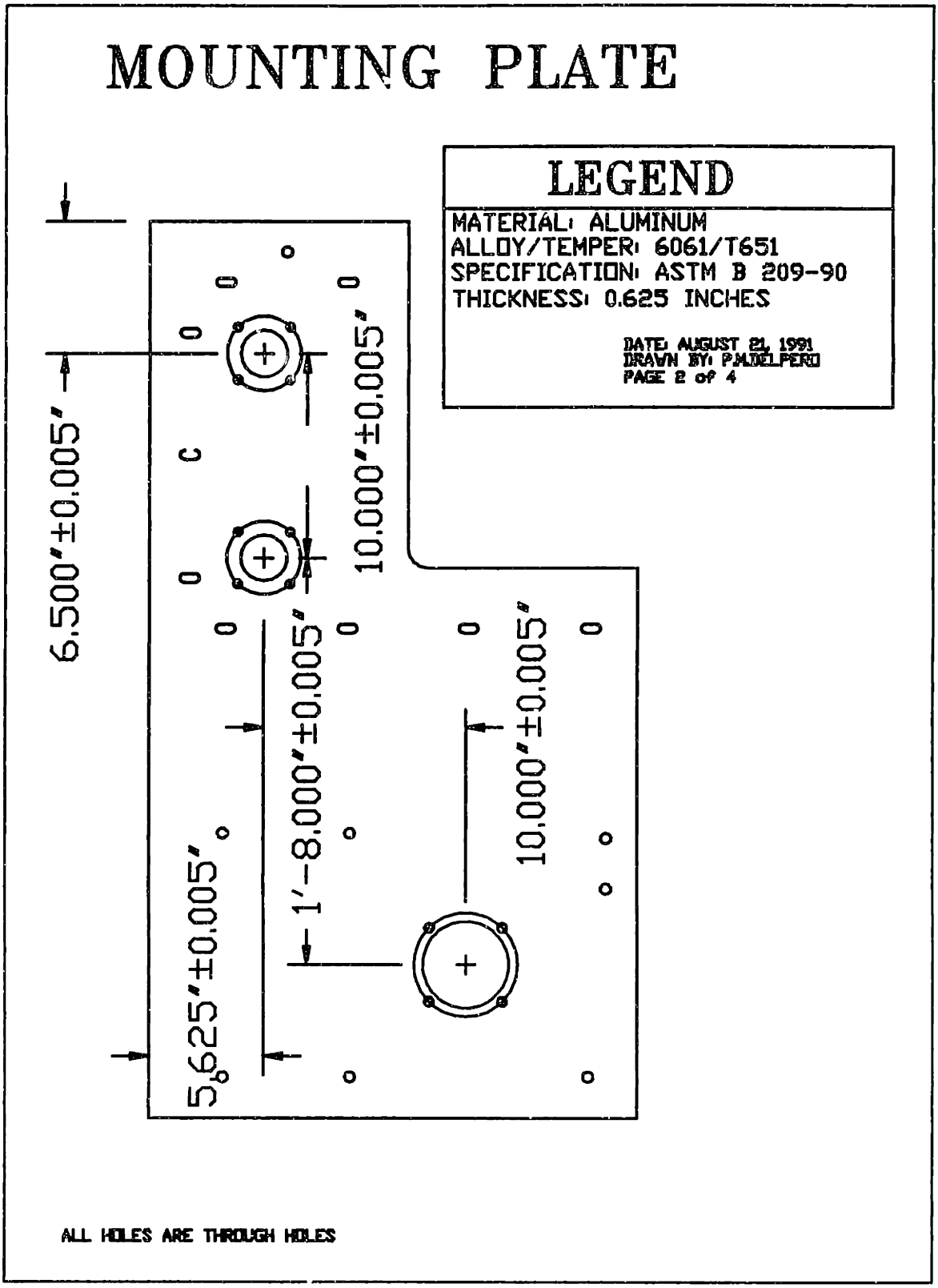

Figure II.12 Mounting Hole Locations

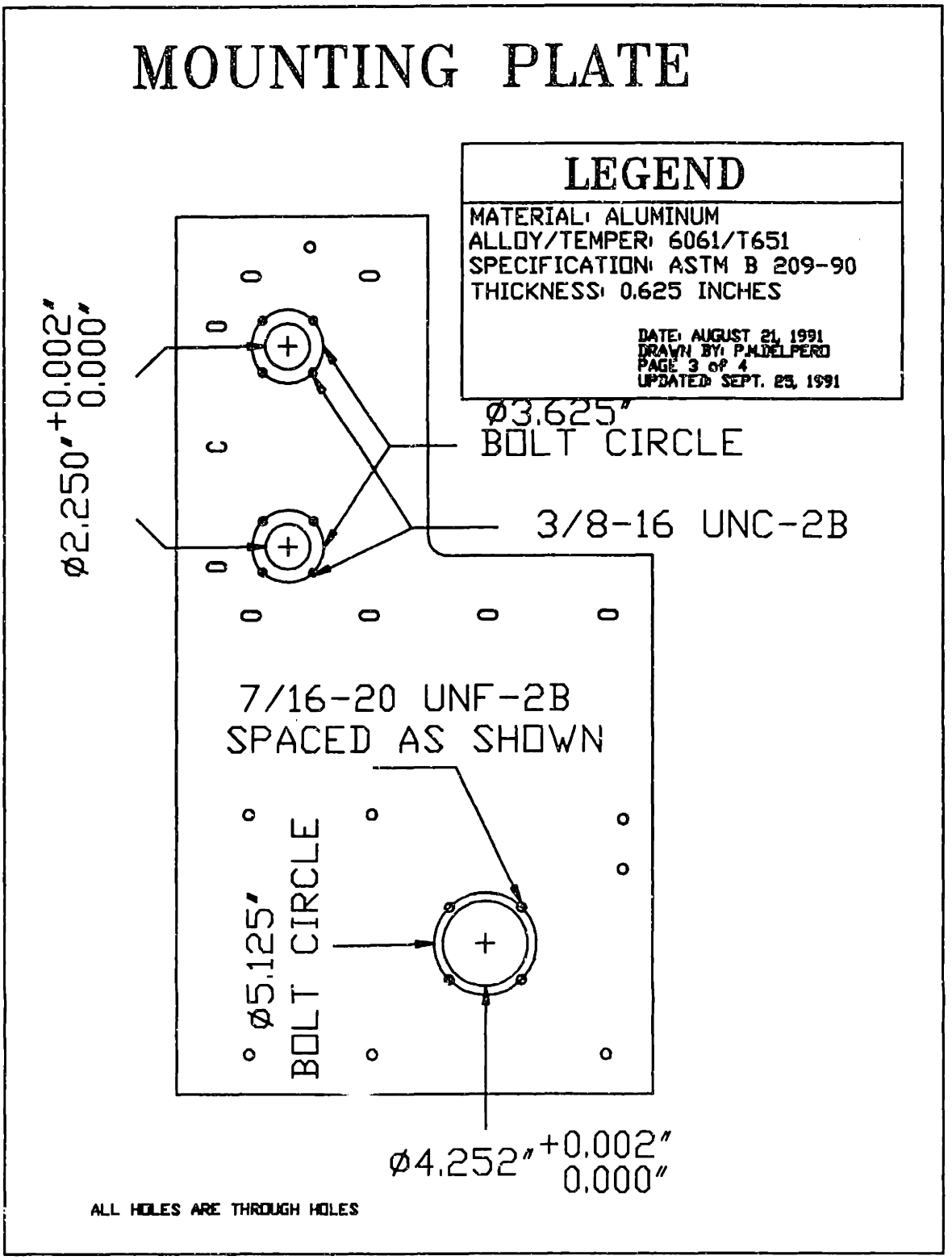

Figure II.13 Mounting Plate Bolt Locations

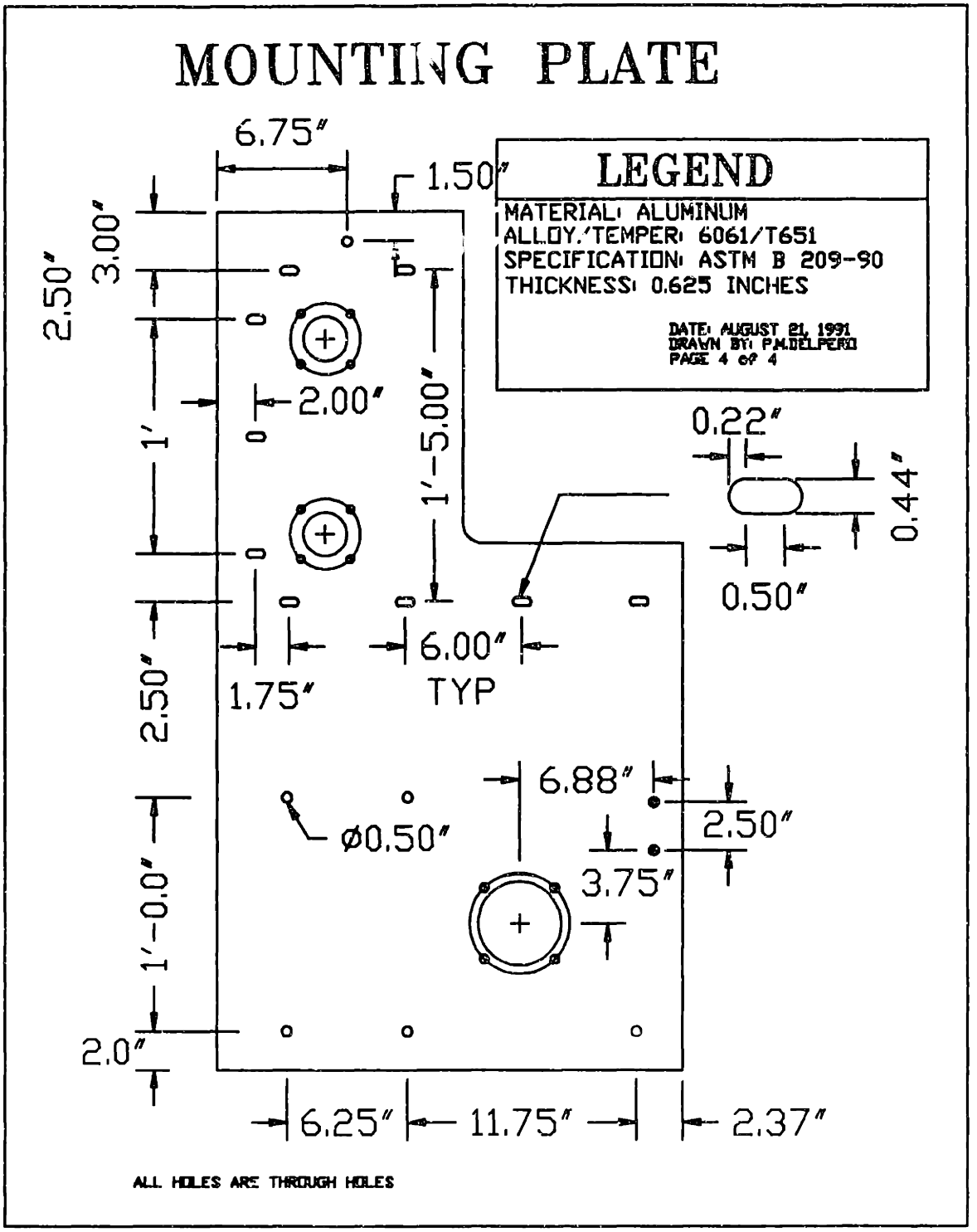

Figure II.14 Mounting Plate Bolt Hole Locations

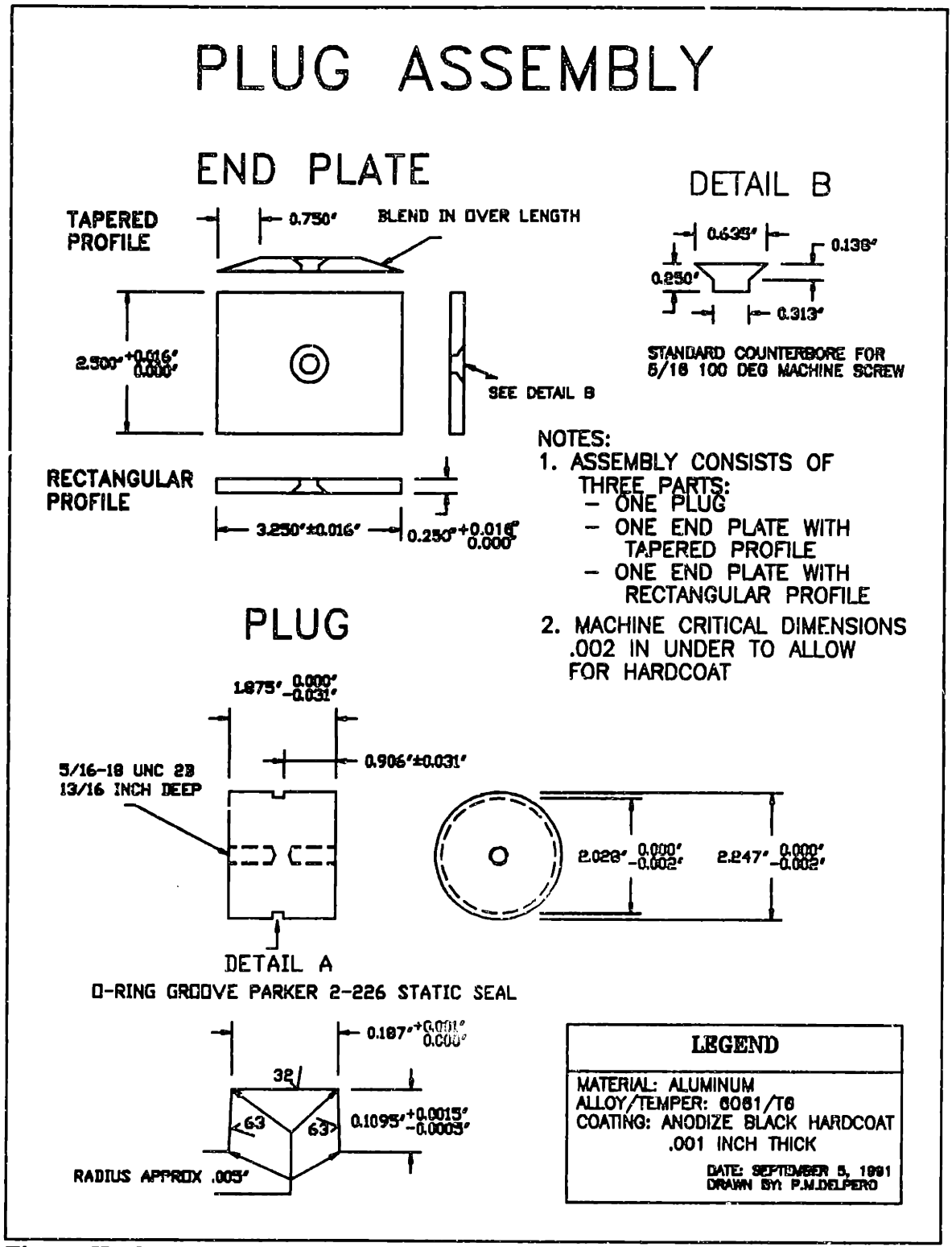

Figure II.15 Window Plug

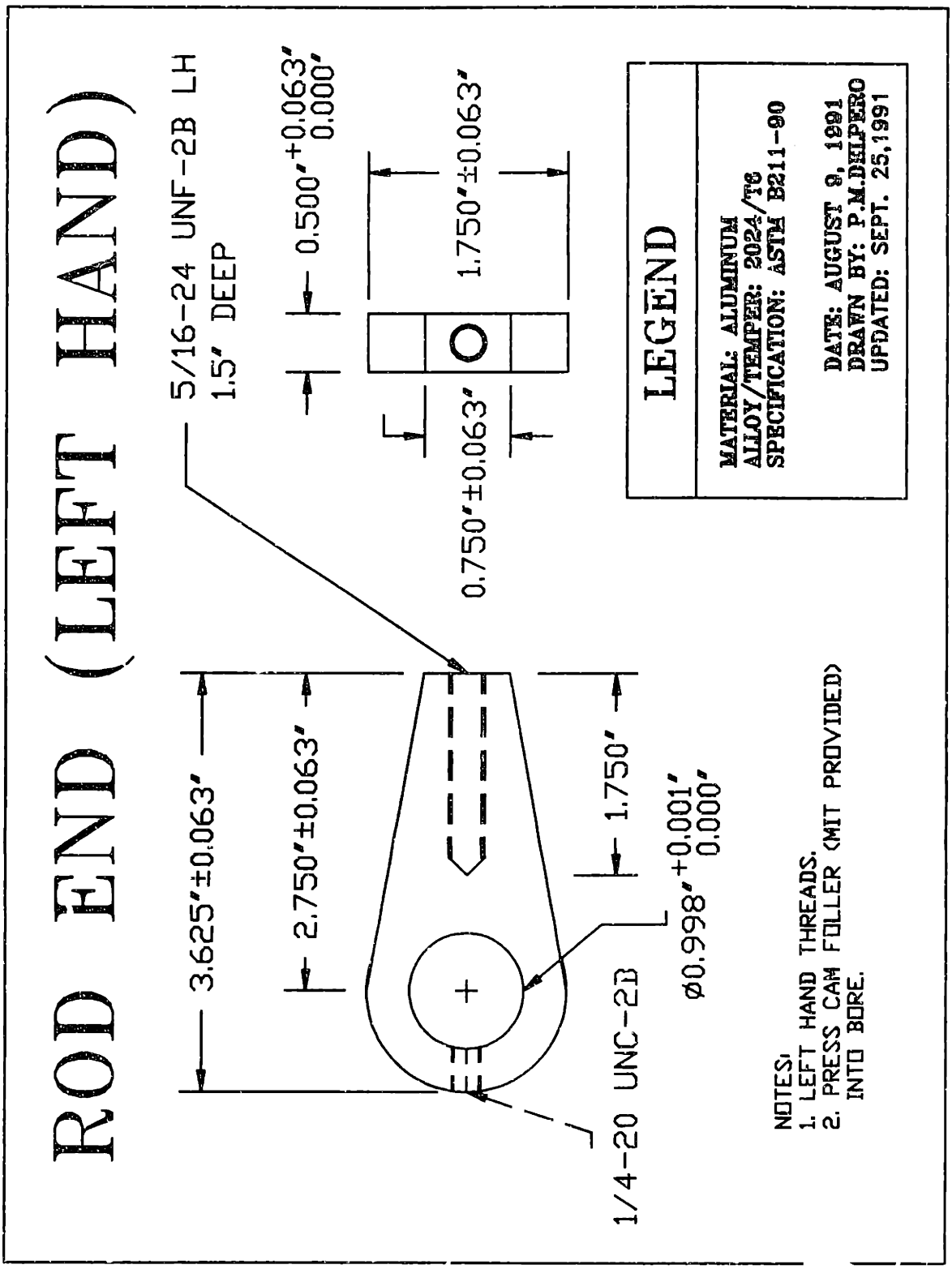

Figure II.16 Left Hand Rod End

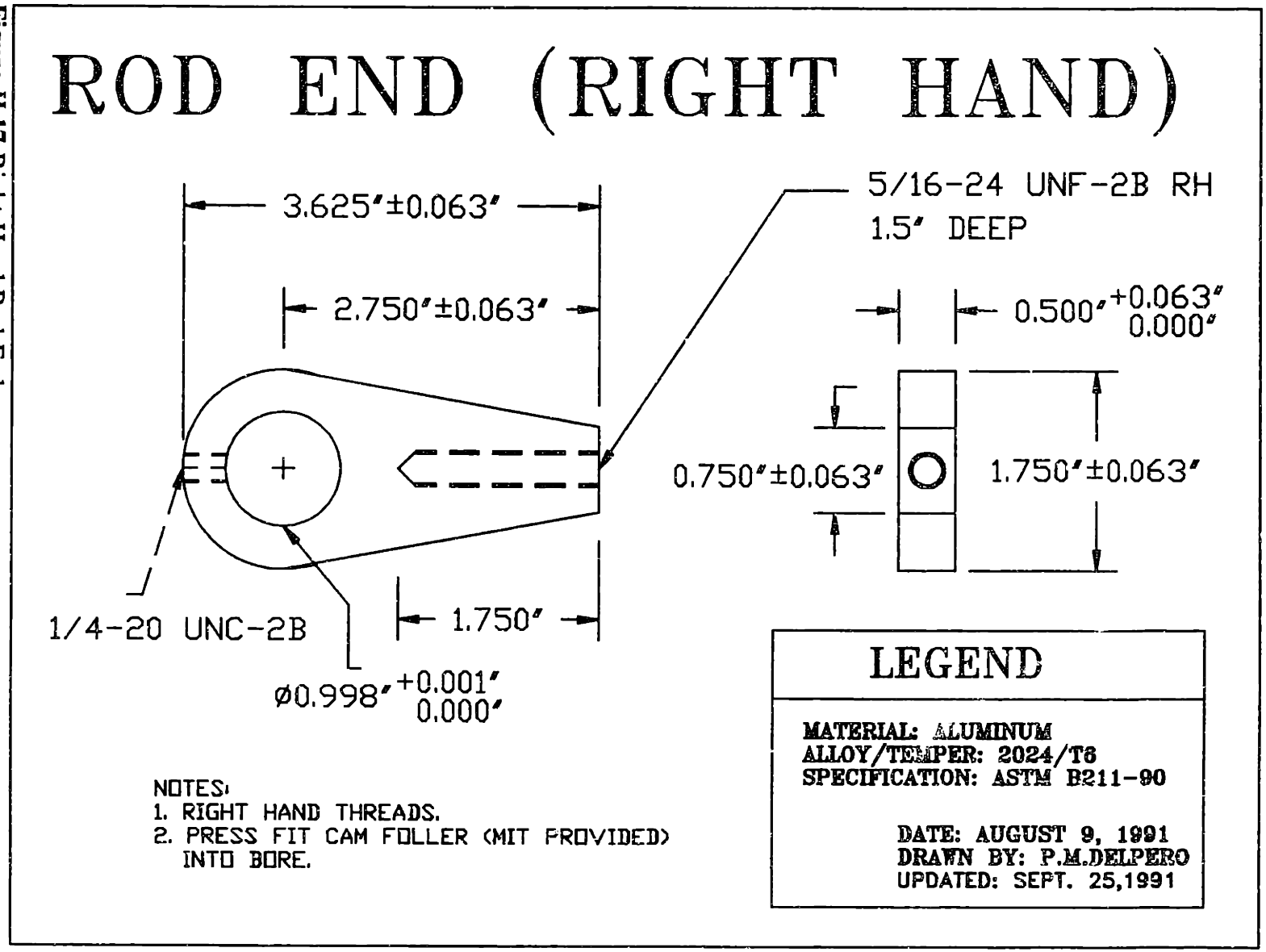

Figure II.17 Right Hand Rod End

Figure II.18 Drive Shaft

SHAFT

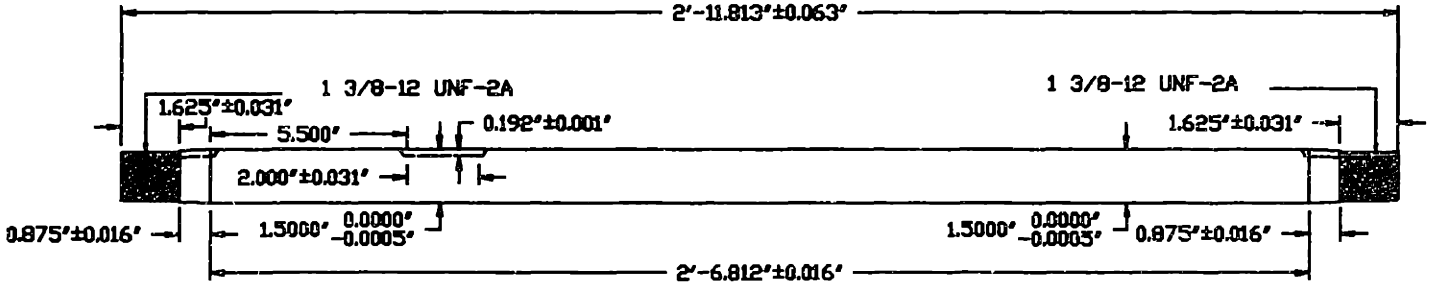

ENLARGED CROSSSECTION

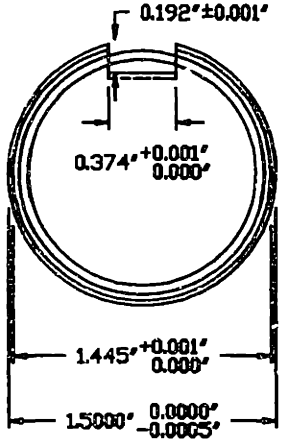

NOTES:
1. THREE KEYWAYS ARE STANDARD 3/8 X 3/8.
2. TAPER IS 3/4 INCH PER FOOT ON THE DIAMETER.

LEGEND

MATERIAL: CARBON STEEL
TYPE: COLD-DRAWN AND STRESS RELIEVED
GRADE: 1050 OR 1144
SPECIFICATION: ASTM A 311 -90B

DATE: AUGUST 4, 1991
DRAWN BY: P.M.DELPERO
UPDATED: SEPTEMBER 8, 1991

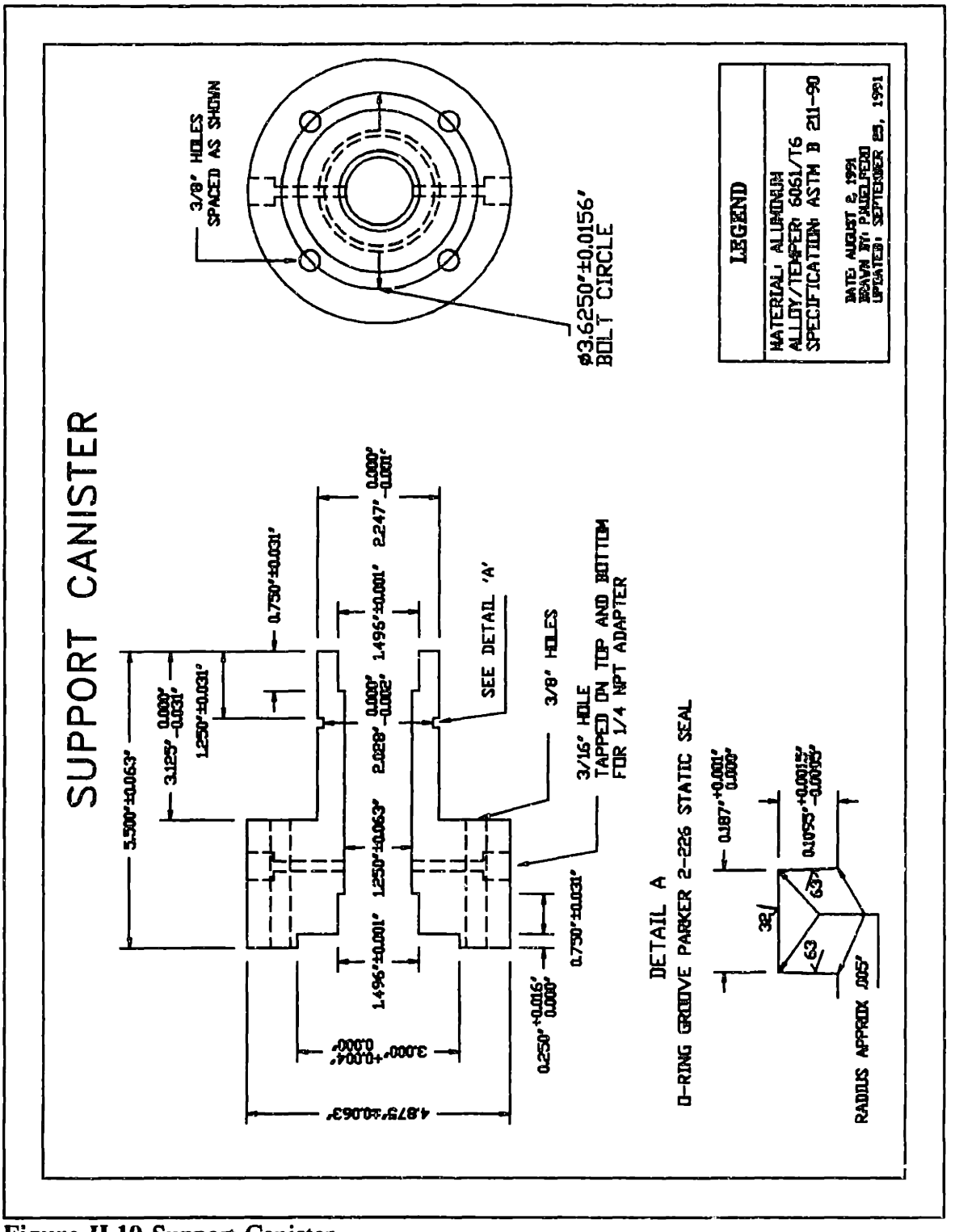

Figure II.19 Support Canister

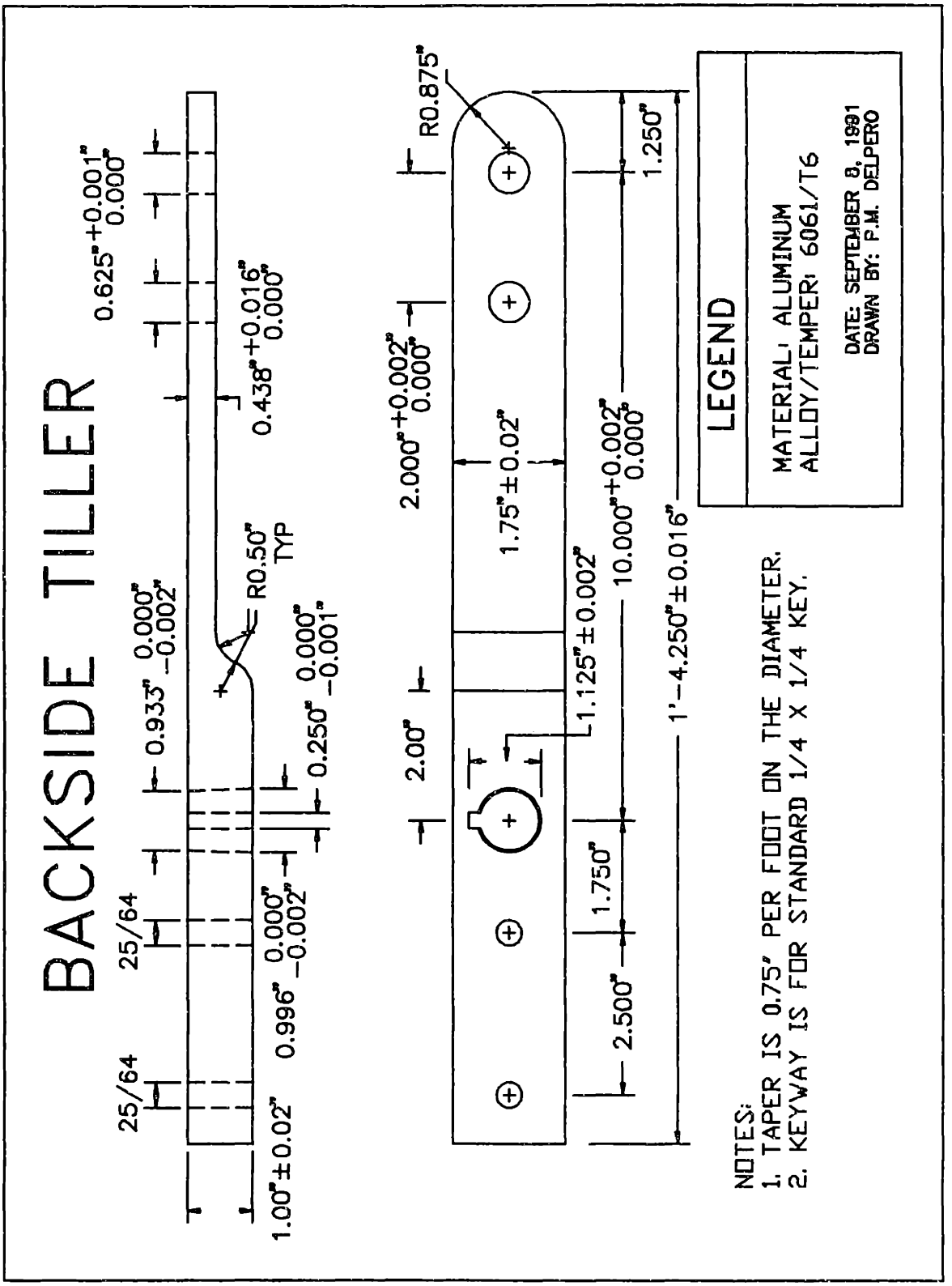

Figure II.20 Backside Tiller

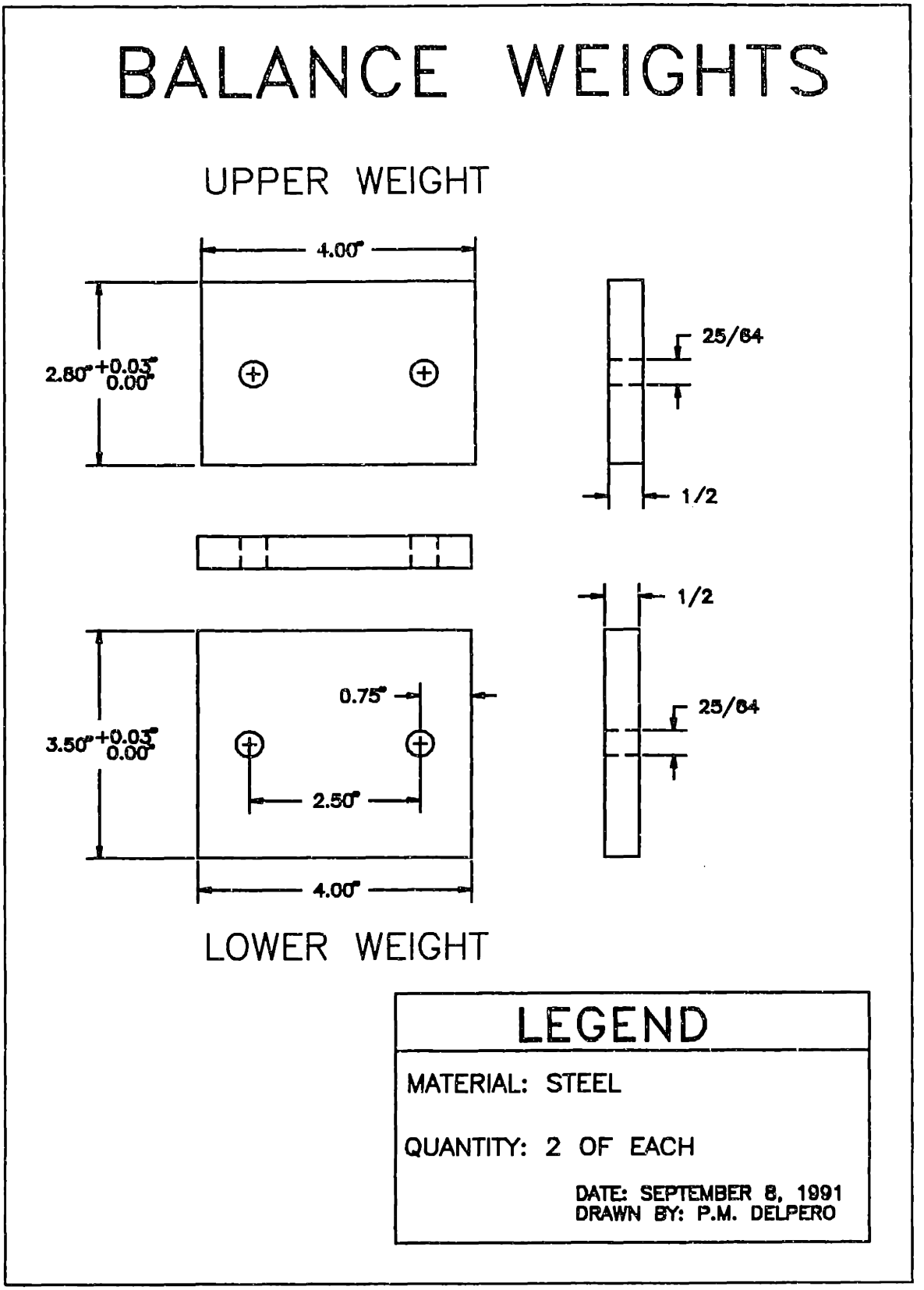

Figure II.21 Tiller Balance Weights

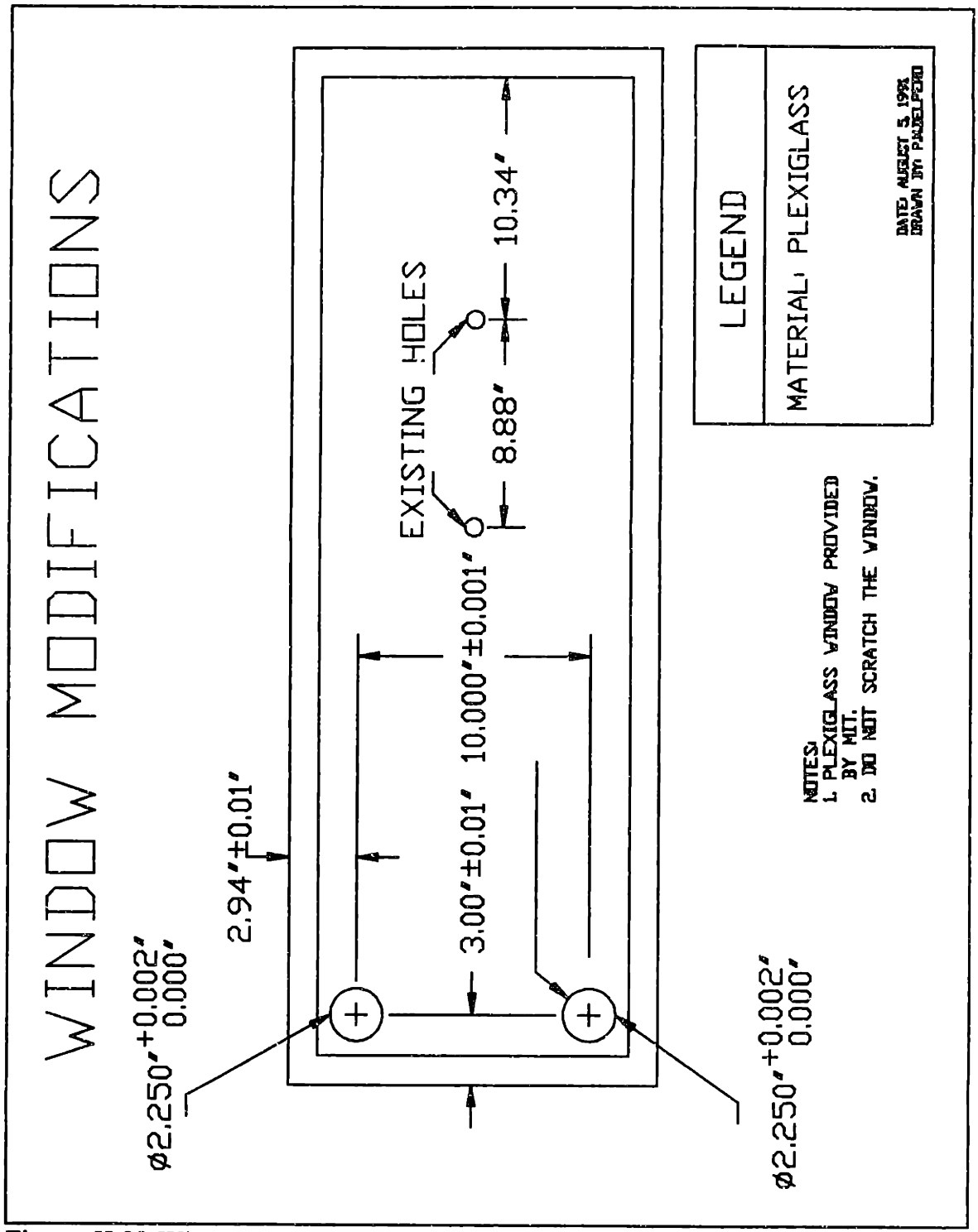

Figure II.22 Window Modification

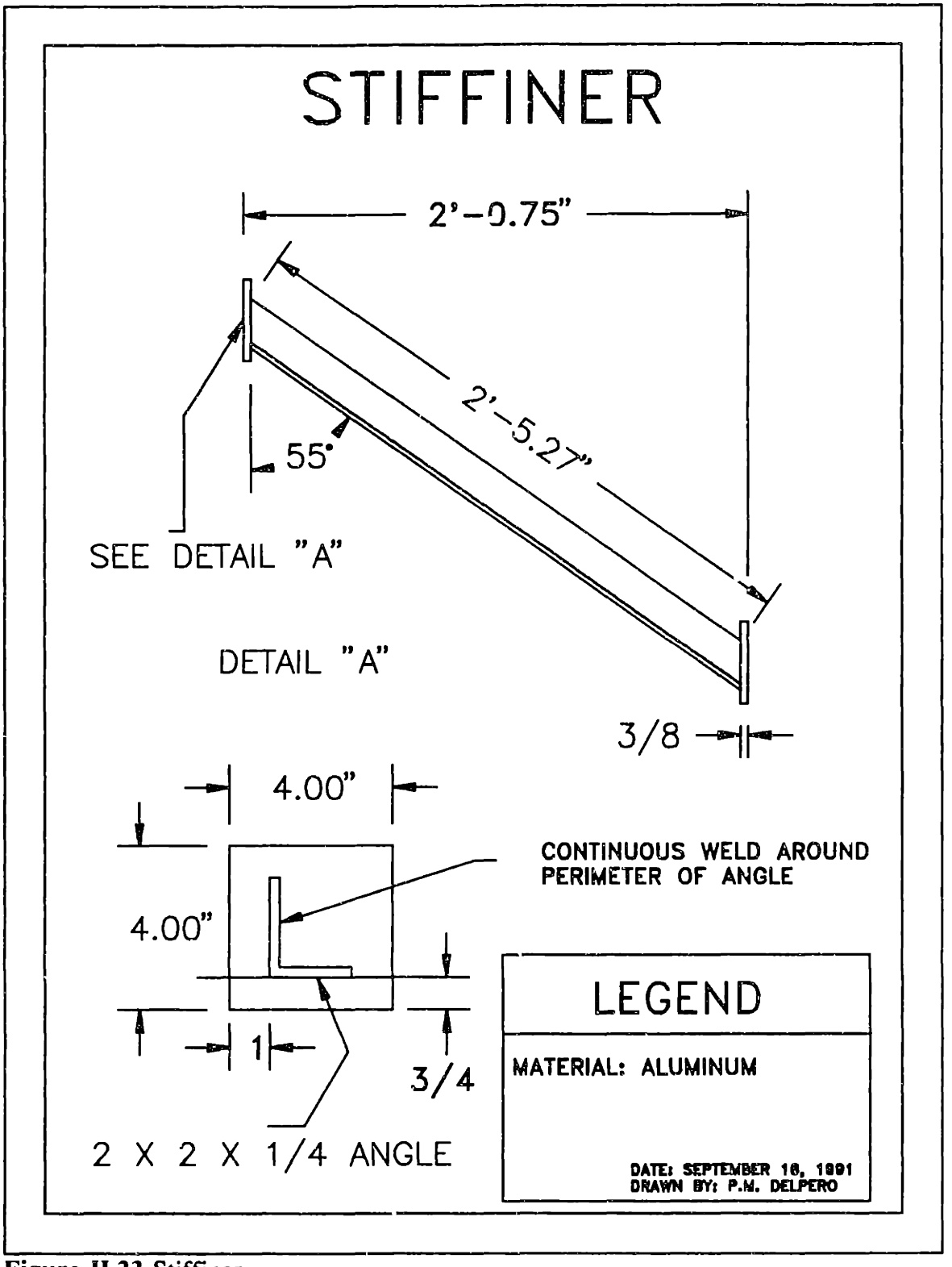

Figure II.23 Stiffiner

Appendix III

Steady State Velocity Profiles

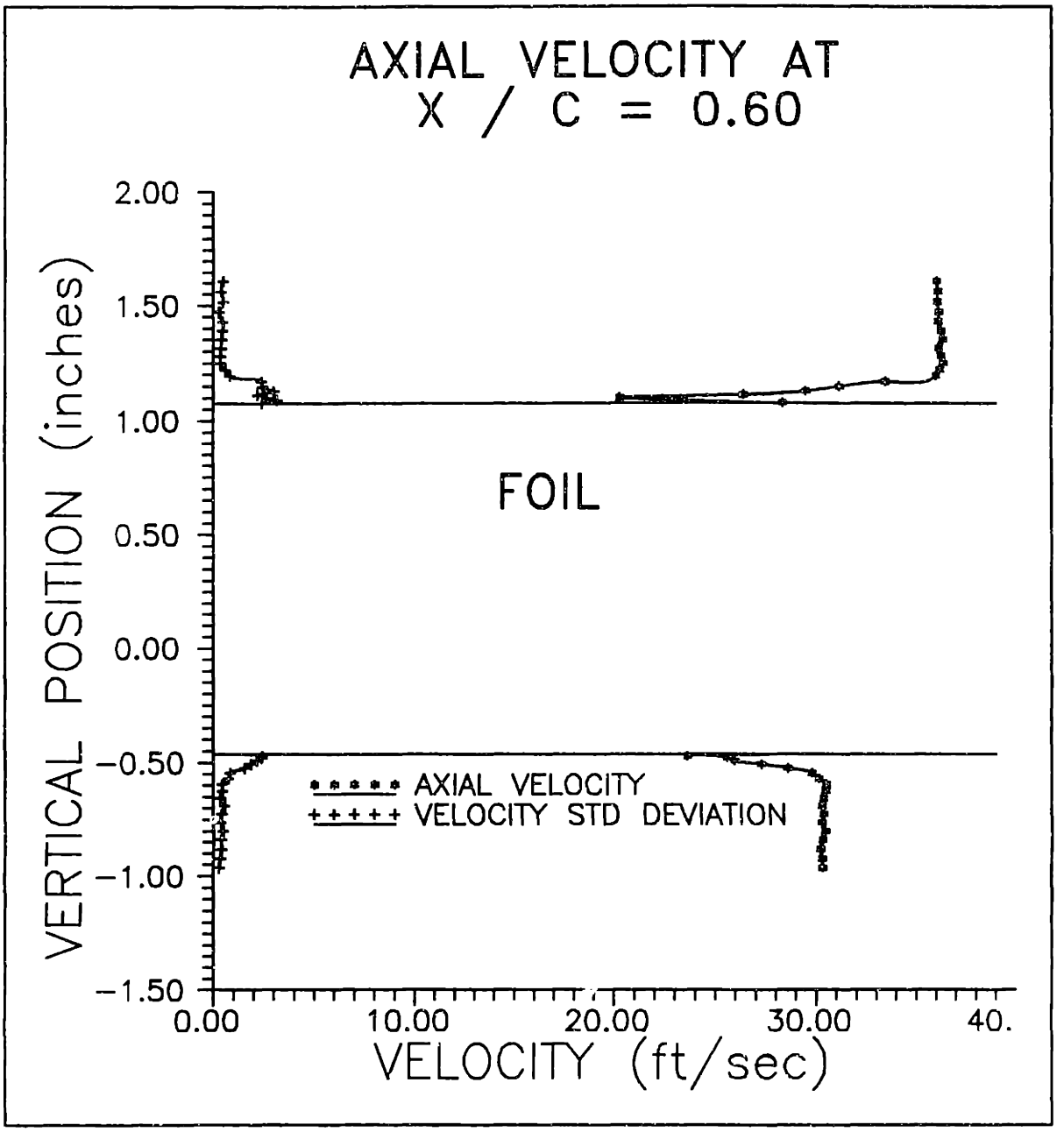

Figure III.1 Velocity Profile at X/C = 60%

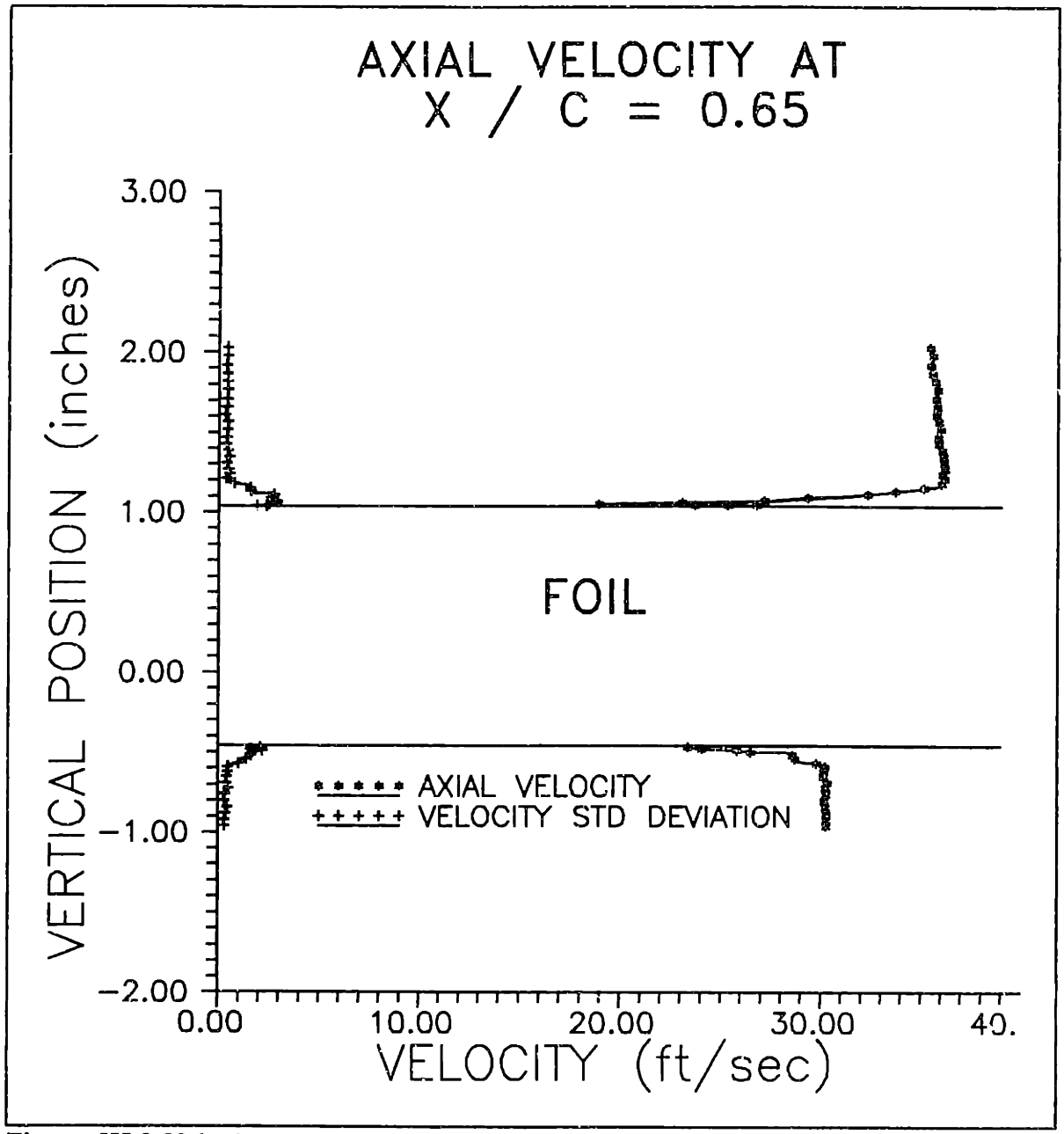

Figure III.2 Velocity Profile at X/C = 65%

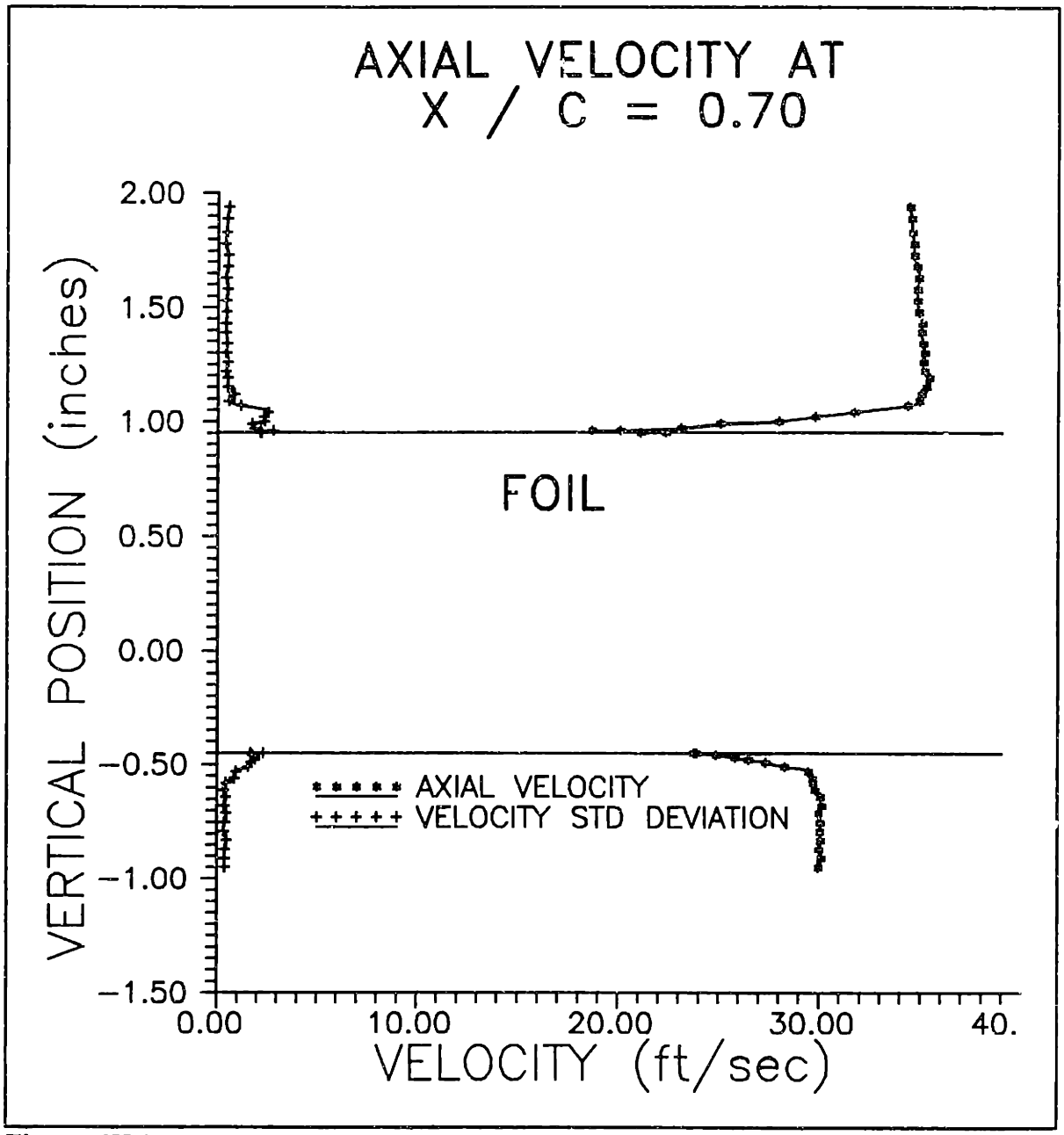

Figure III.3 Velocity Profile at X/C = 70%

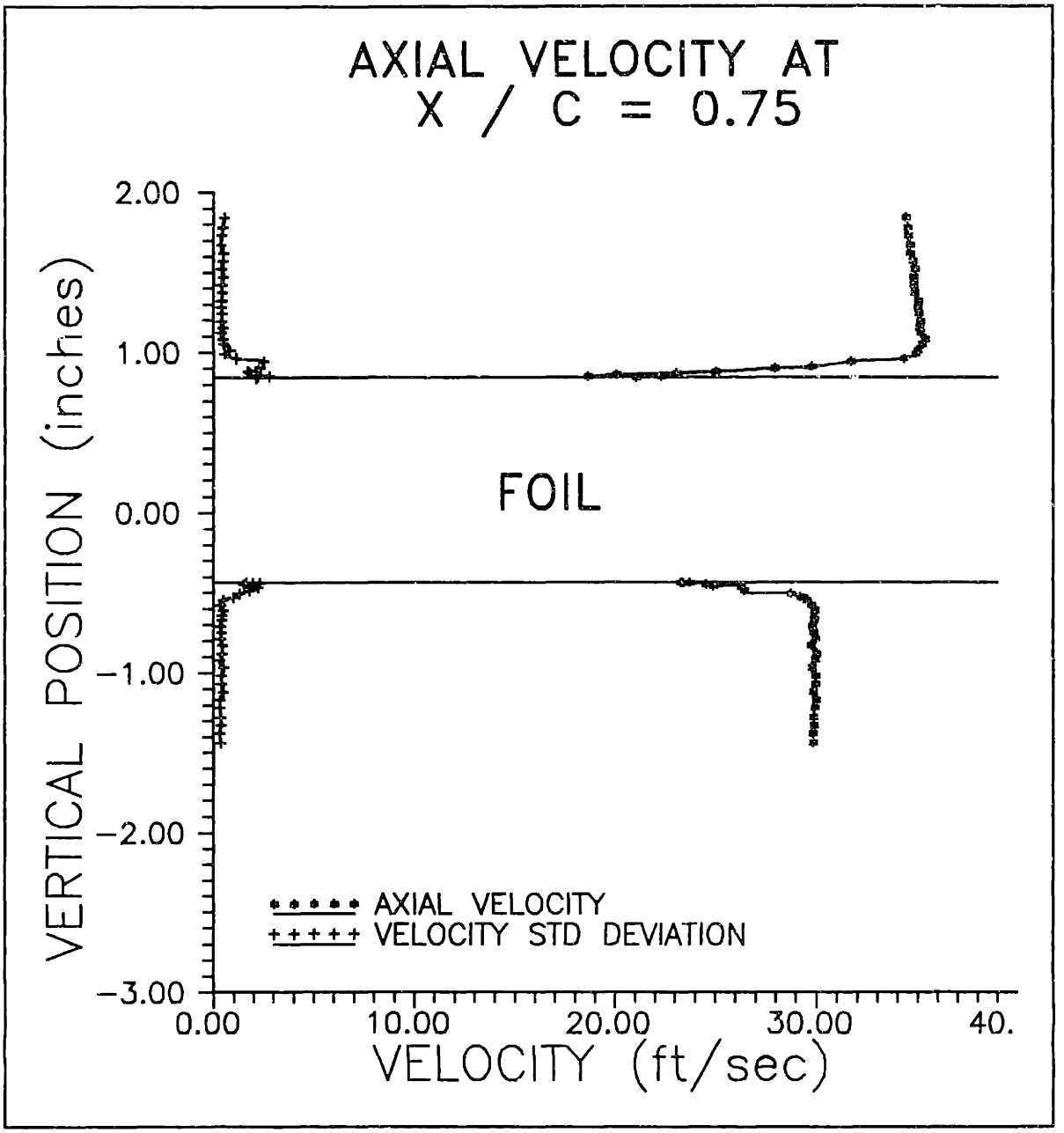

Figure III.4 Velocity Profile at X/C = 75%

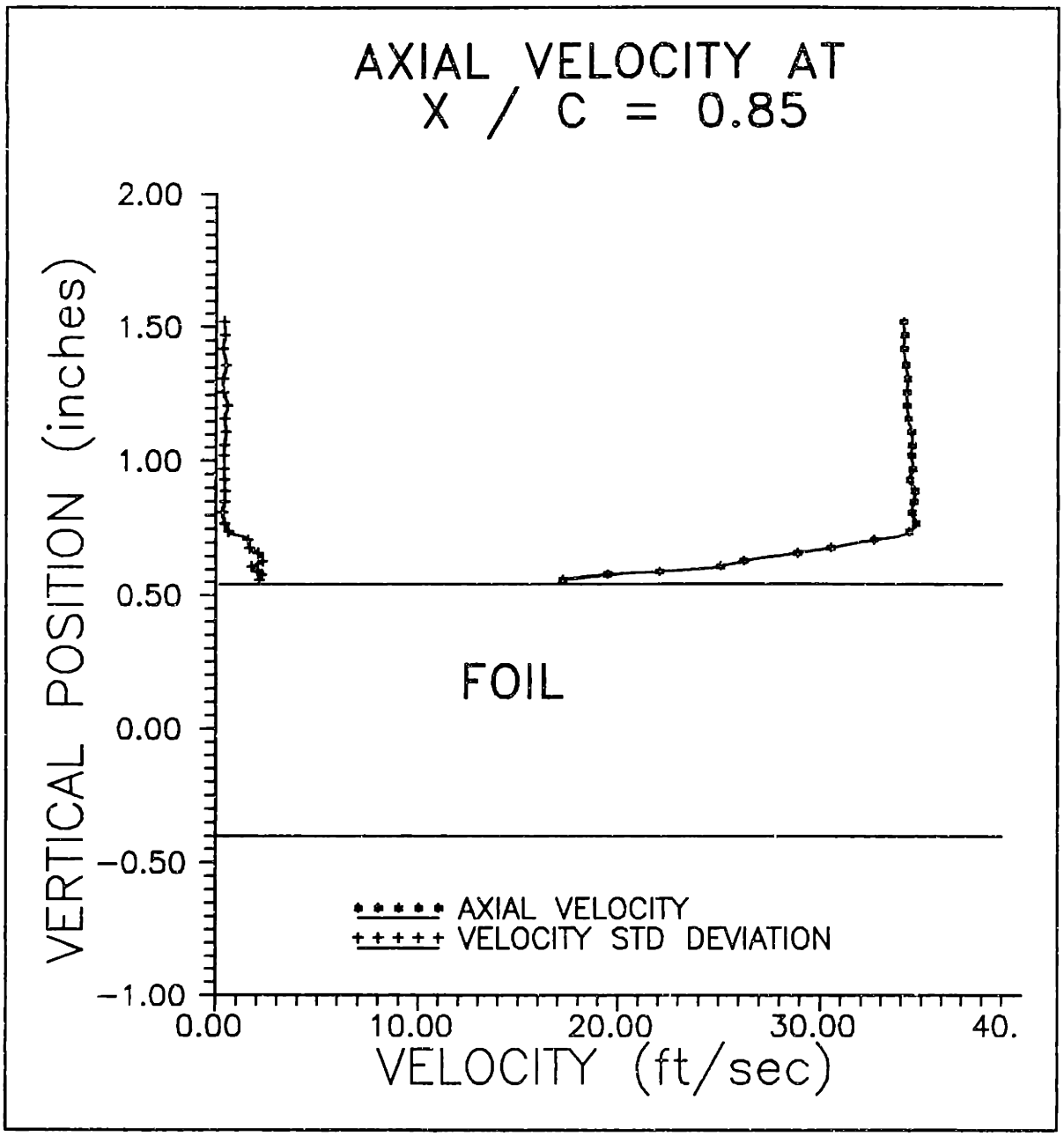

Figure III.5 Velocity Profile at X/C = 85%

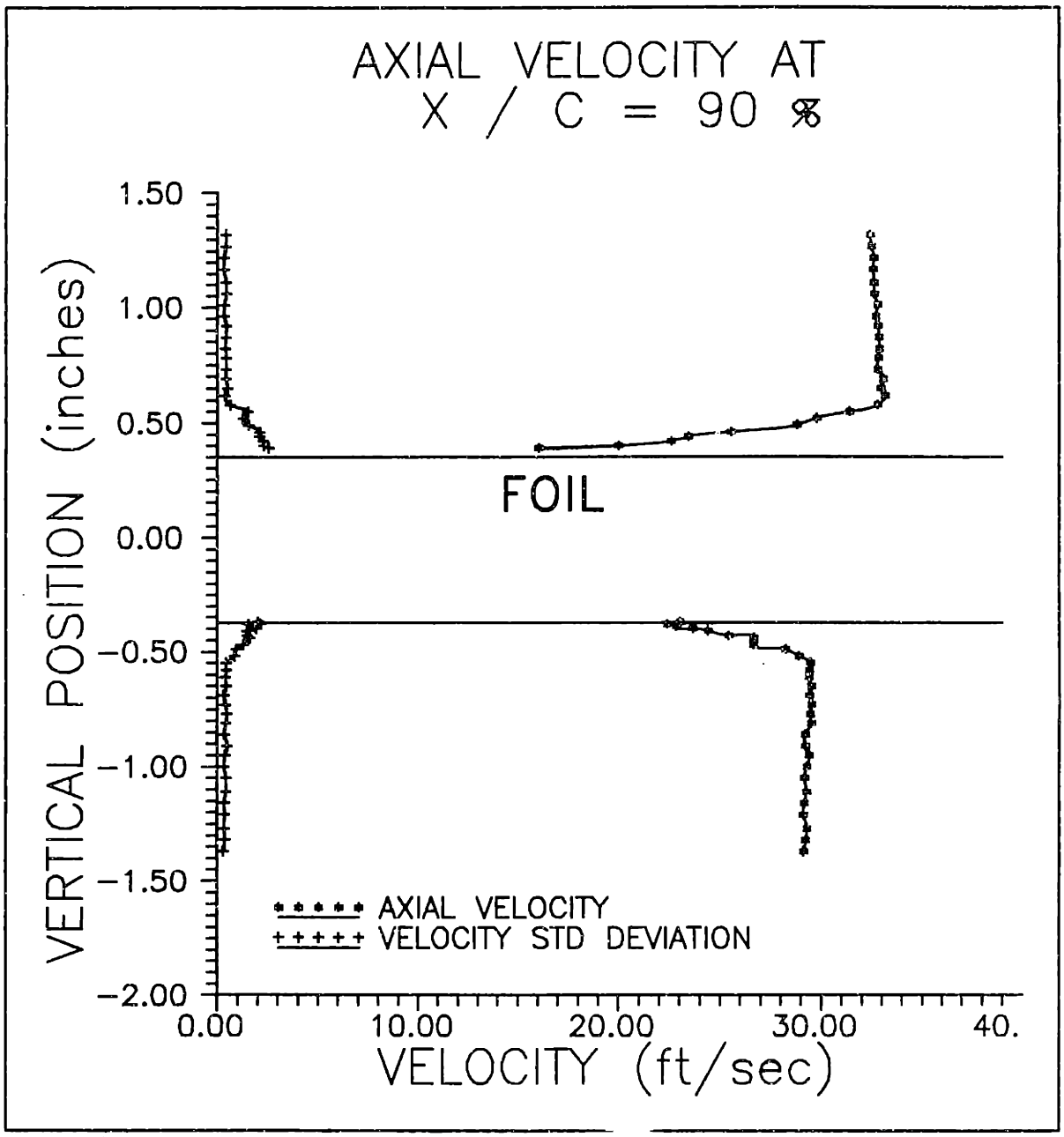

Figure III.6 Velocity Profile at X/C = 90%

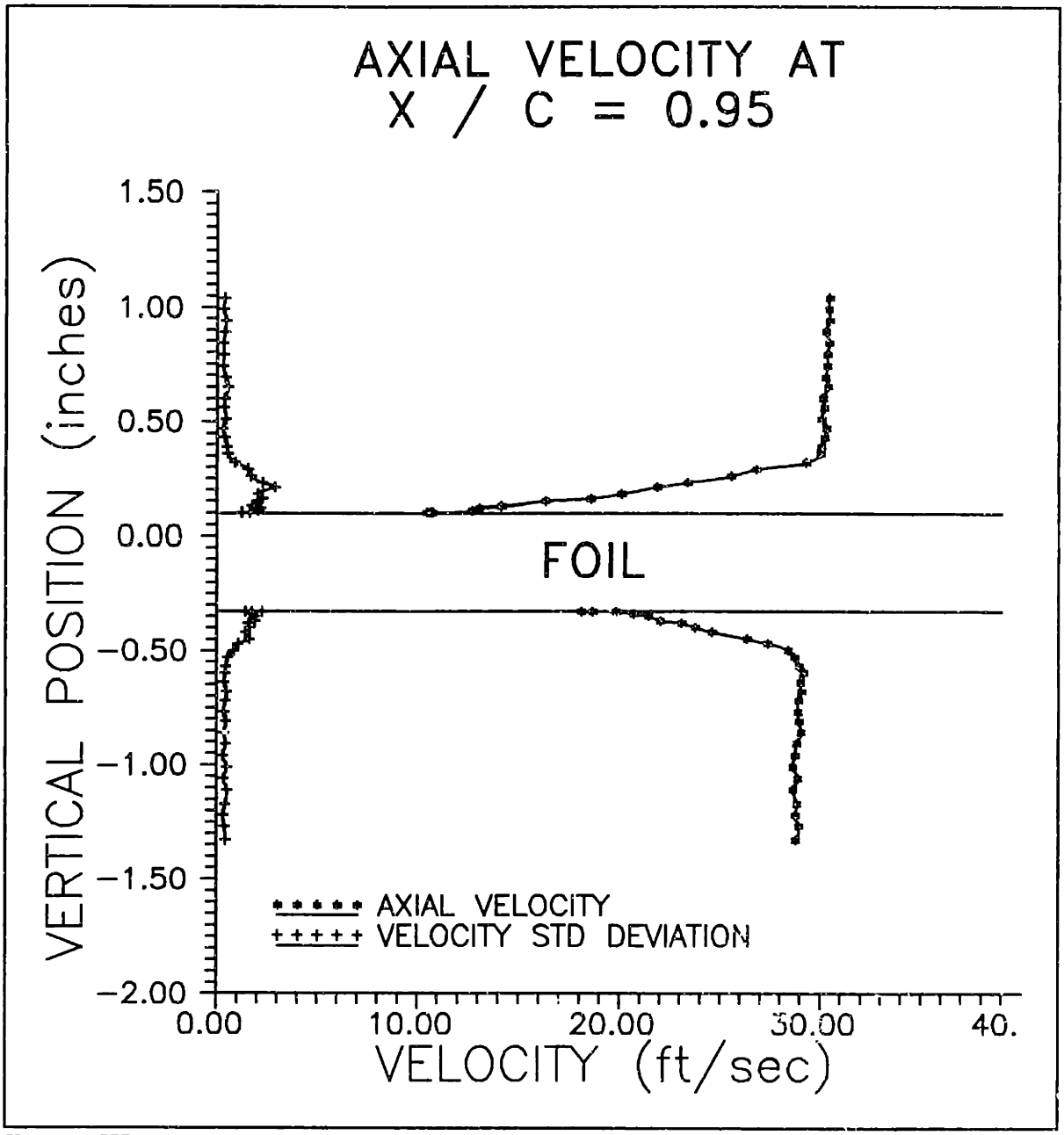

Figure III.7 Velocity Profile at X/C = 95%

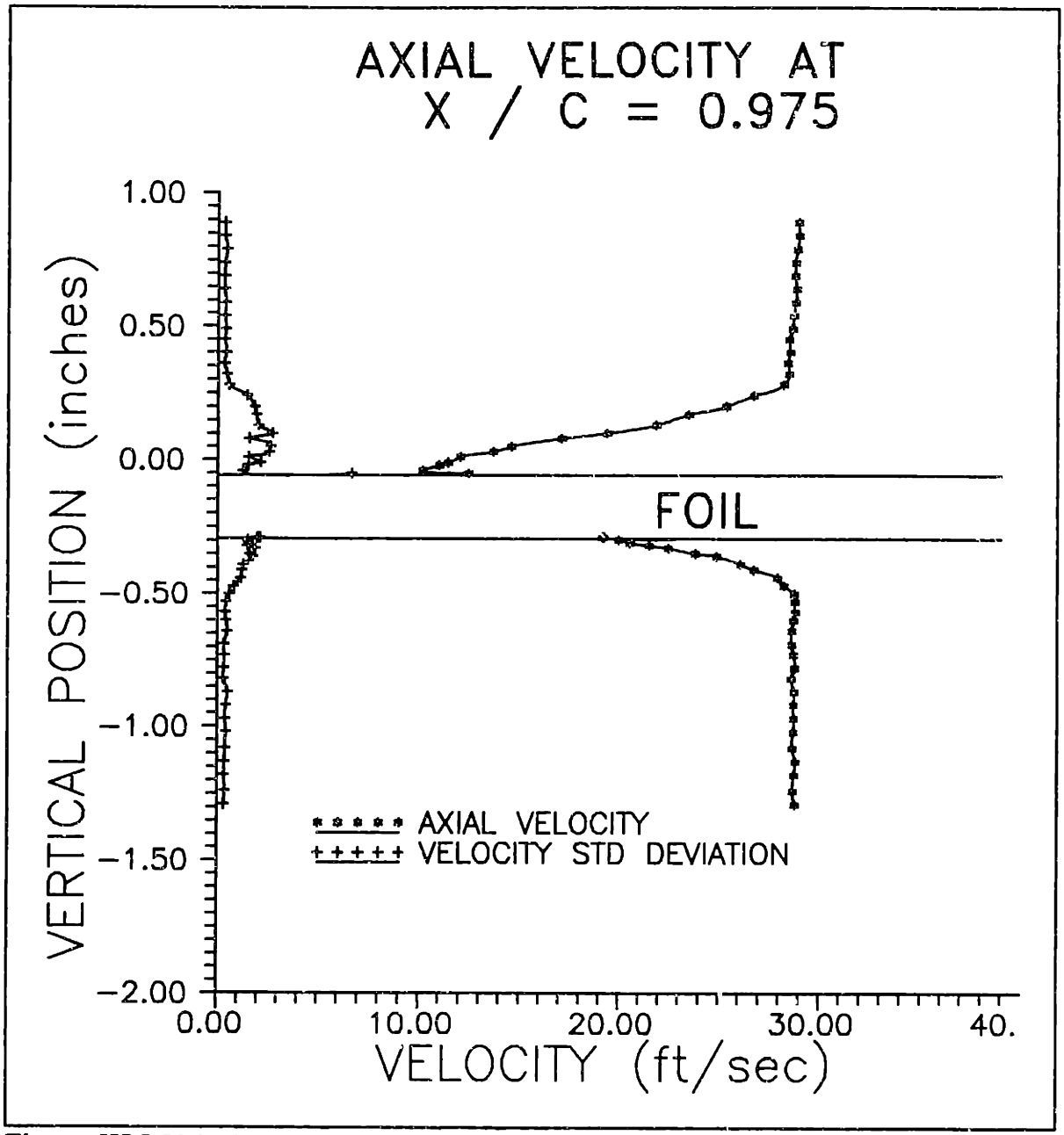

Figure III.8 Velocity Profile at X/C = 97.5%

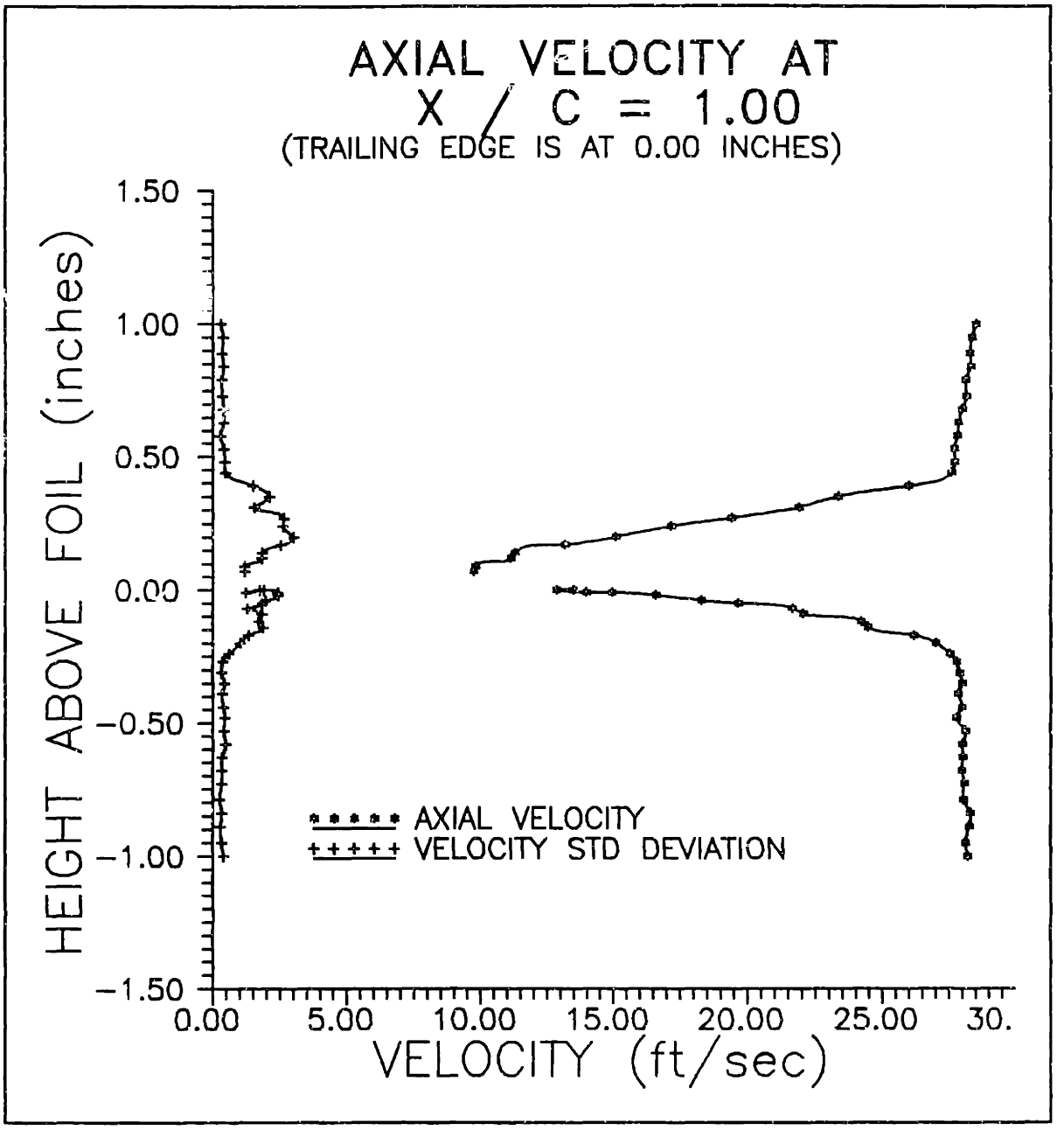

Figure III.9 Velocity Profile at X/C = 100%

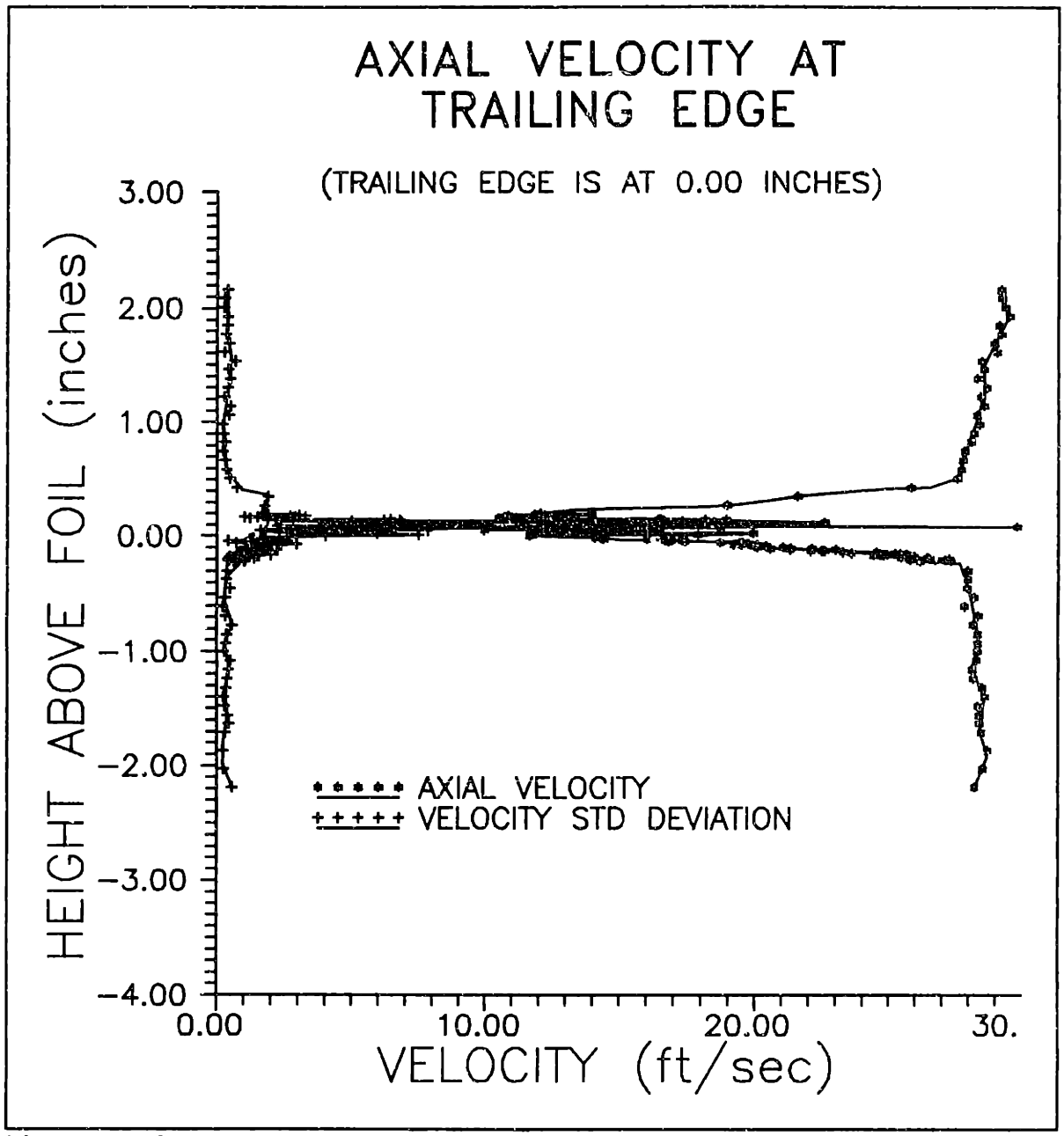

Figure III.10 Velocity Profile at Trailing Edge

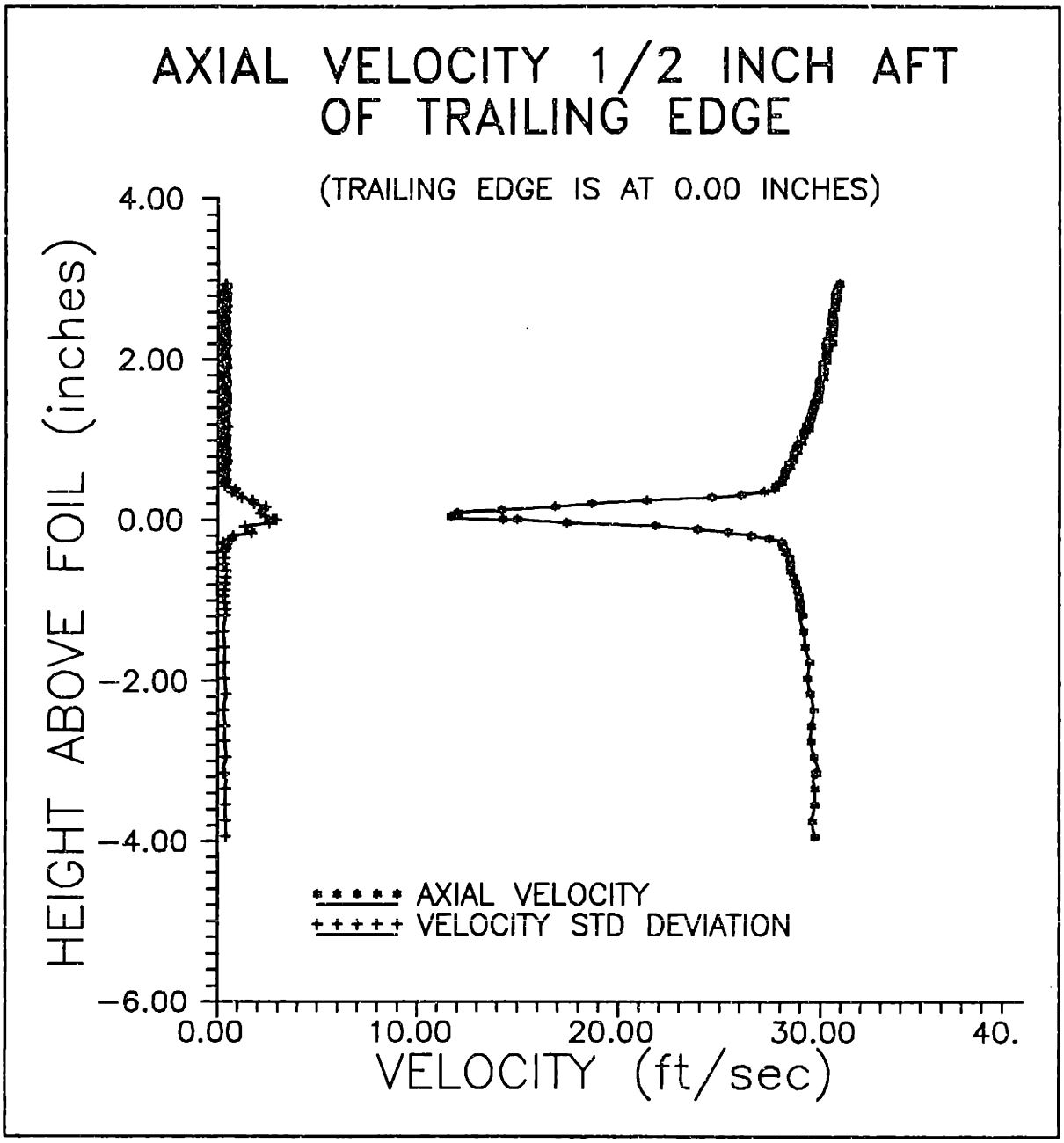

Figure III.11 Velocity Profile 1/2 Inch Aft of Trailing Edge

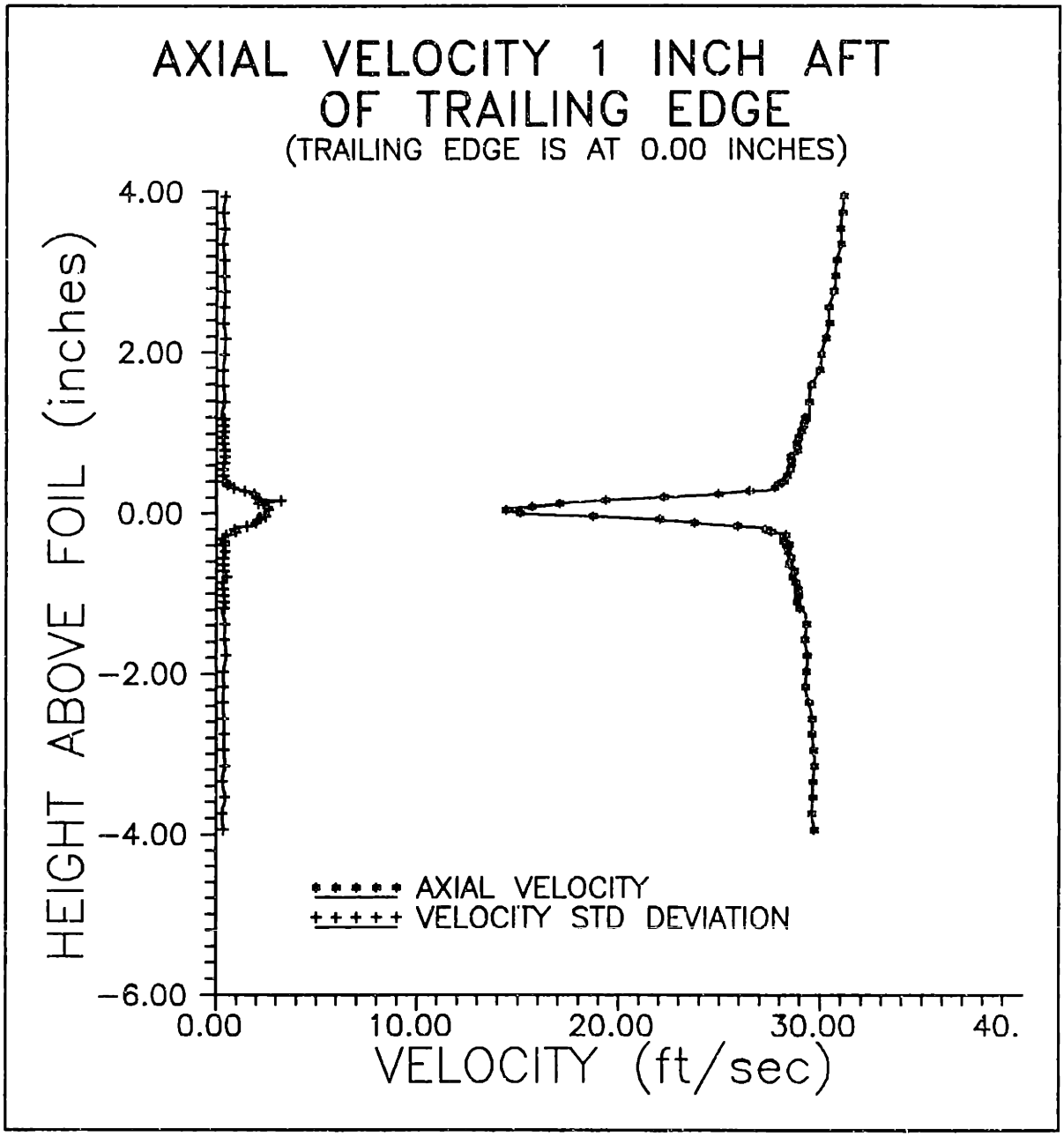

Figure III.12 Velocity Profile 1 Inch Aft of Trailing Edge

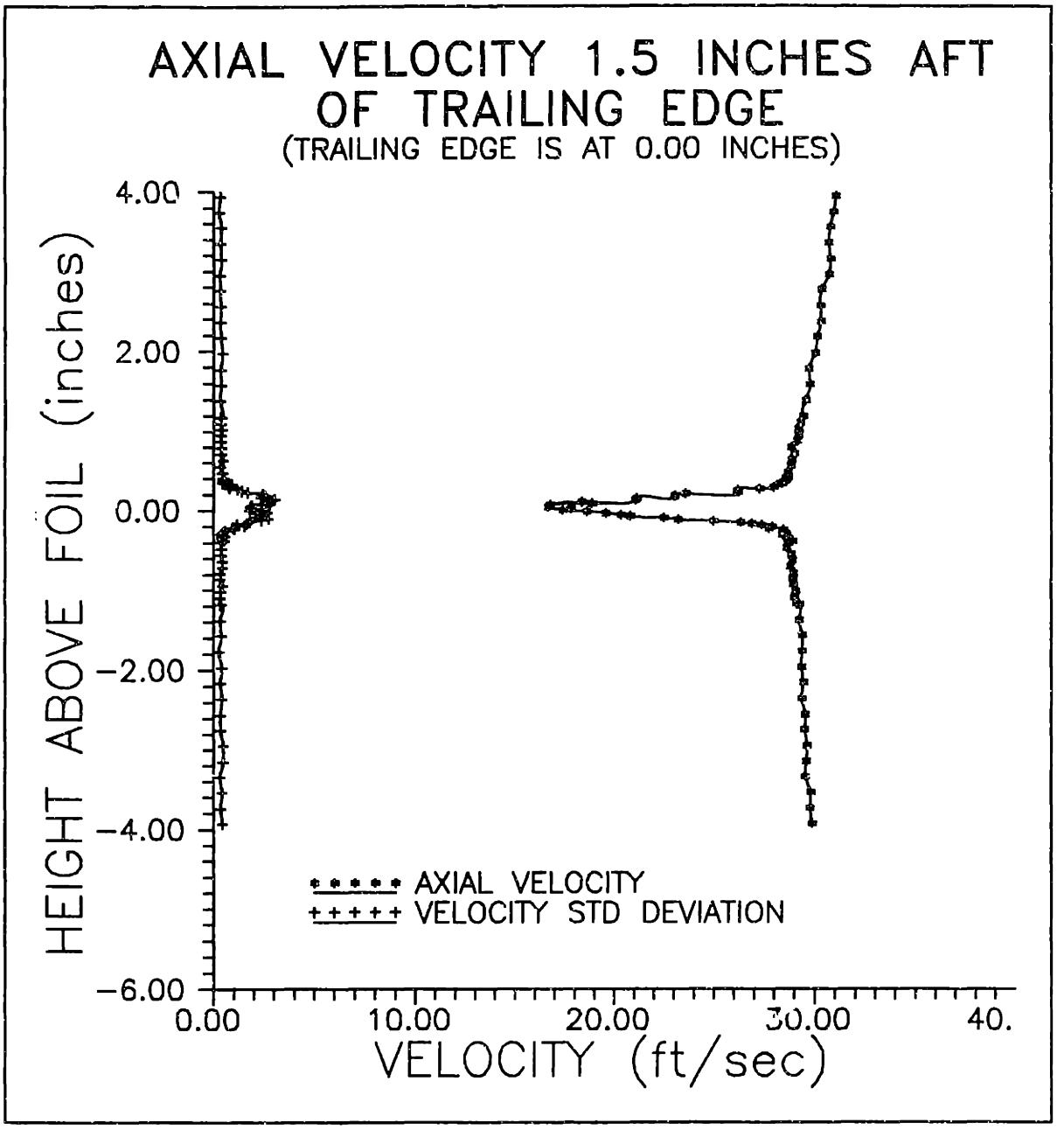

Figure III.13 Velocity Profile 1.5 Inches Aft of Trailing Edge

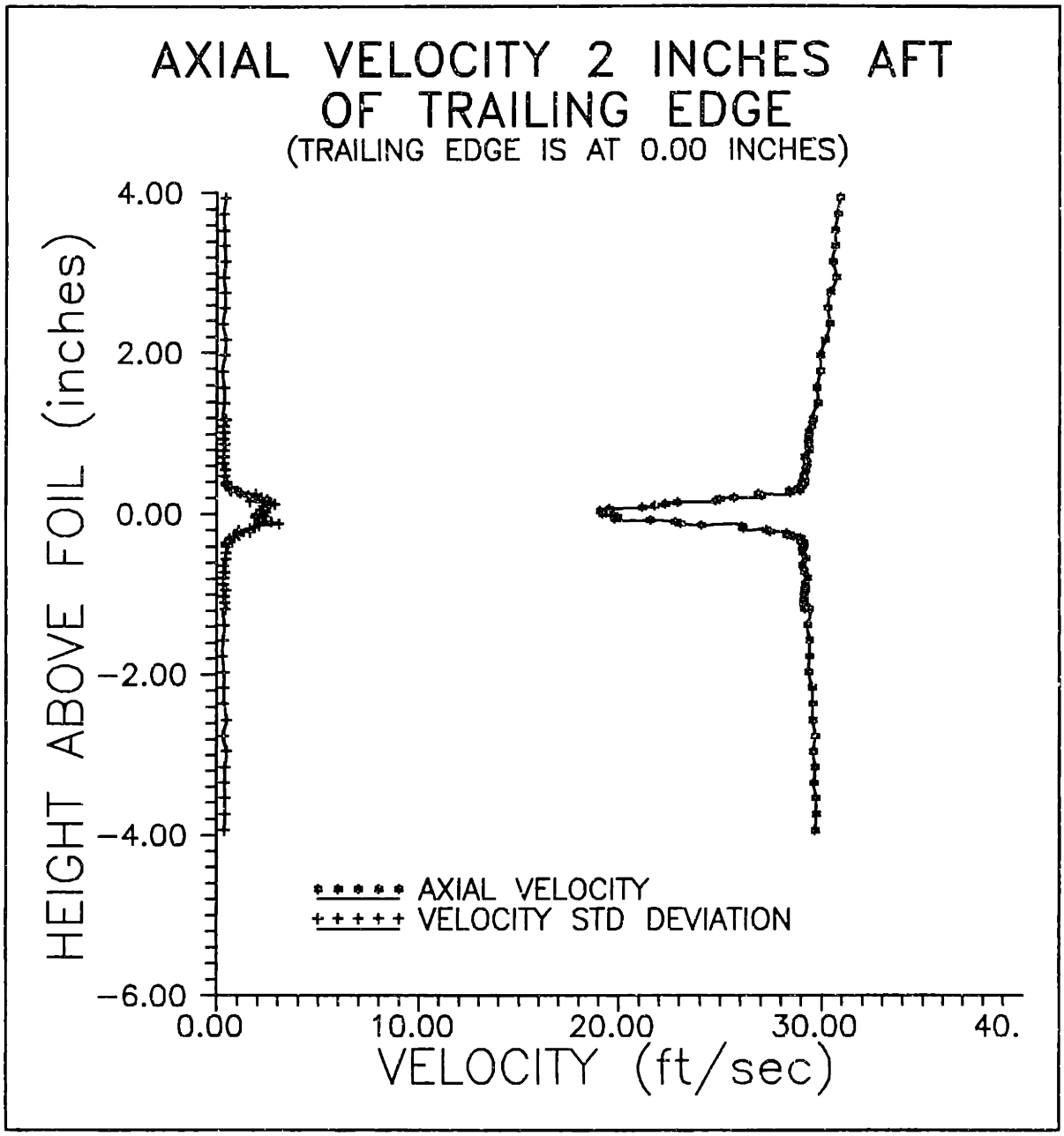

Figure III.14 Velocity Profile 2 Inches Aft of Trailing Edge

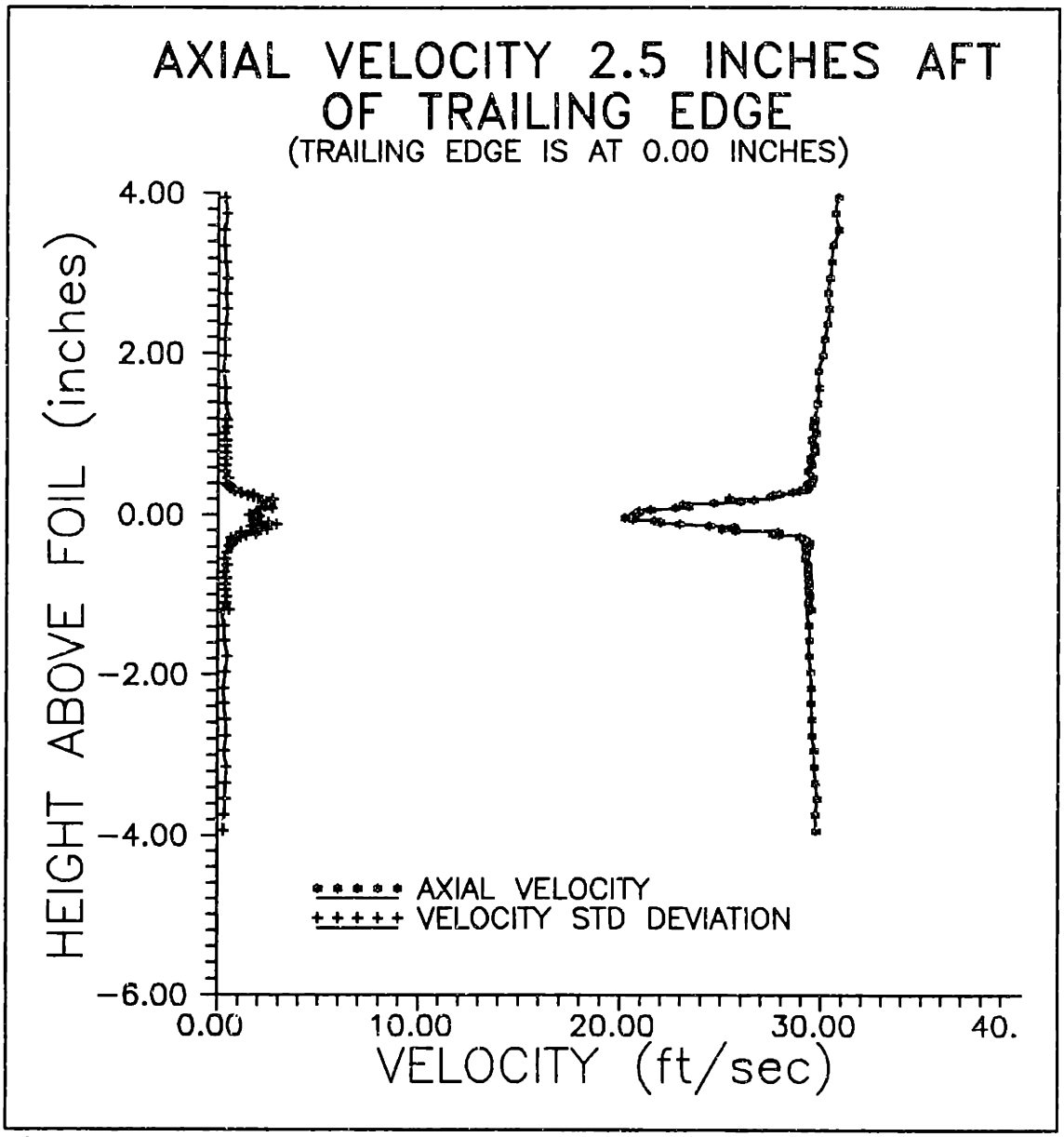

Figure III.15 Velocity Profile 2.5 Inches aft of Trailing Edge

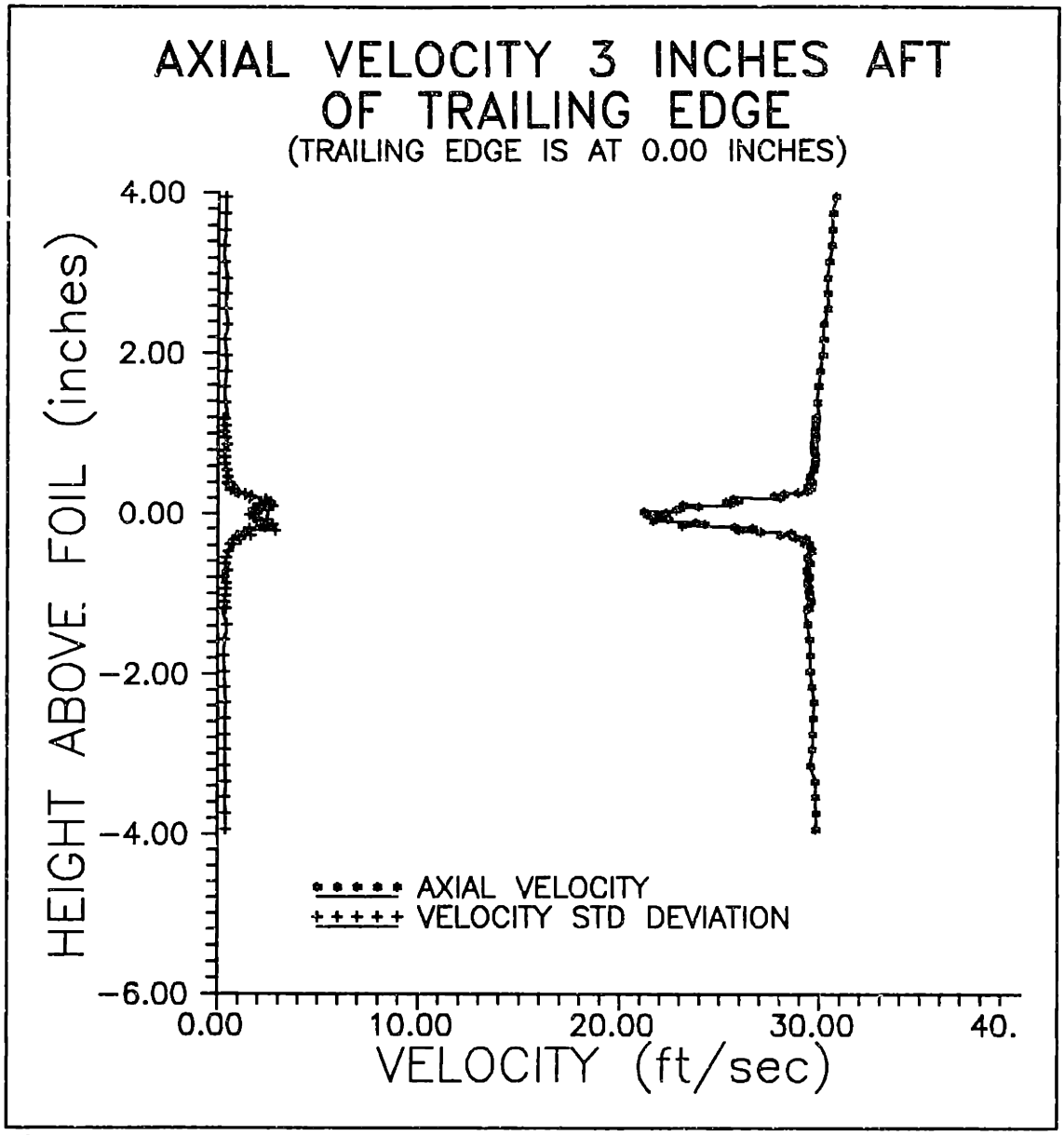

Figure III.16 Velocity Profile 3 Inches Aft of Trailing Edge

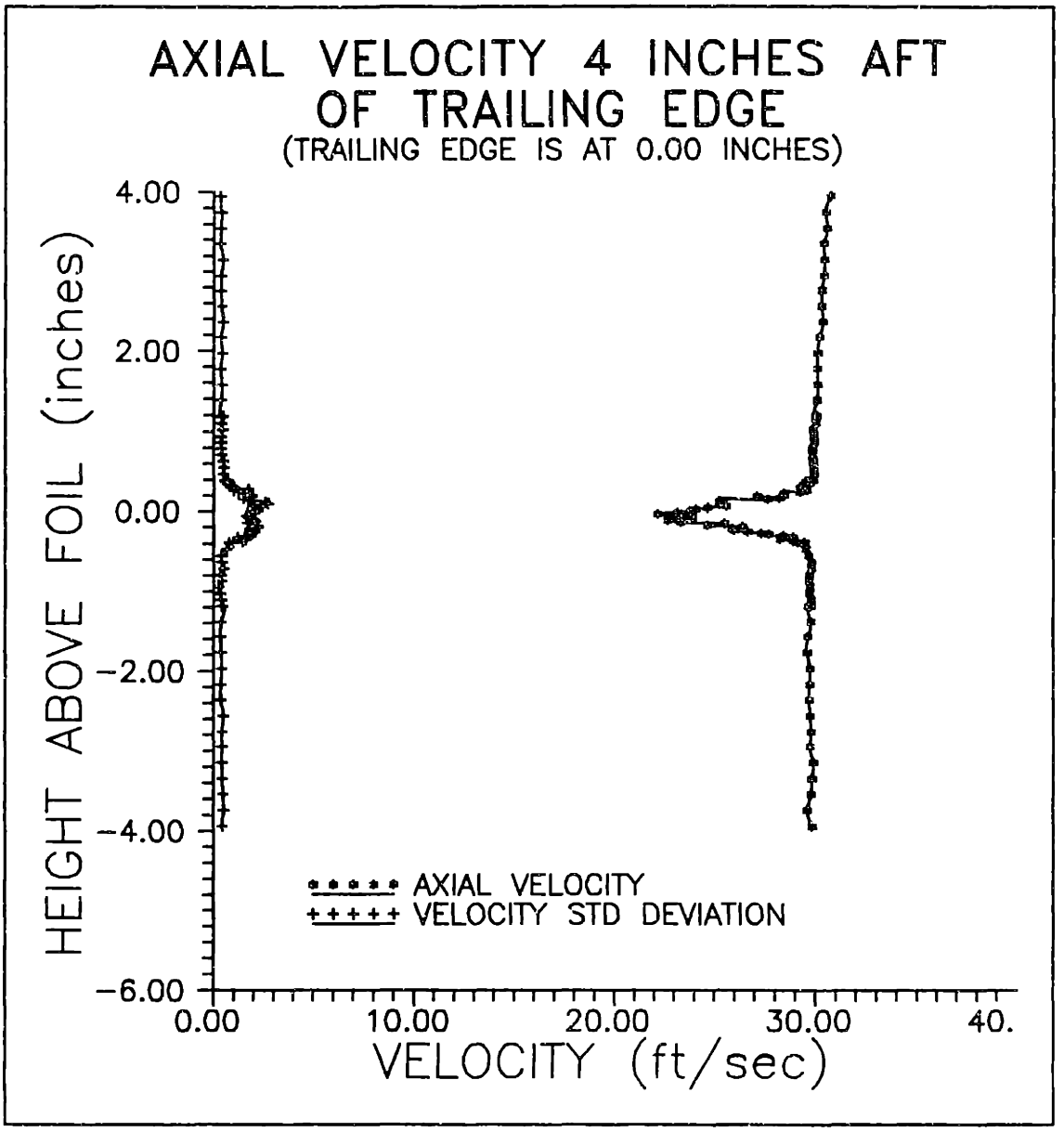

Figure III.17 Velocity Profile 4 Inches Aft of Trailing Edge

The end.